A COMPREHENSIVE SIMULATION STUDY OF THE VOLTAGE STABILITY OF A LARGE POWER SYSTEM

By

WENJIE ZHANG

B. Eng., Huazhong University of Science and Technology, PRC, 1982
M. Sc., Taiyuan University of Technology, PRC, 1985

A THESIS SUBMITTED IN PARTIAL FULFILLMENT OF
THE REQUIREMENTS FOR THE DEGREE OF
DOCTOR OF PHILOSOPHY

in

THE FACULTY OF GRADUATE STUDIES
DEPARTMENT OF ELECTRICAL ENGINEERING

We accept this thesis as conforming
to the required standard

THE UNIVERSITY OF BRITISH COLUMBIA
October 1993

In presenting this thesis in partial fulfilment of the requirements for an advanced degree at the University of British Columbia, I agree that the Library shall make it freely available for reference and study. I further agree that permission for extensive copying of this thesis for scholarly purposes may be granted by the head of my department or by his or her representatives. It is understood that copying or publication of this thesis for financial gain shall not be allowed without my written permission.

Electrical Engineering
The University of British Columbia
2075 Wesbrook Place
Vancouver, Canada
V6T 1W5

Date: December 17, 1993

Abstract

The voltage stability problem has become a growing concern in power system planning and operation. Many large interconnected power systems have experienced voltage instabilities which involve fast transients and/or slow dynamics. Although load flow related static approaches have been well developed to characterize the system maximum loading limit as the voltage collapse point, the mechanism of how system operation approaches its voltage collapse point and how this collapse point is affected by system dynamics are still obscure.

This thesis provides the answers to these two basic questions through the investigation of effects of loads and reactive power controls on system voltage stability by detailed time domain system simulations. The importance of system dynamics in the determination of the voltage stability limit is emphasized.

Firstly, a multimachine power system with steam and hydro electric generating units, various types of loads, and system reactive power–related control devices is appropriately modeled. Secondly, a comprehensive power system simulation program is developed based on the implicit trapezoidal rule and an integration step size control algorithm. A new variable elimination method for load flow, and a new forward–elimination and backward–substitution procedure for solving the system Jacobian matrix equations are devised. Different system disturbances are simulated, and the exact timing of system changes is implemented. Finally, a 21 bus sample power system is chosen for the voltage stability study. In the case studies, the effects of loads, control devices, and system disturbances on system voltage stability are thoroughly examined.

The voltage instability of a power system is a very complicated phenomenon, which,

depending on the location, the type, and the severity of a system disturbance, may involve a fast transient voltage instability, or a slow voltage deterioration followed by a sharp collapse. It is closely associated with system reactive power–related controls, and is strongly affected by the load characteristics. The beneficial and detrimental effects of loads and reactive power controls on voltage stability should be carefully analyzed so that the information can be used in voltage stability control designs.

Table of Contents

List of Tables

List of Figures

Acknowledgements

This thesis is dedicated to my parents, who inspired and encouraged me to take this opportunity of challenge.

I wish to express my grateful thanks to my research supervisor Dr. Y.N. Yu for his invaluable guidance, constant encouragement, and great patience during the research work and the accomplishment of this thesis.

My appreciation goes to Dr. M.D. Wvong and Dr. H.W. Dommel for their readiness to help and inspiring and helpful discussions.

I am also indebted for the financial support from the Natural Science and Engineering Research Council of Canada and the University of British Columbia.

Finally and gratefully, I thank my wife, Wei, for her special thoughtfulness, encouragement, understanding, and patience throughout the difficulties of my graduate program.

Chapter 1

INTRODUCTION

1.1 Power System Voltage Stability Problems

1.1.1 Power System Angle Stability

Since the beginning of large power system interconnections, low frequency system oscillations and transient and dynamic stability problems have developed. The main concern of these stability problems is to keep all synchronous generators in synchronous step by providing them with adequate damping if they oscillate, reducing generation or adding dynamic braking resistance if there is a power surplus, and shedding some loads if there is a power shortage. These problems, which may be classified as the angle stability problem, have been thoroughly studied and are well understood. Control means to stabilize the system, such as dynamic resistance braking, force excitation, fast valving, HVDC modulation, power system stabilizer (PSS), and generation tripping and load shedding, have been very well developed.

1.1.2 Power System Voltage Stability

As large power system interconnections continued, the power demand kept on increasing. But the environmental restriction on the building of new transmission lines also increased. There is a tendency in power system planning and operation to load the existing generation and transmission equipments as much as possible. This practice, coupled with insufficient and inadequate reactive power supplies for a power system, has caused many system voltage failures in the past, which may or may not also involve an angle instability.

Voltage stability has gained a special attention recently [1]. To have a better understanding of this problem, some major system voltage failure events are briefly reviewed as follows.

EDF — December 19, 1978 [4]

It was a severe cold winter morning in France, and the temperature drop was much greater than anticipated. A rapid rise of power demand caused the increase in several power transfers. It was also marked with the increase in active power losses and especially reactive power losses. Several 400 KV lines were overloaded, and system voltages deteriorated very badly.

Some EHV/HV tap changers were blocked, and a 5% distribution voltage drop was ordered in some area. The system was stabilized for a while. But due to the overload of the persistent load demand and the loss of many reactive power supports, many major transmission lines were successively lost resulting in island operation of the entire system.

EDF — January 12, 1987 [1]

It was again a severe cold weather day, and the system was overloaded. Generations were tripped one after another. At one time, the power deficiency was around 9,000 MW and the full installation capacity was 90 GW. The voltage deteriorated from 400 KV to 300 KV and below but did not collapse completely. The underfrequency relay control did not act because there was no significant frequency deterioration warranting the action. Finally, the voltage profile was restored by shedding 1500 MW of load and by tripping some 400/225 KV transformers feeding a load area.

TEPCO — July 23, 1987 [6]

Japan has a 50 Hz system in the north and a 60 Hz system in the south, and the two systems are connected by two 300 MW frequency converters at Sakuma and Shinshinano. The Tokyo Electric Power Company, TEPCO, belongs to the 50 Hz system.

It was a very hot summer day, much warmer than anticipated. After a maximum power demand of 39.1 GW in the morning, the demand dropped to 36.5 GW at 12:40 during the lunch hour. But the demand increased again rapidly at a rate of 400 MW per minute from 13:00, much faster than estimated. It was attributed to the air conditioning devices developed by then, which drew more current fast despite voltage deterioration. The power demand at 13:10 was 39.3 GW.

Although all shunt capacitances were in service, the system voltage dropped from 500 KV to 460 KV at 13:15 and further to 370 KV in the western part of the system and to 350 KV in the central part of the system at 13:19. Three substations of 8.168 GW were tripped, and 2.8 million customers were lost. The three substations were brought back to service from 13:23 to 13:35, and about 60% of total load loss was recovered at 13:36, 80% at 14:30, 90% at 16:00 and completely recovered at 16:40.

To summarize, it is observed that a voltage instability does not necessarily involve an angle instability, and that the voltage does not necessarily collapse completely. It is also very important that, for a comprehensive voltage stability study, special types of loads, like those in the TEPCO event, must be adequately modeled, and that the functions of all reactive power–related generating, consuming and control components must also be taken into consideration.

1.2 Power System Voltage Stability Studies

Although some effort has been made to clarify the mechanism of voltage instability and to devise some methods to prevent a system from voltage collapse, most researches have been devoted to the determination of maximum loading limit (MLL) of a power system by using the steady state formulation for a static voltage stability analysis. In these studies, only small load variations are considered, and the system dynamics are not included.

1.2.1 Static Voltage Stability Studies

While a power–angle curve for equal–area study has a shape of an inverse V with a maximum power point on top, the voltage–power curve for the MLL study has a V shape with the point of maximum load power towards the right as shown in Figure 1.1.

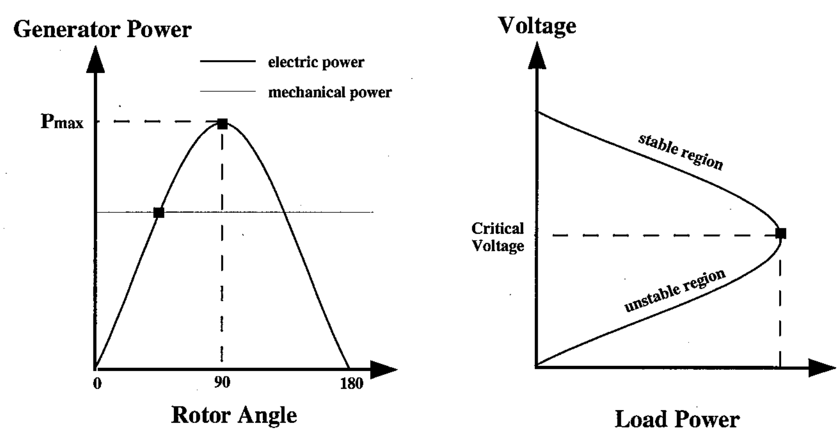

Figure 1.1: Power–Angle and Voltage–Power Curves

It is well known that the upper portion of the voltage–power curve represents a stable operation whereas the lower portion represents the unstable [2][3]. In–between exists a point of critical voltage. Several methods have been developed to find this critical point, and a variety of indicators have been defined for the proximity of the system stable operating state to the point of voltage collapse. All static methods are essentially related to a Jacobian matrix analysis from the results of a system load flow. System voltage may collapse at the point where the load flow Jacobian becomes singular.

1. **Load Flow Analysis** — Venikov et al. [8] found in 1975 that there exists a direct relation between the singularity of the load flow Jacobian and the singularity of the system dynamic state Jacobian and the changes in sign of system eigenvalues. Therefore, the stability of a dynamic system may be estimated by means of load flow. This method was expanded for voltage stability studies by Tamura et al. [9].

2. **Static Bifurcation Theory** — Bifurcation theory is concerned with the branching of static solutions of a dynamic system with a slow change in system parameters. With this technique, Kwatny et al. did a thorough analysis of loss of steady state stability and voltage collapse [10] in 1986. With a slow change in system parameters, the system stable operation determined by load flow will move to a new equilibrium and remain stable until one of the parameters reaches a critical value at which system state branches at a saddle point. This is the very point where the load flow Jacobian matrix becomes singular. When multiple solutions of load flow exist, they correspond to the multiple equilibria of the dynamic system in the neighborhood of the bifurcation point. Therefore, bifurcation analysis can be used to characterize these equilibria and to identify the critical parameters, which are the very important information for system control design.

3. **Sensitivity Method** — Sensitivity in voltage to system parameters near the critical state provides very useful information to system operation. It can be used to identify critical system buses and also effective means of controls [37][58]. Based on the analysis, a variety of indicators of proximity of the system state to the point

of voltage collapse can also be defined [11][14][15]. Therefore, adequate control can be exerted on the system to keep the system state away from voltage collapse.

1.2.2 Dynamic Voltage Stability Studies

Many power system voltage failures were triggered by large disturbances of the system. Due to the dynamic interaction among system components and the nonlinear constraints, the dynamics of a voltage instability process is rather complicated. It depends not only on the stability of generators in the system, the type and location of system contingencies, but also on the load characteristics and system controls. Since the system maximum loading limit (MLL) based on load flow analysis may give an upper bound of the voltage stability region, the system may have lost its voltage stability before that limit can be reached due to system dynamics [16]. Therefore, the MLL can only indicate the loading condition at which system voltage collapse may occur. It cannot answer the questions of how the system voltage approaches the collapse point and how this collapse point is affected by the system dynamics. For this sake, a comprehensive system simulation must be resorted to so that the system dynamics can be adequately included in the voltage stability studies.

1.3 Proposed Thesis Study

1.3.1 System Component Modeling

The major part of this thesis is to investigate the effects of load and system reactive power components on voltage stability. For that, the system behavior will be simulated comprehensively. All important loads and all system components that generate, consume and control the reactive power of the system will be modeled in detail. Other functions, such as the generator rotor field overheat protection, which may affect the reactive power of the system, will also be modeled. There are in general four major components to a power system, the generating plants, the transmission network, the system loads, and the system control devices. All of these components will be modeled.

1.3.2 Dynamic Simulation Techniques

A nine–machine power system is chosen for the simulation study. It is felt that the system is large enough to display the dynamic interactions among system components, such as generators, loads, transmission network and system controls. The high order system model with inherent system nonlinearities requires development of an appropriate simulation technique. The system equations are discretized based on the trapezoidal rule, and Newton–Raphson's iteration method is used to carry out the solution. To avoid direct inversion of a large Jacobian matrix in each integration step, a new technique of solving the Jacobian matrix equation is developed.

1.3.3 Dynamic Simulation of Voltage Stability

The main objective of this thesis is to investigate the general effects of special types of loads and major reactive power–related components on the dynamic behavior of the voltage stability of a multimachine power system. Several types of loads, control devices, and system disturbances of single or double contingencies will be considered.

Since the dynamics of induction motor loads [51], transformer tap changers [17], generator field excitations [37], and reactive power supply deficit [59] play a important role in a voltage collapse process, their effects must be examined on a large power system with detailed system models so that the dynamic interactions among system components can be included. In addition, the persistent PQ load characteristics [54] contributing to the TEPCO voltage failure should also be investigated. For this reason, the case studies are designed and carried out to clarify the effects on voltage stability of induction motor stalling, transformer tap changing, fixed capacitor and SVC compensations, persistent and general static loads and generator overheat protections.

1.4 Thesis Structure

In Chapter 2, the power system component models are presented. System bus loads are modeled by the combination of typical loads. Load dynamics are represented by induction motor loads and constant power and reactive power (PQ) loads with delayed recovery. Conventional static loads are modeled as voltage dependent loads. A generating plant is modeled in detail, including synchronous generator, field excitation system, governor and turbine system, and power system stabilizer. System controls, which have strong effects on system voltage stability, such as on load tap changer of a transformer(OLTC), the static VAR compensator(SVC), and generator rotor overheat protection(ROP) are also modeled. Finally, the transmission network is represented by the system node voltage equations.

Chapter 3 describes the nonlinear time domain simulation technique. The overall system equations can be obtained through a hybrid coordinate system for both generators and the transmission system. Based on the trapezoidal rule, system differential equations are discretized to obtain the corresponding difference equations. Newton–Raphson's method is then used to solve the system equations. A systematic method is developed to solve the high dimension Jacobian matrix equation without involving a direct inversion of a large matrix. In order to capture both fast transients and slow dynamics of a voltage instability, a variable step size mechanism is implemented. System disturbances and sudden topological changes are considered and exactly timed.

In Chapter 4, a 21 bus power system is presented. Since the system has low frequency oscillations for the given operating conditions, power system stabilizers are designed.

Next, the most voltage sensitive bus of the system is identified through system voltage sensitivity analysis. Typical system loads and control actions are considered for the most voltage sensitive bus. Case studies are then conducted to clarify the effects of various loads and controls on system voltage stability. Finally, the results of voltage stability from load flow and simulation studies are compared to demonstrate the effect of system dynamics on the system maximum loading limit.

Finally, conclusions are drawn and future research projects are suggested in Chapter 6.

Chapter 2

MODELING OF POWER SYSTEM COMPONENTS

For voltage stability studies, an appropriate power system model is required. Although a static model, like load flow equations, is adequate for steady state analysis, a more detailed model, including both load dynamics and reactive power generating and control components, must be used in a voltage stability study of a system involving dynamics. This is because the voltage instability phenomenon of a power system may involve both fast transients and slow dynamics [13]. Therefore, all system components involving transients and dynamics should be included in the voltage stability study.

Typical power system load models are presented in section 2.1, generating plant in section 2.2, system control devices in section 2.3, and, finally, transmission network equations in section 2.4.

2.1 Typical Power System Load Models

2.1.1 A Composite Bus Load Model

Examinations of major voltage failures show that system loads have significant effects on the voltage stability of a power system. But, a power system load is usually made up of numerous individual loads with different characteristics, and the information about some individual loads may not be available [18][19]. Therefore, it is almost impossible to derive an exact model for a power system load. Instead, the power system loads may be approximately represented by a few equivalents, e.g., industrial, commercial, and residential loads [20] as shown in Figure 2.1.

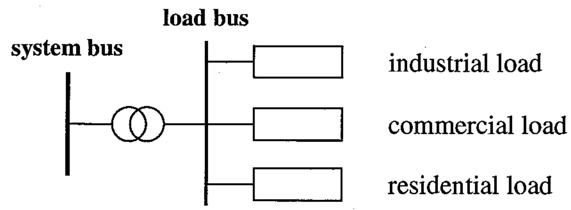

Figure 2.1: Classification of a Composite Bus Load

It is suggested in [21], for example, that a composite system bus load may be modeled by an equivalent induction motor in parallel with a static load as shown in Figure 2.2,

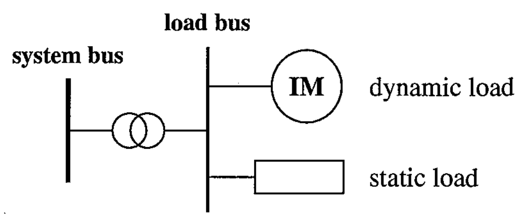

Figure 2.2: Composite Bus Load Modeling

where the equivalent induction motor represents the dynamics associated with the major industrial load, while the static load represents the voltage dependence of commercial and residential loads. Therefore, the load effect on system performance may be found by studying the following typical loads.

2.1.2 Induction Motor Load

Induction motors constitute the major part of an industrial load. They have a fast response to system disturbances to maintain more or less a constant power and draw more reactive power from the power supply. This feature of quick load pick–up and more reactive power absorption during a system disturbance is one of the major causes of a dynamic voltage instability [22].

The basic equations of a three–phase induction motor may be derived from Park's equations for a synchronous generator. However, there is no field winding, and the d and q axis windings are symmetrical for the motor. There is a slip of rotor windings with respect to the stator rotating field of the motor. Neglecting the electromagnetic transients (EMT's) in the stator windings, the induction motor may be described by a third order model as follows.

(a) Rotor motion equation:

$$2\,H\,\dot{s} = T_L - T_E \tag{2.1}$$

(b) Rotor winding voltage equations:

$$\begin{aligned} T_o^{'}\,\dot{e}_d^{'} &= -e_d^{'} - (x_o - x^{'})\,I_{qs} + \omega_b\,T_o^{'}\,s\,e_q^{'} \\ T_o^{'}\,\dot{e}_q^{'} &= -e_q^{'} + (x_o - x^{'})\,I_{ds} - \omega_b\,T_o^{'}\,s\,e_d^{'} \end{aligned} \tag{2.2}$$

(c) Stator winding voltage equations:

$$\begin{aligned} V_{ds} &= e_d^{'} + r_s\,I_{ds} - x^{'}\,I_{qs} \\ V_{qs} &= e_q^{'} + x^{'}\,I_{ds} + r_s\,I_{qs} \end{aligned} \tag{2.3}$$

(d) Electromagnetic torque equation:

$$T_E = e_d^{'} I_{ds} + e_q^{'} I_{qs} \tag{2.4}$$

where

H	:	motor inertia constant
r_s	:	stator resistance
x_o	:	rotor open circuit reactance
x'	:	blocked rotor reactance
T_o'	:	rotor open circuit time constant
e_d', e_q'	:	rotor internal voltages
V_{ds}, V_{qs}	:	stator terminal voltages
I_{ds}, I_{qs}	:	stator currents
s	:	motor slip
T_L	:	mechanical load torque
T_E	:	electromagnetic torque
ω_b	:	synchronous speed of the system

In steady state system condition, both mechanical and electrical transients of the motor are not included. Hence, equations (2.1) and (2.2) are reduced to algebraic equations to represent the steady state behavior of the motor. In that case, the motor torque, power, and reactive power can be determined by

$$\begin{aligned} T_E &= f_E(s, \mathbf{p})V^2 \\ P_m &= f_P(s, \mathbf{p})V^2 \\ Q_m &= f_Q(s, \mathbf{p})V^2 \\ V &= \sqrt{V_{ds}^2 + V_{qs}^2} \end{aligned} \tag{2.5}$$

where f_E, f_P and f_Q are functions of motor slip s and motor parameters $\mathbf{p}$. The derivation of equation (2.5) is given in Appendix A.

2.1.3 Voltage Dependent PQ Load

Since a voltage instability does not necessarily involve system frequency deterioration, the frequency dependence of commercial and residential loads may be neglected. The power and reactive power drawn from a system bus may then be described as a function of bus voltage. It has been a common practice that a bus load is divided into a constant power, a constant current, and a constant impedance load components. This concept leads directly to a load model of quadratic form [23].

$$\begin{aligned} P &= P_0[p_p + p_i\left(\tfrac{V}{V_0}\right) + p_z\left(\tfrac{V}{V_0}\right)^2] \\ Q &= Q_0[q_p + q_i\left(\tfrac{V}{V_0}\right) + q_z\left(\tfrac{V}{V_0}\right)^2] \end{aligned} \tag{2.6}$$

where P_0 and Q_0 are power and reactive power at normal operating voltage V_0, p_p, p_i and p_z are the coefficients of power portion of constant power, constant current, and constant impedance loads, and q_p, q_i and q_z are those of the reactive power portion of the load. These coefficients must satisfy

$$\begin{aligned} p_p + p_i + p_z &= 1 \\ q_p + q_i + q_z &= 1 \end{aligned}$$

A more general static PQ load model [24] has exponential forms as follows.

$$\begin{aligned} P &= P_0\left(\tfrac{V}{V_0}\right)^{\alpha} \\ Q &= Q_0\left(\tfrac{V}{V_0}\right)^{\beta} \end{aligned} \tag{2.7}$$

Here, again, P_0 and Q_0 are power and reactive power at normal operating voltage V_0, and α and β characterize the voltage dependence of the load. Equation (2.7) also includes three special cases, that is, the constant power load with $\alpha = \beta = 0$, the constant current load with $\alpha = \beta = 1$, and the constant impedance load with $\alpha = \beta = 2$.

The appropriate selection of a combination of p_p, p_i, p_z, q_p, q_i, and q_z in equation (2.6), and the exponents of α and β in equation (2.7) should be made by investigating the actual system load.

2.1.4 Constant PQ Load with a Recovery Time Constant

This type of load demands a constant power through self control to maintain the required power despite a system voltage decrease. A typical load power response to a step change in voltage may be in the form as shown in Figure 2.3.

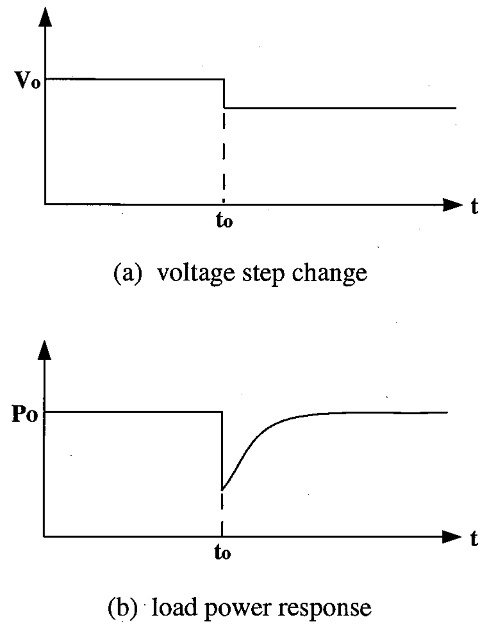

Figure 2.3: Constant PQ with a Delayed Recovery

The sudden dip in voltage causes an instant decrease in load power demand followed by a recovery to its normal value P_0. The demand is persisting, but involving a time delay. There is a such kind of load of modern air conditioning device as reported in TEPCO power failure [6]. This type of constant power load, which may be referred to as persistent PQ load, may be modeled by a changing load equivalent admittance with a time delay. The time delay is associated with the time needed for the control devices to respond, and may also involve a human factor [25].

Assuming an exponential recovery in both power and reactive power, this type of PQ load may be modeled as follows.

$$
\begin{aligned}
T_G \dot{G}_L &= P_0 - G_L V^2 \\
T_B \dot{B}_L &= Q_0 - B_L V^2
\end{aligned}
\tag{2.8}
$$

where V is the load terminal voltage; G_L and B_L are the varying equivalent load conductance and susceptance; T_G and T_B are the corresponding time constants; and P_0 and Q_0 are the load power and reactive power at normal operating condition with

$$
\begin{aligned}
P_0 &= G_{L0} V_0^2 \\
Q_0 &= B_{L0} V_0^2
\end{aligned}
\tag{2.9}
$$

2.2 Component Models of a Generating Plant

A generating plant consists of a synchronous generator, a field excitation system, a governor controlled turbine system, and probably a supplementary control, such as a power system stabilizer. These components contribute the major dynamics of a power system, which should be adequately modeled in a dynamic system study.

2.2.1 Synchronous Generator

Neglecting electromagnetic transients in armature windings, a synchronous generator may be represented by a fifth order model as follows.

(a) Rotor motion equations:

$$
\begin{aligned}
M \dot{\omega} &= T_m - T_e - D \omega \\
\dot{\delta} &= \omega_b (\omega - 1.0)
\end{aligned}
\tag{2.10}
$$

(b) Rotor winding voltage equations:

$$
\begin{aligned}
T'_{do}\,\dot{E}'_q &= -E'_q - (x_d - x'_d)\,I_d + E_{FD} \\
T''_{do}\,\dot{E}''_q &= -E''_q - (x'_d - x''_d)\,I_d + E'_q + T''_{do}\,\dot{E}'_q \\
T''_{qo}\,\dot{E}''_d &= -E''_d + (x_q - x''_q)\,I_q
\end{aligned}
\tag{2.11}
$$

(c) Armature winding voltage equations:

$$
\begin{aligned}
V_d &= E''_d - r_a\,I_d + x''_q\,I_q \\
V_q &= E''_q - x''_d\,I_d - r_a\,I_q
\end{aligned}
\tag{2.12}
$$

(d) Electromagnetic torque equation:

$$
T_e = E''_d I_d + E''_q I_q + (x''_q - x''_d) I_d I_q \tag{2.13}
$$

The voltages and currents are described in individual machine d–q coordinates.

In the foregoing equations,

M	:	inertia constant
D	:	mechanical damping coefficient
ω	:	rotor speed
δ	:	rotor angle
T_m, T_e	:	mechanical and electromagnetic torques
r_a	:	armature resistance
x'_d	:	d–axis transient reactance
x''_d, x''_q	:	d– and q–axis sub–transient reactances
T'_{do}	:	d–axis transient time constant
T''_{do}, T''_{qo}	:	d– and q–axis sub–transient time constant

E_q' : q–axis transient voltage

E_d'', E_q'' : d– q–axis sub–transient voltages

E_{FD} : field voltage

V_d, V_q : d and q components of terminal voltage

I_d, I_q : d and q components of armature current

ω_b : synchronous speed of the system

where δ is in radian, M and time constants are in seconds, and all other variables are in per unit.

2.2.2 Field Excitation System

A fast–response exciter and voltage regulator system shown in Figure 2.4 is chosen for the study.

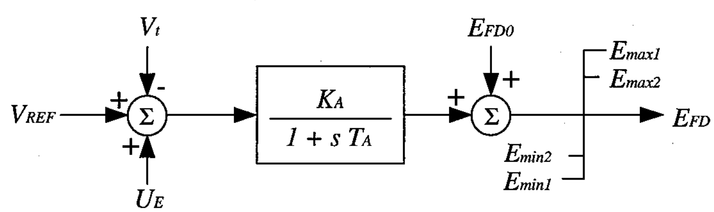

Figure 2.4: A Fast Excitation System

It may be described by the differential equation

$$T_A\,\dot{E}_{FD} = -E_{FD} + E_{FD0} + K_A\,(U_E + V_{REF} - V_t) \tag{2.14}$$

where K_A and T_A are respectively the equivalent gain and time constant of the excitation system. V_t and V_{REF} are the generator terminal voltage and its reference, respectively.

U_E is the supplementary excitation control. E_{FD0} is the initial value of excitation voltage E_{FD}.

The excitation voltage has physical limits, which may be called the first limit

$$E_{min1} \leq E_{FD} \leq E_{max1}$$

It also has a lower operating limits (E_{min2}, E_{max2}), which may be called the second limit, determined from the consideration of the generator rotor overheat protection. When a generator has been excited continuously over the second limit for a prescribed period of time, relay protection will cramp the excitation voltage to the second limit, or even trip off the generator.

2.2.3 Governor and Turbine Systems

(a) Mechanical–Hydraulic Governor and Hydro Turbine System

The block diagram of a mechanical–hydraulic governor and turbine system for a hydro–electric plant is shown in Figure 2.5.

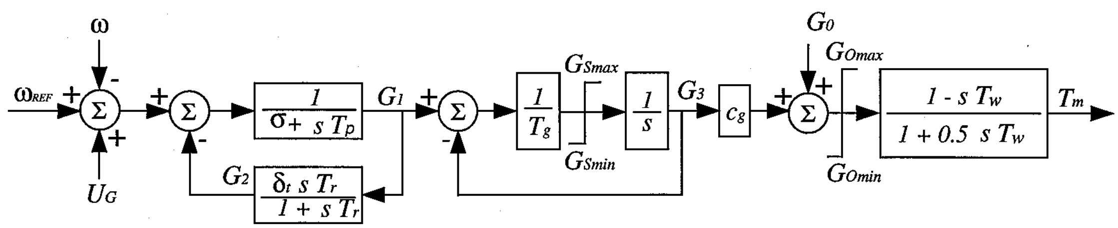

Figure 2.5: Hydro Turbine and Governor System

The corresponding differential equations are

$$\begin{aligned}
T_p \dot{G}_1 &= -\sigma G_1 + U_G + \omega_{REF} - \omega - G_2 \\
T_r \dot{G}_2 &= -G_2 + \delta_T T_r \dot{G}_1 \\
T_g \dot{G}_3 &= -G_3 + G_1 \\
0.5 T_w \dot{T}_m &= -T_m + C_g G_3 + G_0 - T_w \dot{G}_3
\end{aligned} \tag{2.15}$$

subject to the governor speed and opening constraints by

$$G_{Smin} \leq \dot{G}_3 \leq G_{Smax}$$
$$G_{Omin} \leq (C_g G3 + G_0) \leq G_{Omax}$$

where

$1/\sigma$	:	overall gain of speed governor
δ_t	:	transient regulation constant
T_p, T_r, T_g, T_w	:	time constants of actuator, dashpot, servomotor, and water, respectively
G_1, G_2	:	outputs of servo actuator and dashpot, respectively
G_3	:	gate incremental opening
G_0	:	initial gate opening
ω_{REF}	:	speed reference
U_G	:	supplementary governor control

(b) Electrical–Hydraulic Governor and Steam Turbine System

The block diagram of an electrical–hydraulic governor and non–reheat steam turbine for an steam electric plant is shown in Figure 2.6.

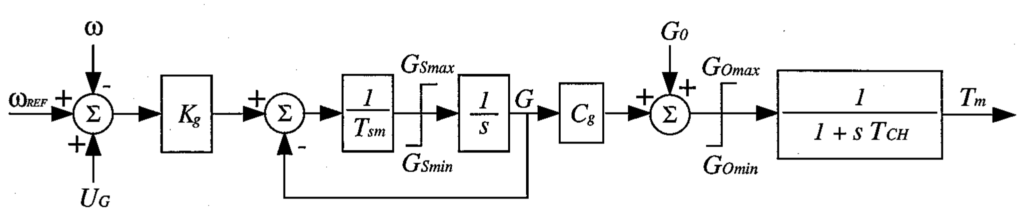

Figure 2.6: Non-Reheat Steam Turbine and Governor System

The corresponding differential equations are

$$\begin{aligned} T_{sm} \dot{G} &= -G + K_g (U_G + \omega_{REF} - \omega) \\ T_{CH} \dot{T}_m &= -T_m + C_g G + G_0 \end{aligned} \tag{2.16}$$

subject to governor speed and opening constraints

$$G_{Smin} \le \dot{G} \le G_{Smax}$$
$$G_{Omin} \le (C_g G + G_0) \le G_{Omax}$$

where

K_g : overall gain of speed governor

T_{sm} : servo motor time constant

G : valve incremental opening

T_{CH} : steam chest time constant

In a multi–machine power system, the power output of a generator is expressed on the system base, while the governor output is usually expressed on the individual generator base with a full load output as 1 per unit. As a result, an interfacing factor C_g must be introduced as shown in the Figures.

2.2.4 Power System Stabilizer (PSS)

For a voltage stability study, the low frequency system oscillation phenomena must be isolated by power system stabilizer applications. A power system stabilizer with two compensation components and one reset block is shown in Figure 2.7.

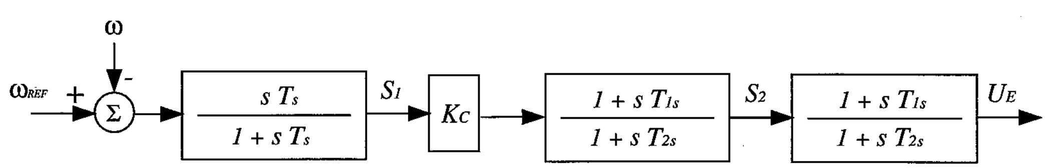

Figure 2.7: A Power System Stabilizer

The differential equations for the PSS are

$$\begin{aligned}
T_s \dot{S}_1 &= -S_1 - T_s \dot{\omega} \\
T_{2s} \dot{S}_2 &= -S_2 + K_c S_1 + K_c T_{1s} \dot{S}_1 \\
T_{2s} \dot{U}_E &= -U_E + S_2 + T_{1s} \dot{S}_2
\end{aligned} \tag{2.17}$$

where K_c is the overall gain, T_s is the time constant of the reset block, and T_{1s} and T_{2s} are those of the compensation blocks.

2.3 System Voltage Control Devices

Obviously, system voltage controls have significant effects on system voltage behavior. These control devices may include synchronous condensers, transformer tap changers, and static VAR compensators. In addition, a generator rotor overheat protection may limit the excitation voltage and hence the reactive power output of the generator, which may result in a loss of system voltage control ability. Therefore, It may also be considered as a voltage control device.

2.3.1 On Load Transformer Tap Changer

Distribution transformers are usually equipped with on–load tap changers (OLTC's). An OLTC controlled load bus is shown in Figure 2.8. The secondary voltage V_s is controlled through the change of the transformer ratio a which has limits.

$$\begin{gathered}
a = \mu(V_s) \\
a_{min} \leq a \leq a_{max}
\end{gathered} \tag{2.18}$$

Since a transformer has only limited number of taps, the ratio a must be changed in steps. In addition, time is required for completion of each tap changing. Therefore, the control function μ may be modeled in discrete way with time delay. That is, for voltage

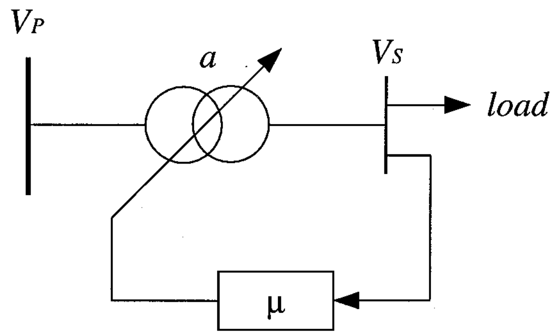

Figure 2.8: A Transformer with OLTC

controlled bus i with normal operating voltage V_i^0, a tap step of Δa_i, and a prescribed voltage tolerance ϵ, the tap changing function may be described by

$$a_i(k+1) = a_i(k) + \mu_i \Delta a_i \tag{2.19}$$

where μ is a sign function as follows.

$$\mu_i = \begin{cases} 1 & \text{if } V_i - V_i^0 < -\epsilon \\ 0 & \text{if } |V_i - V_i^0| < \epsilon \\ -1 & \text{if } V_i - V_i^0 > \epsilon \end{cases}$$

2.3.2 Static VAR Compensator (SVC)

Static VAR compensators (SVC's) have a significant influence on the system voltage behavior. A thyristor–controlled reactor (TCR) compensator with fixed shunt capacitors is shown in Figure 2.9 with a block diagram of SVC control circuit in Figure 2.10.

The differential equations for the SVC system are

$$\begin{aligned} T_b \dot{B}_1 &= -B_1 + K_b(V_{REF} - V_t) \\ T_{2b} \dot{B}_2 &= -B_2 + T_{1b} \dot{B}_1 + B_1 \\ B_L &= B_2 + B_{L0} \end{aligned} \tag{2.20}$$

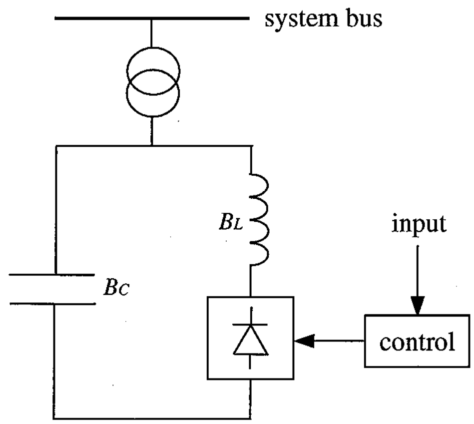

Figure 2.9: A TCR with Fixed Capacitor

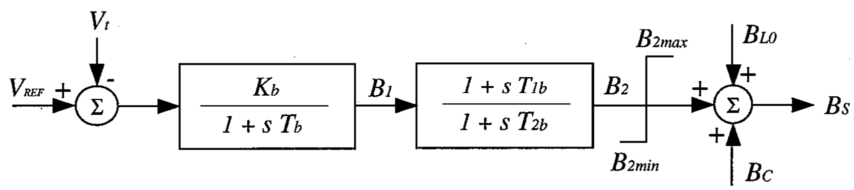

Figure 2.10: Block Diagram of an SVC with Voltage Control

with constraints

$$B_{2min} \leq B_2 \leq B_{2max}$$

where K_b and T_b are the gain and time constant of voltage regulator. T_{1b} and T_{2b} are time constants associated with the thyristor firing system.

2.3.3 Generator Rotor Overheat Protection

A generator rotor overheat protection may be approximately modeled by an excitation reduction of the generator which has been excited continuously over its operating limit or the second excitation limit E_{max2} (see in Figure 2.4) for a certain period of time. The timing of excitation reduction depends on the accumulated heat and temperature rise of a field winding due to actual excitation at a level over E_{max2} as in Figure 2.11. For instance,

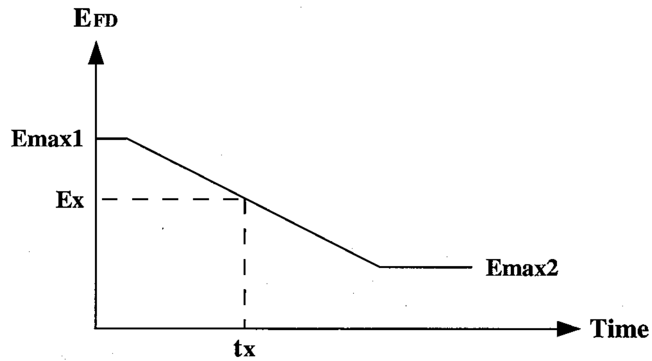

Figure 2.11: Overheat protection characteristic

if the excitation voltage E_{FD} is higher than E_x continuously over a time period of t_x, the overheat protection will cramp the excitation voltage immediately to its second limit E_{max2}.

2.4 Modeling of Transmission Network

Neglecting the electromagnetic transients in the transmission system, the network equation, which describes the relationship between bus voltage and current injection, may be expressed algebraically with network admittance matrix $\mathbf{Y_N}$ in the following phasor form,

$$[\mathbf{I_{BUS}}] = [\mathbf{Y_N}]\,[\mathbf{V_{BUS}}] \tag{2.21}$$

or alternatively in X–Y real number coordinates as

$$[I_{X,Y}] = [Y_{GB}]\,[V_{X,Y}] \tag{2.22}$$

In equation (2.22), $[V_{X,Y}]$ and $[I_{X,Y}]$ respectively denote the system bus voltages and current injections in X and Y coordinates as

$$\begin{aligned} [V_{X,Y}] &= [V_{X1}, V_{Y1}, V_{X2}, V_{Y2}, \cdots, V_{X_N}, V_{Y_N}]^T \\ [I_{X,Y}] &= [I_{X1}, I_{Y1}, I_{X2}, I_{Y2}, \cdots, I_{X_N}, I_{Y_N}]^T \end{aligned}$$

and the corresponding matrix Y_{GB} has the form of

$$[Y_{GB}] = \begin{bmatrix} [Y_{11}] & [Y_{12}] & \cdots & [Y_{1N}] \\ [Y_{21}] & [Y_{22}] & \cdots & [Y_{2N}] \\ \vdots & \vdots & \ddots & \vdots \\ [Y_{N1}] & [Y_{N2}] & \cdots & [Y_{NN}] \end{bmatrix}$$

with

$$[Y_{ij}] = \begin{bmatrix} G_{ij} & -B_{ij} \\ B_{ij} & G_{ij} \end{bmatrix}$$

where N denotes the total system bus number, G_{ij} and B_{ij} are respectively the real and the imaginary components of $\mathbf{Y}_{\mathbf{N}ij}$.

Hence, the network injection current at system bus i can be expressed as

$$\begin{aligned} I_{Xi} &= \textstyle\sum_{j=1}^{N} (G_{ij} V_{Xj} - B_{ij} V_{Yj}) \\ I_{Yi} &= \textstyle\sum_{j=1}^{N} (B_{ij} V_{Xj} + G_{ij} V_{Yj}) \end{aligned} \tag{2.23}$$

Power system component models are presented in this chapter. While synchronous generators are described in individual machine's d–q coordinates, other components are expressed in a coordinate system which rotates at synchronous speed. Coordinate system transformation and the overall system presentation are given in Chapter 3.

Chapter 3

SIMULATION TECHNIQUE FOR VOLTAGE STABILITY STUDIES

The voltage instability phenomenon of a power system is far more complicated than that of a conventional transient and dynamic angle instability of the system. They differ in nature. Voltage stability depends not only on the stability of synchronous generators, but also largely on the load characteristics and power and reactive power control dynamics of the system. For different system operating conditions, voltage instability may involve a fast voltage drop or a slow voltage decline followed by a voltage collapse. In other words, a heavily loaded power system may experience either a slow or a fast system voltage instability, which depends on the type, the location and the severity of system disturbances, the load characteristics and inadequate system controls [13].

The stability of a power system can be best assessed by the time responses of system state variables to different system disturbances. This requires the solutions of the system equations which usually constitute a very complicated high order system with many inherent nonlinearities. Therefore, computer simulation methods must be resorted. As part of the thesis work, a comprehensive system simulation program is developed.

Following a discussion of coordinate transformation of machines and transmission network, a complete set of system equations are presented in section 3.1. A simultaneous implicit integration method based on trapezoidal rule is described in section 3.2. Finally, a flowchart of the system simulation program with some detailed discussions are presented in section 3.3.

3.1 Complete System Equations

3.1.1 Machine and Transmission Coordinates

In Chapter 2, synchronous machines are described in individual machine's d and q coordinates, while transmission network was initially described in static coordinates but may be deemed as synchronously rotating X–Y coordinates. To interface the machines with the transmission network at machine terminals, coordinate transformations of terminal currents and voltages are necessary. The relationship between the kth synchronous machine coordinates d_k–q_k and the common network coordinates X–Y is shown as in Figure 3.1.

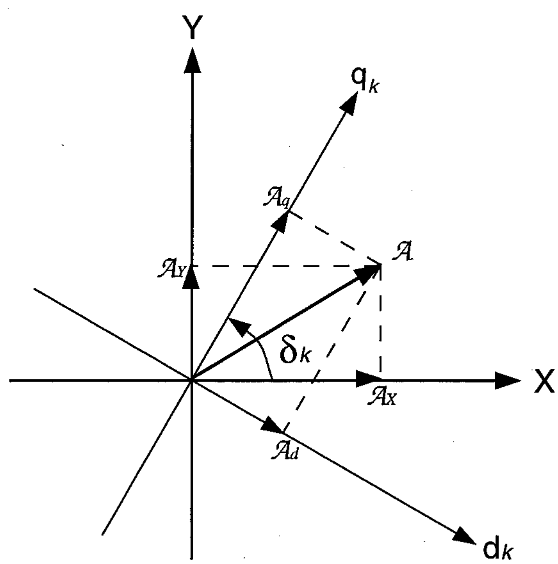

Figure 3.1: Machine and Transmission Network Coordinates

Therefore, the voltage and current transformations of the kth generator and the ith transmission bus may be written as follows.

$$\begin{bmatrix} V_{dk} \\ V_{qk} \end{bmatrix} = \begin{bmatrix} \sin\delta_k & -\cos\delta_k \\ \cos\delta_k & \sin\delta_k \end{bmatrix} \begin{bmatrix} V_{Xi} \\ V_{Yi} \end{bmatrix} \tag{3.1}$$

and

$$\begin{bmatrix} I_{dk} \\ I_{qk} \end{bmatrix} = \begin{bmatrix} \sin\delta_k & -\cos\delta_k \\ \cos\delta_k & \sin\delta_k \end{bmatrix} \begin{bmatrix} I_{Xi} \\ I_{Yi} \end{bmatrix} \tag{3.2}$$

where δ_k is the rotor angle of the kth generator.

To save the computation of coordinate transformation, a hybrid coordinate system is preferred [39], by which synchronous machine terminal voltages are transformed into the common network coordinates, while machine currents remain in individual d and q coordinates. As a result, for the kth synchronous generator connected to the ith system bus, the generator armature winding voltage equation (2.12) and the network injection current equation at the ith system bus (2.23) become

$$\begin{bmatrix} \sin\delta_k & -\cos\delta_k \\ \cos\delta_k & \sin\delta_k \end{bmatrix} \begin{bmatrix} V_{Xi} \\ V_{Yi} \end{bmatrix} = \begin{bmatrix} E''_{dk} \\ E''_{qk} \end{bmatrix} - \begin{bmatrix} r_{ak} & -x_{qk} \\ x_{dk} & r_{ak} \end{bmatrix} \begin{bmatrix} I_{dk} \\ I_{qk} \end{bmatrix} \tag{3.3}$$

and

$$\begin{bmatrix} \sin\delta_k & \cos\delta_k \\ -\cos\delta_k & \sin\delta_k \end{bmatrix} \begin{bmatrix} I_{dk} \\ I_{qk} \end{bmatrix} = \begin{bmatrix} \sum_{j=1}^{N} (G_{ij}V_{Xj} - B_{ij}V_{Yj}) \\ \sum_{j=1}^{N} (B_{ij}V_{Xj} + G_{ij}V_{Yj}) \end{bmatrix} \tag{3.4}$$

Equation (3.4) shows that the network injection current at a generator bus has been transformed into the corresponding machine coordinates.

3.1.2 Complete System Equations

The overall internal system behavior is the result of interactions among system components. For a power system with N_g generating plants, N_l system bus loads, and N_c system control devices, a block diagram of component interaction of the power system may be shown as in Figure 3.2.

With this block diagram and the coordinate system, equations (3.3) and (3.4), the complete system equations can be derived by aggregating all system component equations

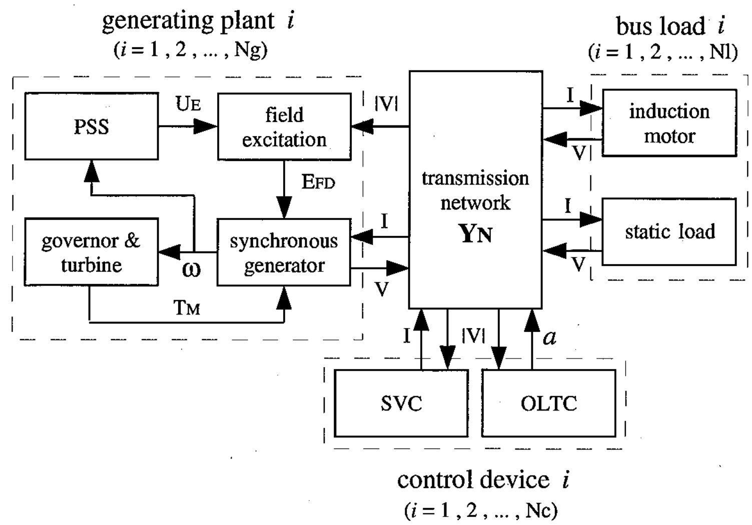

Figure 3.2: Block Diagram of Component Interaction

described in Chapter 2, which can be organized into a set of differential and algebraic equations as follows.

$$\mathbf{F}(\dot{\mathbf{X}}, \mathbf{X}, \mathbf{Y}, \mathbf{D}) = \mathbf{0} \tag{3.5}$$

$$\mathbf{G}(\mathbf{X}, \mathbf{Y}, \mathbf{D}) = \mathbf{0} \tag{3.6}$$

where $\mathbf{X}$ is the vector of system differential variables and $\mathbf{Y}$ the vector of system algebraic variables of system voltage and current and their related variables such as machine electromagnetic torque. $\mathbf{X}$ and $\mathbf{Y}$ together constitute the system state variable vector, which may be subjected to certain operating constraints. $\mathbf{D}$ is the parameter vector of external system changes, such as the changes of system references, load variations, or the system contingencies. $\mathbf{F}$ and $\mathbf{G}$ are vector functions which depend on the system component models and parameters and subject to change due to the changes in system topology and/or system operating conditions.

The state variables $\mathbf{X}$ and $\mathbf{Y}$ and their possible constraints of system equations obtained in Chapter 2 may be summarized as follows.

1. Typical system loads:

   (a) Induction motor load

$$\begin{aligned} \mathbf{x} &= [s\ e_d^{'}\ e_q^{'}]^T \\ \mathbf{y} &= [V_{ds}\ V_{qs}\ I_{ds}\ I_{qs}\ T_E]^T \end{aligned}$$

   (b) Voltage dependent PQ load

$$\mathbf{y} = [V_X\ \ V_Y\ \ I_X\ \ I_Y]^T$$

   (c) Persistent PQ load

$$\mathbf{x} = [G_L\ \ B_L]^T$$

2. Generating plant:

   (a) Synchronous generator

$$\begin{aligned} \mathbf{x} &= [\omega\ \delta\ E_q^{'}\ E_d^{''}\ E_q^{''}]^T \\ \mathbf{y} &= [V_d\ V_q\ I_d\ I_q\ T_e]^T \end{aligned}$$

   (b) Field excitation system

$$\mathbf{x} = [E_{FD}]$$

$$E_{min1} \leq E_{FD} \leq E_{max1}$$

   (c) Mechanical–hydraulic governor and hydro turbine

$$\mathbf{x} = [G_1\ \ G_2\ \ G_3\ \ T_m]^T$$

$$G_{Smin} \leq \dot{G}_3 \leq G_{Smax}$$

$$G_{Omin} \leq (C_G G_3 + G_0) \leq G_{Omax}$$

(d) Electrical–hydraulic governor and steam turbine

$$\mathbf{x} = [G \;\; T_m]^T$$

$$G_{Smin} \leq \dot{G} \leq G_{Smax}$$

$$G_{Omin} \leq (C_G G + G_0) \leq G_{Omax}$$

(e) Power system stabilizer

$$\mathbf{x} = [S_1 \;\; S_2 \;\; U_E]^T$$

$$U_{Emin} \leq U_E \leq U_{Emax}$$

3. System control device

(a) On load transformer tap changer

$$\mathbf{y} = [a]$$

$$a_{min} \leq a \leq a_{max}$$

(b) Static VAR compensator

$$\mathbf{x} = [B_1 \;\; B_2]^T$$

$$B_{2min} \leq B_2 \leq B_{2max}$$

4. Transmission network

$$\mathbf{y} = [V_{Xi} \;\; V_{Yi} \;\; I_{Xi} \;\; I_{Yi}]^T \quad i = 1, 2, \cdots, N$$

3.2 Simultaneous Implicit Integration of System Equations

3.2.1 Implicit Trapezoidal Rule

For accuracy and numerical stability, simultaneous implicit integration methods are often used to solve the system differential and algebraic equations like (3.5) and (3.6). In this method, both differential and algebraic equations are replaced by finite difference equations through discretizations, and then solved simultaneously by Newton-Raphon's method. The simultaneous implicit integration method may be implemented with different algorithms depending on the accuracy of the difference equations used to approximate the corresponding differential equations. In general, the higher the discretization order is, the better the accuracy of the result will be, but a more complex algorithm will be involved.

For power system stability studies, it has been suggested that low order integration would be best in both efficiency and stability [40]. Implicit trapezoidal integration method would then be the most suitable candidate for power system stability study. Firstly, as a single step discretization method, the trapezoidal rule is easy to implement. Secondly, and more importantly, the trapezoidal rule has an order of two and has an essential characteristic of symmetrical A–stability. The latter means that if the difference equation is symmetrically A–stable, it demonstrates the same stability results as those determined by the solution of the original differential equation [40].

The basic idea of implicit trapezoidal rule may be illustrated by Figure 3.3. To integrate the differential equation

$$\begin{aligned} \frac{dx}{dt} &= f(x,t) \\ x(t_n) &= x_n \end{aligned} \tag{3.7}$$

with known x_n, the solution of x at t_n, the solution of x at $t_{n+1} = t_n + \Delta t_n$, or x_{n+1} can

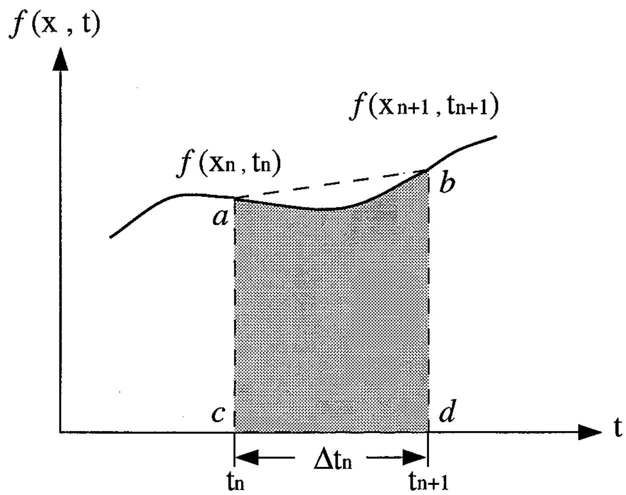

Figure 3.3: Illustration of Implicit Trapezoidal Rule

be obtained by integrating equation (3.7) from t_n to t_{n+1} as follows.

$$x_{n+1} = x_n + \int_{t_n}^{t_{n+1}} f(x,t)\,dt \tag{3.8}$$

As shown in Figure 3.3, the shaded area corresponds to the definite integral in equation (3.8). If the Δt_n is small enough, the arc between points a and b may be replaced by the dashed line ab, and the shaded area may then be approximated by the area of the trapezoid $abcd$, which results in

$$\int_{t_n}^{t_{n+1}} f(x,t)\,dt = \frac{\Delta t_n}{2}[f(x_n,t_n) + f(x_{n+1},t_{n+1})] + e_{LT} \tag{3.9}$$

where e_{LT} is the local truncation error introduced in the integration interval $(t_n,\ t_{n+1})$, which can be estimated [42] as

$$e_{LT} = -\frac{1}{12}x'''(\xi_n)(\Delta t_n)^3 \tag{3.10}$$

for some $\xi_n \in (t_n, t_{n+1})$.

Equation (3.8) then becomes

$$x_{n+1} = x_n + \frac{\Delta t_n}{2}[f(x_n, t_n) + f(x_{n+1}, t_{n+1})] + e_{LT} \tag{3.11}$$

The evaluation of e_{LT} will be presented in section 3.3.3.

The trapezoidal integration algorithm for the differential equation (3.7) is obtained by dropping the error term in equation (3.11).

$$x_{n+1} = x_n + \frac{\Delta t_n}{2}[f(x_n, t_n) + f(x_{n+1}, t_{n+1})] \tag{3.12}$$

With x_n and $f(x_n, t_n)$ known at $t = t_n$, a difference equation constant, z_n, can be defined as

$$z_n = x_n + \frac{\Delta t_n}{2} f(x_n, t_n) \tag{3.13}$$

Equation (3.12) can then be written in the following standard form.

$$x_{n+1} = z_n + \frac{\Delta t_n}{2} f(x_{n+1}, t_{n+1}) \tag{3.14}$$

This is the discretization algorithm of implicit trapezoidal integration.

3.2.2 Discretization of System Differential Equations

With the implicit trapezoidal integration rule of equation (3.14), all differential equations of system components described in Chapter 2 can be discretized and summarized as follows. For convenience, define $h = \Delta t\,/\,2$.

1. Typical system loads:

   (a) Induction motor load

$$\begin{aligned}
2\,H\,s\,|_{(t+\Delta t)} &= z_{m1}|_t + h\,(T_L - T_E)|_{(t+\Delta t)} \\
T_o^{'}\,e_d^{'}|_{(t+\Delta t)} &= z_{m2}|_t + h\,[-e_d^{'} - (x_o - x^{'})\,I_{qs} + \omega_b\,T_o^{'}\,s\,e_q^{'}]|_{(t+\Delta t)} \\
T_o^{'}\,e_q^{'}|_{(t+\Delta t)} &= z_{m3}|_t + h\,[-e_q^{'} + (x_o - x^{'})\,I_{ds} - \omega_b\,T_o^{'}\,s\,e_d^{'}]|_{(t+\Delta t)}
\end{aligned} \tag{3.15}$$

with the difference equation constants

$$\begin{aligned} z_{m1}|_t &= 2H\,s\,|_t + h\,(T_L - T_E)|_t \\ z_{m2}|_t &= T_o^{'}\,e_d^{'}|_t + h\,[-e_d^{'} - (x_o - x^{'})\,I_{qs} + \omega_b\,T_o^{'}\,s\,e_q^{'}]|_t \\ z_{m3}|_t &= T_o^{'}\,e_q^{'}|_t + h\,[-e_q^{'} + (x_o - x^{'})\,I_{ds} - \omega_b\,T_o^{'}\,s\,e_d^{'}]|_t \end{aligned}$$

(b) Persistent PQ load

$$\begin{aligned} T_G G_L|_{(t+\Delta t)} &= z_{c1}|_t + h\,(P_0 - G_L V^2)|_{(t+\Delta t)} \\ T_B B_L|_{(t+\Delta t)} &= z_{c2}|_t + h\,(Q_0 - B_L V^2)|_{(t+\Delta t)} \end{aligned} \tag{3.16}$$

with the difference equation constants

$$\begin{aligned} z_{c1}|_t &= T_G G_L|_t + h\,(P_0 - G_L V^2)|_t \\ z_{c2}|_t &= T_B B_L|_t + h\,(Q_0 - B_L V^2)|_t \end{aligned}$$

2. Generating plant:

(a) Synchronous generator

$$\begin{aligned} M\,\omega|_{(t+\Delta t)} &= z_{g1}|_t + h\,(T_m - T_e - D\,\omega)\,|_{(t+\Delta t)} \\ \delta|_{(t+\Delta t)} &= z_{g2}|_t + h\,\omega_b\,(\omega - 1.0)|_{(t+\Delta t)} \\ T_{do}^{'}\,E_q^{'}|_{(t+\Delta t)} &= z_{g3}|_t + h\,[-E_q^{'} - (x_d - x_d^{'})\,I_d + E_{FD}]|_{(t+\Delta t)} \\ T_{do}^{''}\,(E_q^{''} - E_q^{'})|_{(t+\Delta t)} &= z_{g4}|_t + h\,[-E_q^{''} - (x_d^{'} - x_d^{''})\,I_d + E_q^{'}]|_{(t+\Delta t)} \\ T_{qo}^{''}\,E_d^{''}|_{(t+\Delta t)} &= z_{g5}|_t + h\,[-E_d^{''} + (x_q - x_q^{''})\,I_q]|_{(t+\Delta t)} \end{aligned} \tag{3.17}$$

with the difference equation constants

$$\begin{aligned} z_{g1}|_t &= M\,\omega|_t + h\,(T_m - T_e - D\,\omega)\,|_t \\ z_{g2}|_t &= \delta|_t + h\,\omega_b\,(\omega - 1.0)|_t \\ z_{g3}|_t &= T_{do}^{'}\,E_q^{'}|_t + h\,[-E_q^{'} - (x_d - x_d^{'})\,I_d + E_{FD}]|_t \\ z_{g4}|_t &= T_{do}^{''}\,(E_q^{''} - E_q^{'})|_t + h\,[-E_q^{''} - (x_d^{'} - x_d^{''})\,I_d + E_q^{'}]|_t \\ z_{g5}|_t &= T_{qo}^{''}\,E_d^{''}|_t + h\,[-E_d^{''} + (x_q - x_q^{''})\,I_q]|_t \end{aligned}$$

(b) Field excitation system

$$T_A\, E_{FD}|_{(t+\Delta t)} = z_e|_t + h\,[-E_{FD} + E_{FD0} + K_A\,(U_E + V_{REF} - V_t)]|_{(t+\Delta t)} \tag{3.18}$$

with the difference equation constant

$$z_e|_t = T_A\, E_{FD}|_t + h\,[-E_{FD} + E_{FD0} + K_A\,(U_E + V_{REF} - V_t)]|_t$$

(c) Mechanical–hydraulic governor and hydro turbine

$$\begin{aligned}
T_p\, G_1|_{(t+\Delta t)} &= z_{h1}|_t + h\,[-\sigma\, G_1 + U_G + \omega_{REF} - \omega - G_2]|_{(t+\Delta t)} \\
(T_r\, G_2 - \delta_T\, T_r\, G_1)|_{(t+\Delta t)} &= z_{h2}|_t - h\, G_2|_{(t+\Delta t)} \\
T_g\, G_3|_{(t+\Delta t)} &= z_{h3}|_t + h\,(-G_3 + G_1)|_{(t+\Delta t)} \\
(0.5\, T_w\, T_m + T_w\, G_3)|_{(t+\Delta t)} &= z_{h4}|_t + h\,(-T_m + C_g G_3 + G_0)|_{(t+\Delta t)}
\end{aligned} \tag{3.19}$$

with the difference equation constants

$$\begin{aligned}
z_{h1}|_t &= T_p\, G_1|_t + h\,[-\sigma\, G_1 + U_G + \omega_{REF} - \omega - G_2]|_t \\
z_{h2}|_t &= (T_r\, G_2 - \delta_T\, T_r\, G_1)|_t - h\, G_2|_t \\
z_{h3}|_t &= T_g\, G_3|_t + h\,(-G_3 + G_1)|_t \\
z_{h4}|_t &= (0.5\, T_w\, T_m + T_w\, G_3)|_t + h\,(-T_m + C_g G_3 + G_0)|_t
\end{aligned}$$

(d) Electrical–hydraulic governor and steam turbine

$$\begin{aligned}
T_{sm}\, G|_{(t+\Delta t)} &= z_{s1}|_t + h\,[-G + K_g\,(U_G + \omega_{REF} - \omega)]|_{(t+\Delta t)} \\
T_{CH}\, T_m|_{(t+\Delta t)} &= z_{s2}|_t + h\,(-T_m + C_g G + G_0)|_{(t+\Delta t)}
\end{aligned} \tag{3.20}$$

with the difference equation constants

$$\begin{aligned}
z_{s1}|_t &= T_{sm}\, G|_t + h\,[-G + K_g\,(U_G + \omega_{REF} - \omega)]|_t \\
z_{s2}|_t &= T_{CH}\, T_m|_t + h\,(-T_m + C_g G + G_0)|_t
\end{aligned}$$

(e) Power system stabilizer

$$
\begin{aligned}
T_s(S_1+\omega)|_{(t+\Delta t)} &= z_{p1}|_t - h\,S_1|_{(t+\Delta t)} \\
(T_{2s}S_2 - K_c T_{1s}S_1)|_{(t+\Delta t)} &= z_{p2}|_t + h\,(-S_2+K_c S_1)|_{(t+\Delta t)} \\
(T_{2s}U_E - T_{1s}S_2)|_{(t+\Delta t)} &= z_{p3}|_t + h\,(-U_E+S_2)|_{(t+\Delta t)}
\end{aligned}
\tag{3.21}
$$

with the difference equation constants

$$
\begin{aligned}
z_{p1}|_t &= T_s(S_1+\omega)|_t - h\,S_1|_t \\
z_{p2}|_t &= (T_{2s}S_2 - K_c T_{1s}S_1)|_t + h\,(-S_2+K_c S_1)|_t \\
z_{p3}|_t &= (T_{2s}U_E - T_{1s}S_2)|_t + h\,(-U_E+S_2)|_t
\end{aligned}
$$

3. Control devices

(a) Static VAR compensator

$$
\begin{aligned}
T_b B_1|_{(t+\Delta t)} &= z_{v1}|_t + h\,[-B_1 + K_b(V_{REF} - V_t)]|_{(t+\Delta t)} \\
(T_{2b}B_2 - T_{1b}B_1)|_{(t+\Delta t)} &= z_{v2}|_t + h\,[-B_2 + B_1]|_{(t+\Delta t)}
\end{aligned}
\tag{3.22}
$$

with the difference equation constants

$$
\begin{aligned}
z_{v1}|_t &= T_b B_1|_t + h\,[-B_1 + K_b(V_{REF} - V_t)]|_t \\
z_{v2}|_t &= (T_{2b}B_2 - T_{1b}B_1)|_t + h\,[-B_2 + B_1]|_t
\end{aligned}
$$

In the above difference equations, the difference equation constants, z's, are known at time t and the values of state variables $(\mathbf{x}, \mathbf{y})$ at time $(t+\Delta t)$ are to be solved.

Finally, with some manipulations of equations (3.15) – (3.22), the overall system difference equations may be written in a compact form as

$$
\mathbf{X}_{t+\Delta t} = \mathbf{Z}_t + \frac{\Delta t}{2}\mathbf{H}(\mathbf{X}_{t+\Delta t}, \mathbf{Y}_{t+\Delta t}, \mathbf{D}_t) \tag{3.23}
$$

where Δt is the integration step size and $\mathbf{D}_t$ is determined at time t and assumed not to change during $(t, t+\Delta t)$. With $\mathbf{X}_t$, $\mathbf{Y}_t$, $\mathbf{D}_t$ and $\mathbf{H}(\mathbf{X}_t, \mathbf{Y}_t, \mathbf{D}_t)$ known at time t, the difference equation constant vector $\mathbf{Z}_t$ is defined as

$$
\mathbf{Z}_t = \mathbf{X}_t + \frac{\Delta t}{2}\mathbf{H}(\mathbf{X}_t, \mathbf{Y}_t, \mathbf{D}_t) \tag{3.24}
$$

Therefore, for a system solution $(\mathbf{X}_{\mathrm{t}}, \mathbf{Y}_{\mathrm{t}})$ at time t and a chosen integration step size Δt, equation (3.23) together with discretized system algebraic equation (3.6) forms the simultaneous implicit integration algorithm based on the trapezoidal rule for the system equations (3.5) and (3.6)

$$\mathbf{X}_{t+\Delta t} - \frac{\Delta t}{2}\mathbf{H}(\mathbf{X}_{t+\Delta t}, \mathbf{Y}_{t+\Delta t}, \mathbf{D}_t) - \mathbf{Z}_t = \mathbf{0} \tag{3.25}$$

$$\mathbf{G}(\mathbf{X}_{t+\Delta t}, \mathbf{Y}_{t+\Delta t}, \mathbf{D}_t) = \mathbf{0} \tag{3.26}$$

These are nonlinear algebraic equations and can be solved for $(\mathbf{X}_{t+\Delta t}, \mathbf{Y}_{t+\Delta t})$ by Newton–Raphson's method.

3.3 Power System Simulation Program

Based on the simultaneous implicit integration method described in the previous section, a comprehensive power system simulation program is developed in this section for system voltage stability studies. The program consists of the following major functions.

1. System data input and pre–processing
2. Load flow and initial system condition
3. Selection of system contingencies
4. System state monitoring, recording and control logics
5. Topology change and new initial system values
6. System equation integration and variable constraints
7. Step size control and exact timing
8. System data output

The program is very involved since it has to deal with various types of load and reactive power component models, nonlinear constraints and logics, such as generator rotor overheat protection, etc.. Some details of the simulation program are presented as follows.

3.3.1 Load Flow Calculation

For the dynamic system simulation studies of a power system, a load flow is required to determine the initial steady state values of the system. For that, the initial system generation and loading conditions must be specified. With a load flow, all initial system state values $(\mathbf{X_0}\,\mathbf{Y_0})$ can be determned.

In a load flow, generator buses are usually specified as PV buses, while load buses as PQ buses. However, the power and reactive power drawn by a dynamic load may be a function of its terminal voltage and other state variables which can not be specified a priori. For example, the power and reactive power drawn by an induction motor in steady state are determined by equation (2.5), which are functions of not only motor terminal voltage V but also the motor slip s. In order to determine load power and reactive power, the steady state equations of the load must be included in load flow. Since most loads are also nonlinear, their effects must be reflected in the following load flow Jacobian equation.

$$\begin{bmatrix} \mathbf{\Delta P(\Theta, V)} \\ \mathbf{\Delta Q(\Theta, V)} \end{bmatrix} = [\mathbf{J_{LF}}] \begin{bmatrix} \mathbf{\Delta\Theta} \\ \mathbf{\Delta V} \end{bmatrix} \tag{3.27}$$

where $\mathbf{\Delta P}$ and $\mathbf{\Delta Q}$ are power and reactive power mismatch functions, $\mathbf{\Theta}$ and $\mathbf{V}$ are respectively the angle and magnitude of system bus voltage, and $\mathbf{J_{LF}}$ is the corresponding load flow Jacobian matrix.

There are two different methods in dealing with the load flow equations with nonlinear loads, the sequential method and the unified method [38]. By the former, the steady state equations of the load are solved separately in each iteration. The nonlinear effect of the load is included only in the power mismatch equations, but not in the system Jacobian matrix, which may reslut in possible convergence problems. By the united method, the idea is to add the load variables, such as motor slip, into the solution vector. It amounts to an extension of a very large load flow Jacobian matrix, which is obviously inconvenient.

In this thesis, a new method is devised to overcome these difficulties, all extra load variables, such as motor slip, are eliminated from the load equations first, and then both power and reactive power drawn by the load and their derivatives with respect to load terminal voltage are computed, which may be done numerically if necessary. The load nonlinearity can then be included in both power mismatch equations and in load flow Jacobian matrix without variable extensions.

For a static load, the load power and reactive power may be directly expressed as functions of the terminal voltage, such as equations (2.6) and (2.7). The calculations of load power, reactive power and their derivatives with respect to terminal voltage are straightforward.

For a dynamic load, variable elimination may be involved. For example, the steady state operating condition of an induction motor load is determined by the equations (2.5) which is rewritten as follows.

$$T_L = T_E = f_E(s, \mathbf{p})\, V^2 \tag{3.28}$$

$$P_m = f_P(s, \mathbf{p})\, V^2 \tag{3.29}$$

$$Q_m = f_Q(s, \mathbf{p})\, V^2 \tag{3.30}$$

With T_L specified, the motor slip s can be eliminated by solving it from equation (3.28) and substituting the result into equations (3.29) and (3.30). Thus, the power P_m and reactive power Q_m determined by the terminal voltage V can be included in the power mismatch equations. The derivatives of power and reactive power with respect to voltage can be computed by

$$\frac{dP_m}{dV} = \frac{df_P(s,\mathbf{p})}{ds}\frac{ds}{dV}V^2 + 2Vf_P(s,\mathbf{p}) \tag{3.31}$$

$$\frac{dQ_m}{dV} = \frac{df_Q(s,\mathbf{p})}{ds}\frac{ds}{dV}V^2 + 2Vf_Q(s,\mathbf{p}) \tag{3.32}$$

where $\frac{ds}{dV}$ can be obtained by differentiating equation (3.28) with respect to V as

$$0 = \frac{df_E(s,\mathbf{p})}{ds}\frac{ds}{dV}V^2 + 2\,V\,f_E(s,\mathbf{p}) \tag{3.33}$$

or

$$\frac{ds}{dV} = -2\,f_E(s,\mathbf{p})\,/\,(\frac{df_E(s,\mathbf{p})}{ds}\,V) \tag{3.34}$$

Therefore, with load flow Jacobian matrix modified by equations (3.31) and (3.32), the nonlinearity of the load has been fully included in the load flow.

3.3.2 Solution of System Jacobian Equations

The major task of solving the nonlinear system equations (3.25) and (3.26) by Newton Raphson's method is to solve the corresponding system Jacobian matrix equation

$$\mathbf{\Delta R} = \mathbf{J_S}\,\mathbf{\Delta S} \tag{3.35}$$

where $\mathbf{\Delta R}$ is the function residue vector, $\mathbf{\Delta S}$ is the system state variable deviation vector and $\mathbf{J_S}$ the system Jacobian matrix. $\mathbf{\Delta R}$ has the form of $\mathbf{\Delta R} = [\mathbf{\Delta F}\ \ \mathbf{\Delta I}]^{\mathbf{T}}$ with $\mathbf{\Delta F}$ for the function residue vector of all system components but the system network equations, and $\mathbf{\Delta I}$ for those of system network equations. $\mathbf{\Delta S}$ has the form of $\mathbf{\Delta S} = [\mathbf{\Delta X}\ \ \mathbf{\Delta V}]^{\mathbf{T}}$ with $\mathbf{\Delta X}$ for the vector of all system non–terminal–voltage variable deviations and $\mathbf{\Delta V}$ for the system terminal–voltage deviations.

For a multi–machine power system with nonlinear load and control dynamics, the order of Jacobian matrix equation (3.35) is usually very high. For instance, it has more than two hundred variables for a nine machine power system used in this thesis project. Therefore, the direct formulation and solution of the Jacobian matrix equation are both heavy memory demanding and very time consuming.

Although the order of the Jacobian matrix may be reduced by eliminating some system variables from equation (3.25) using the existing relations, this amounts to have a new model for the original system. It will be very complicated in dealing with original component model changes during integration.

To save the computation in solving the Jacobian matrix equation (3.35) yet to keep the original system component models, a new and systematic method is developed in this thesis. It consists of two steps, a forward elimination and a backward substitution. In the forward elimination step, all system non–terminal–voltage variable deviations are eliminated and the result is used to modify the sub–Jacobian matrix corresponding to the transmission network equations. All system terminal–voltage deviations are then solved. In the backward substitution step, the terminal-voltage deviations are back substituted and all non–terminal–voltage variable deviations are then obtained. Both forward elimination and backward substitution are designed in such a way that the system components are arranged in a definite order and processed systematically one after another.

In this method, the system buses are ordered in such a way that the N_g generator buses come first, followed by N_m induction motor buses, and then N_s SVC buses, followed by N_l nonlinear load buses. Any other different types of components can be easily grouped and added in similar way. As an illustration example, a power system with $N_g = 2$ generator buses and $N_m = 2$ motor buses is considered. The system Jacobian matrix equation may then have the form as in Figure 3.4.

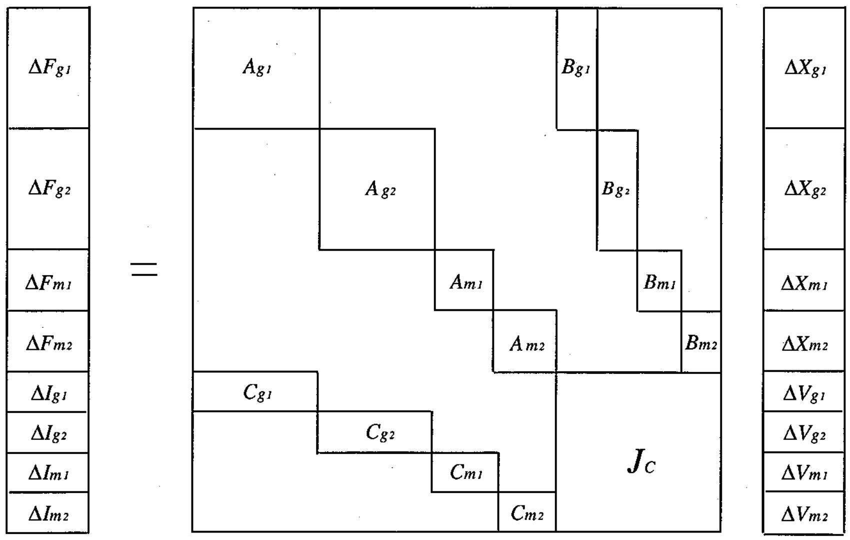

Figure 3.4: An Example of System Jacobian Matrix Equation

where ΔX_{gi} denotes the non–terminal–voltage variable deviation vector for the ith generator, and ΔX_{mi} that for the ith motor. ΔV_{gi} and ΔV_{mi} are the corresponding terminal–voltage deviations vectors. While ΔF_i is the residue function vector of generator or motor equations, ΔI_i is residue function vector of the network equations. Finally, A_i, B_i, C_i, and J_c are corresponding sub–Jacobian matrices.

Forward Elimination

Referring to Figure 3.4, the residue function vector ΔF_i of the ith system component and the residue current vector ΔI_i of the corresponding network equations may be written as

$$\Delta F_i = A_i \Delta X_i + B_i \Delta V_i \tag{3.36}$$

$$\Delta I_i = C_i \Delta X_i + J_{ci} \mathbf{\Delta V} \tag{3.37}$$

where J_{ci} is the ith row sub–matrix of J_c and $\mathbf{\Delta V}$ is the vector of all system bus terminal voltage deviations, including ΔV_i.

Next, the ith component of the non–terminal–voltage deviation vector, ΔX_i, can be eliminated by solving it from equation (3.36) and substituting the result into equation (3.37) resulting in

$$\Delta I_i' = J_{ci}\,\mathbf{\Delta V} - C_i A_i^{-1} B_i \Delta V_i \tag{3.38}$$

where

$$\Delta I_i' = \Delta I_i - C_i A_i^{-1} \Delta F_i$$

With equation (3.38), J_{ci} is then modified by subtracting $C_i A_i^{-1} B_i$ from the ith element of J_{ci}.

Finally, when all system components have been processed one by one in the same way as described above, the sub–Jacobian matrix J_c is modified and all system bus voltage deviations can then be solved through the following matrix equation, which finishes the forward elimination process.

$$\mathbf{\Delta I}' = \mathbf{J}_{\mathbf{c}}' \mathbf{\Delta V} \tag{3.39}$$

where $\mathbf{\Delta I}'$ is the vector with $\Delta I_i'$ as its elements, and $\mathbf{J}_{\mathbf{c}}'$ is the modified matrix of sub–Jacobian matrix J_c.

Backward Substitution

Once the system bus voltage deviation $\mathbf{\Delta V}$ is obtained through forward elimination, the non–terminal–voltage variable deviation of the ith system component ΔX_i can be solved by substituting ΔV_i back into the component equation (3.36), which gives

$$\Delta X_i = A_i^{-1}(\Delta F_i - B_i \Delta V_i) \tag{3.40}$$

When all system components have been processed one by one in the same substitution procedure, the whole system Jacobian matrix equation (3.35) is finally solved.

With this forward elimination and backward substitution procedure, the system Jacobian matrix equation can be solved systematically and efficiently. There are three advantages. Firstly, since the form of all system component equations remains unchanged, the tedious work involved in equation reductions is then avoided. As a result, it is very straightforward in dealing with changes in component equations. In addition, since all system components are handled in the same way, it is very easy to add or remove components to or from the system. Secondly, since system components are processed one at a time, the highest order of the matrix involved in the forward elimination and backward substitution is the highest order among J_c and A_i ($i = 1, 2, \cdots, N_c$) where N_c is the total number of system components. To reduce the order of the sub-Jacobian matrix J_c, the system buses with constant impedance loads and fixed capacitor banks can be eliminated by lumping the corresponding equivalent admittance of the components into the diagonal elements of the respective submatrix of the system admittance matrix $\mathbf{Y_N}$. Finally, since matrices A_i's and J_c are usually sparse, triangular factorization technique can be used to save computation associated with forward elimination and backward substitution procedures.

3.3.3 Integration Step Size Control and Exact Timing

Power system equations (3.5) and (3.6) may have wide–ranged values of time constants associated with the system dynamics. For example, a generator sub–transient may involve a time constant of a small fraction of a second, while a time constant associated with load dynamics may be several minutes. Small time constants determine the fast system transients while large time constants dominate the slow system dynamics. For system problems like voltage instability phenomenon involving both fast transients and slow system dynamics, a too large integration step size may result in poor accuracy for fast transients, while a too small step size may result in excessive computation for the slow dynamics. Therefore, to take care of both small and large time constants of the system, a step size control procedure is imperatively needed for the system integration.

In an implicit integration method, the solutions of differential equations are approximated by those of the corresponding difference equations of finite order. For example, the original system differential equation (3.5) is approximated by the difference equation (3.25). The approximation is made by truncating the higher order terms of the difference equations. The error of the approximation introduced in a single integration step is called the local truncation error e_{LT}. It is shown in [43] that the relationship between local truncation error and integration step size can be expressed as

$$e_{LT} \approx C \frac{d^{(p+1)}x}{dt^{(p+1)}} \Delta t^{p+1} \tag{3.41}$$

where p is the order of the numerical integration method, for example, $p = 2$ for integration algorithm based on trapezoidal rule, Δt is the integration step size, C is a constant which depends on the system equation and the integration method being used, and x is the solution of the system equation.

The basic idea of step size control is to keep the local truncation error e_{LT} within the tolerance limit while maximizing the integration step size Δt.

Computation of e_{LT} from equation (3.41) requires information regarding the order of the method p, the constant C, and the $(p+1)$th derivative of x. In this thesis, instead of computing the $(p+1)$th derivative of x by extrapolation with a polynomial of degree $p+1$, an alternative approach, the step doubling approach, described in [40] is used to estimate the local truncation error. This method involves integrating the system equations by taking two steps of step size Δt and reintegrating over the same interval with a single step of length $2\Delta t$. With these solutions, the local truncation error e_{LT} can be estimated as follows.

Let x_s be the solution by taking two single steps, x_d the solution by taking a double step, and x_t the corresponding true solution which is unknown. We have the following equations

$$x_s = x_t + 2\,e_{LTs} \tag{3.42}$$

$$x_d = x_t + e_{LTd} \tag{3.43}$$

where e_{LTs} and e_{LTd} are local truncation errors of single step and double step integrations, respectively, which, from the equation (3.41), are given by

$$\begin{aligned} e_{LTs} &= C\,\frac{d^{(p+1)}x}{dt^{(p+1)}}\,\Delta t^{\,p+1} \\ e_{LTd} &= C\,\frac{d^{(p+1)}x}{dt^{(p+1)}}\,(2\,\Delta t)^{p+1} \end{aligned}$$

Subtracting (3.42) from (3.43), we get

$$\begin{aligned} x_d - x_s &= e_{LTd} - 2\,e_{LTs} \\ &= C\,\tfrac{d^{(p+1)}x}{dt^{(p+1)}}\,\Delta t^{p+1}(2^{p+1}-2) \\ &= (2^{p+1}-2)e_{LTs} \end{aligned} \tag{3.44}$$

which gives the local truncation error of single step integration

$$e_{LT} = (x_d - x_s)/(2^{p+1}-2) \tag{3.45}$$

From equation (3.45), we can see that computation of e_{LT} by step doubling approach avoids the computation of the derivatives and the knowledge of constant C. Only the order of the integration method needs to be known. On the other hand, step doubling method has an obvious disadvantage. It incurs much more computations because x_s and x_d have to be computed in order to obtain e_{LT}. However, as also indicated in [40], in addition to easy implementation, this method usually gives more reliable and steady result. This means that the changes in step size during integration are more consistent which is also observed in the simulation studies in this thesis. These benefits are nearly sufficient to compensate the extra computation cost.

With the local truncation error e_{LT} available, the integration step size Δt can be so chosen that the e_{LT} satisfies

$$e_{min} \leq e_{LT} \leq e_{max} \tag{3.46}$$

where e_{min} and e_{max} are prescribed lower and upper bounds of local truncation error e_{LT}. If the e_{LT} is within its bounds, the current step size is acceptable and the integration continues with the step size. Otherwise, if the e_{LT} is less than e_{min} or greater than e_{max}, then the step size is doubled or halved. In order to avoid too large or too small step size, Δt is also bounded by its upper and lower limits

$$\Delta t_{min} \leq \Delta t \leq \Delta t_{max} \tag{3.47}$$

Therefore, whenever there is a system change which causes some system variables to vary sharply, a small integration step size must be chosen for accuracy. After fast system transients, the step size will be increased gradually while keeping the local truncation error within the prescribed limits.

Due to the variation in step size during the integration, the simulation may overshoot and miss the exact timing of faulting and clearing, tap changing and rotor overheat protecting, etc.. In the simulation program, the exact timing t_c of an event, is pinpointed by changing the last step size according to

$$\Delta t_{new} = \Delta t_{old} - t + t_c \tag{3.48}$$

and the new step size is then used to re–integrate the last step as shown in Figure 3.5.

3.3.4 System Contingencies

Most system instabilities are caused by system disturbances. Different disturbances occurring at different locations have different impacts on system stability. System disturbances may include system load changes, system network changes, and system generation changes. There may also be single or double contingencies.

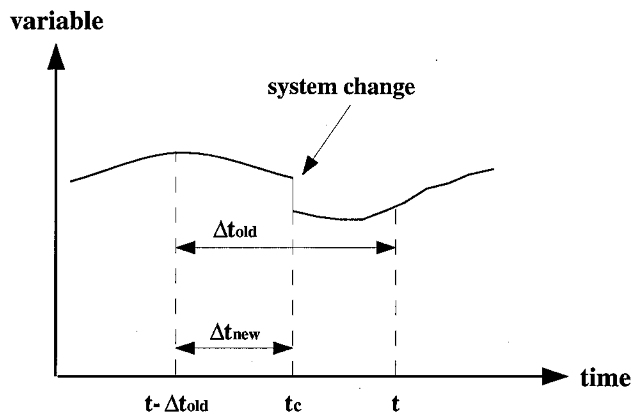

Figure 3.5: Step Size Change for Exact Timing

1. System load changes

   (a) Step change in power and reactive power of a nonlinear PQ load.

   (b) Step change in load torque of an induction motor.

   (c) Gradual inrease in system load.

2. System network changes

   (a) opening of a transmission line

   (b) tripping of a transformer.

   (c) Ground of a system bus.

3. System generation changes

   (a) Tripping of a generator.

   (b) Switching–in or –out of a capacitor.

Whenever there is an sudden change in system topology, system variables **Y** will change instantly since the fast electromagnetic transients in transmission network are neglected. Although the differential variables $\mathbf{X}$ remain unchanged, system equation (3.5) and (3.6) must be solved at that time instant in order to find new initial value of $\mathbf{Y}$ for the next step integration.

3.3.5 Flowchart of System Simulation Program

The complete system simulation program may be recapitulated by an overall flowchart as shown in Figure 3.6.

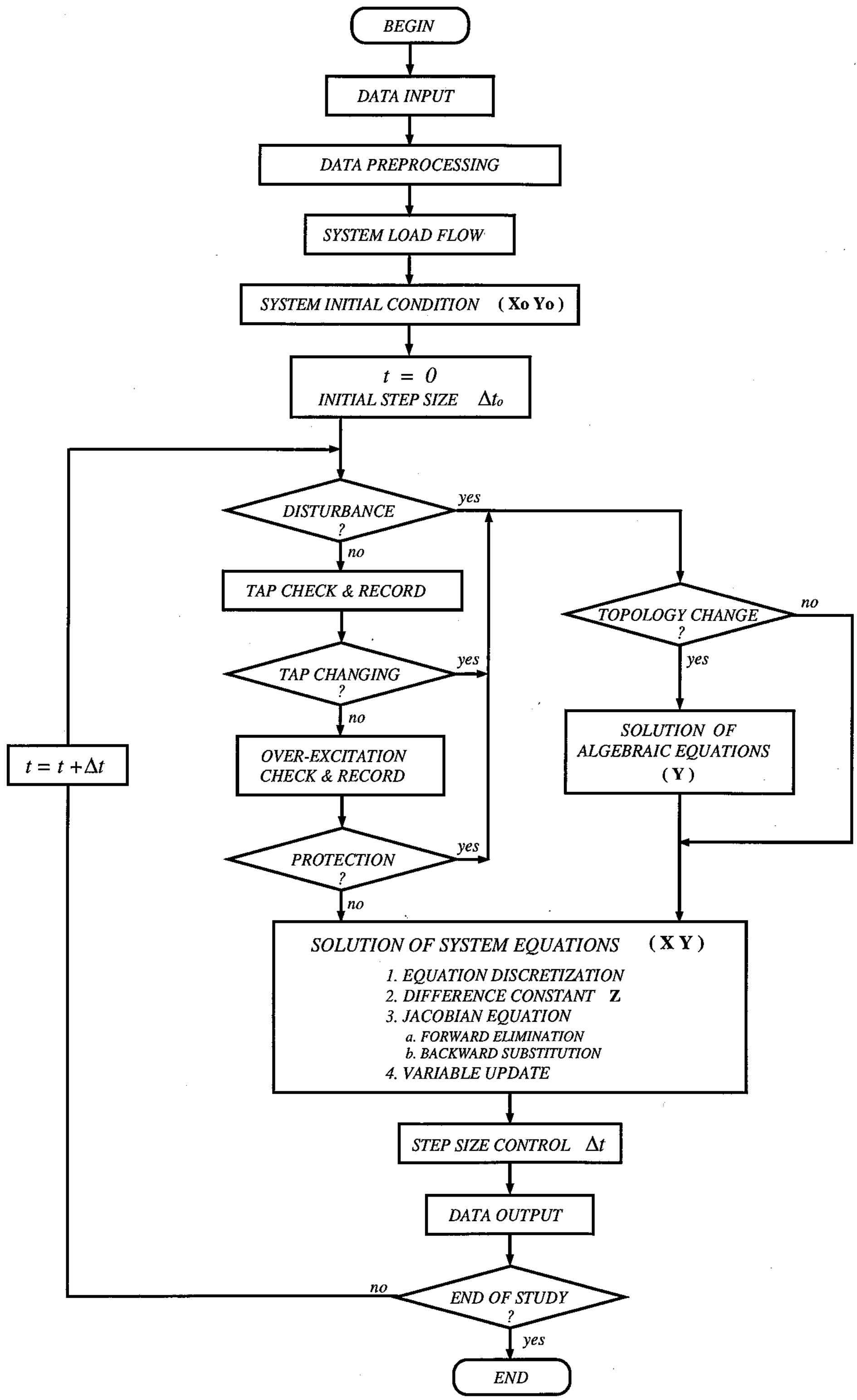

Figure 3.6: Overall Flowchart of System Simulation Program

Chapter 4

DYNAMIC VOLTAGE STABILITY STUDIES

Voltage stability studies have been concentrated on the determination of maximum loading limit (MLL) of a power system based on load flow related analysis. When the system loading reaches its MLL determined by conventional load flow, the load flow Jacobian will become singular, which indicates a possible voltage collapse. Such defined MLL may be referred to as static voltage stability limit. Thus, the distance between current system loading condition and the MLL can then be used as an index to measure the degree of system voltage stability. However, when the MLL is determined through load flow analysis, system dynamics are not included. As a result, it may not lead to a realistic solution due to the harmful or favorable system dynamics. Moreover, even if an exact MLL could be found, it can only tell a system loading condition where a possible voltage collapse may occur. It can not provide any information of how system voltage approaches the collapse point and how this collapse point is affected by system dynamics.

Therefore, the evaluation of system MLL and clarification of voltage collapse mechanism require a detailed system dynamic simulation which may take into account the effects of all system dynamics on voltage stability. It is believed that the unfavored dynamic interactions among system components play a key role in the process of voltage deterioration and collapse. With system models described in Chapter 2 and time domain simulation technique developed in Chapter 3, the effects of load and control dynamics on voltage collapse process can be better investigated by dynamic simulation of a sample power system.

In this chapter, a 21 bus sample power system with basic system data is presented in Section 4.1. Critical system load buses are defined and identified in Section 4.2 based on bus voltage–reactive power sensitivity analysis. Following that, the effects of different system loads on voltage stability are investigated in Section 4.3, and system control effects in Section 4.4. Finally, the results of system maximum loading limit (MLL) from load flow and those from dynamic simulation are compared and discussed in Section 4.5.

4.1 A Sample Power System for Voltage Stability Studies

4.1.1 A 21 Bus Sample Power System

A sample power system with 21 buses and 23 branches of transmission system is shown in Figure 4.1. The system has 9 generating plants, two of them at buses 4 and 9 are hydro–electric, and the others are steam–electric. There are 11 load buses with a VAR compensation at bus 21. The system is connected to an infinite system through line $11 - 1$.

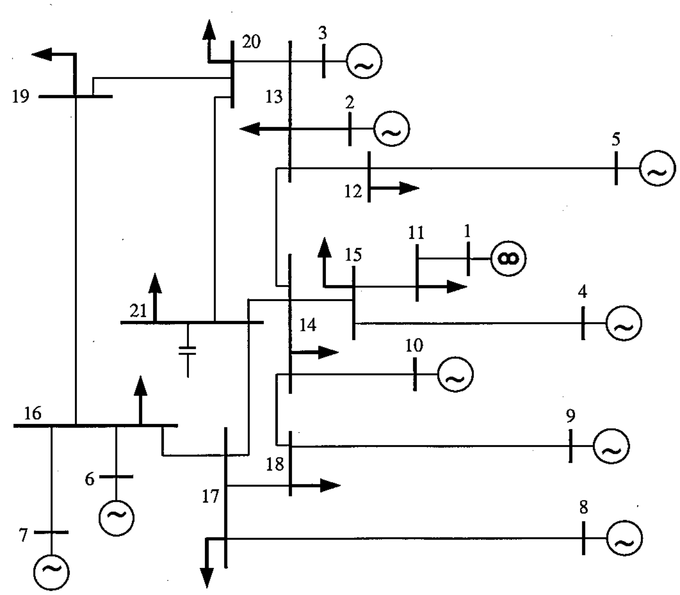

Figure 4.1: A Sample Power System under Study

4.1.2 Basic System Data

The basic system data for the transmission system, the generating plants and a specified system generation and loading condition are given as follows. The data for typical system loads and system control devices are given in the subsequent sections. All data are in per unit unless otherwise specified.

A. Transmission System

Table 4.1: Data of Transmission System

Line	*Bus I*	*Bus J*	*Resistance(R)*	*Reactance(X)*
1	2	13	0.0000	0.0590
2	3	13	0.0000	0.0135
3	5	12	0.0000	0.2900
4	12	13	0.0068	0.0680
5	6	16	0.0000	0.0500
6	16	19	0.0300	0.3000
7	7	16	0.0000	0.1000
8	16	17	0.0015	0.0145
9	19	20	0.0106	0.1060
10	20	21	0.0240	0.2400
11	21	17	0.0161	0.1610
12	21	14	0.0025	0.0250
13	13	14	0.0120	0.1200
14	13	20	0.0048	0.0480
15	14	15	0.0070	0.0700
16	15	4	0.0200	0.2320
17	15	11	0.0070	0.0700
18	14	10	0.0120	0.1200
19	14	18	0.0102	0.1020
20	18	9	0.0000	0.2800
21	17	18	0.0057	0.0570
22	17	8	0.0320	0.3200
23	11	1	0.0000	0.0320

The impedances of transformers in the transmission system are combined with those of transmission lines. All line capacitances are ignored.

B. Given System Generation and Loading Condition

Table 4.2: Data of Generator PV and Load PQ

PV Bus			*PQ Bus*		
Bus	P_{gen}	V_{gen}	*Bus*	P_{load}	Q_{load}
2	3.000	1.040	11	2.500	0.200
3	3.500	1.035	12	1.500	0.100
4	2.000	1.030	13	2.400	0.200
5	1.000	1.035	14	4.500	0.500
6	2.500	1.040	16	3.500	0.200
7	2.500	1.040	17	2.000	0.200
8	2.000	1.010	18	2.000	0.000
9	2.000	1.015	19	1.500	0.100
10	3.500	1.060	21	3.500	−1.700
Slack Bus: V_1=1.060			*Bus* 15, 20: *No Load*		

For different system loading conditions, generator voltages may be adjusted for a normal system voltage profile. The power balance is taken care by the infinite system.

C. Generating Plant

Synchronous Generators

Table 4.3: Data of Generator Parameters

Bus	x_d	x_q	x_d'	x_d''	x_q''	M	D	T_{do}'	T_{do}''	T_{qo}''
2	0.700	0.700	0.120	0.098	0.098	25.000	0.050	7.000	0.091	0.455
3	0.600	0.600	0.100	0.084	0.084	30.000	0.050	7.000	0.091	0.455
4	0.500	0.400	0.150	0.070	0.070	20.000	0.050	8.000	0.104	0.520
5	1.600	1.600	0.230	0.224	0.224	12.800	0.050	7.000	0.091	0.455
6	0.950	0.950	0.150	0.133	0.133	19.800	0.050	7.000	0.091	0.455
7	0.950	0.950	0.150	0.133	0.133	19.800	0.050	7.000	0.091	0.455
8	1.000	1.000	0.170	0.140	0.140	18.000	0.050	7.000	0.091	0.455
9	1.000	1.000	0.170	0.140	0.140	18.000	0.050	7.000	0.091	0.455
10	0.390	0.320	0.060	0.055	0.055	32.000	0.050	6.000	0.078	0.390

where M, T'_{do}, T''_{do}, and T''_{qo} are in seconds.

Field Excitation Systems

The excitation systems for the sample power system may be divided into two groups. Group A has smaller time constants and larger gains, while group B has larger time constants and smaller gains as shown in Table 4.4. The excitation systems of generators at buses 2, 3, 4, 5, 6, and 7 belong to group A, and those at buses 8, 9, and 10 belong to group B.

Table 4.4: Data of Field Excitation System

$Group$	K_A	T_A	E_{min1}	E_{max1}
A	100.00	0.050	−7.000	7.000
B	50.00	0.100	−7.000	7.000

where T_A is in second.

Governor and Turbine Systems

(a) Mechanical–Hydraulic (M–H) Governor and Hydro Turbine System

Table 4.5: Data of M–H Governor and Hydro Turbine

σ	δ_t	T_p	T_r	T_g	T_w
0.050	0.250	0.020	4.800	0.500	1.600
C_g	G_{Smin}	G_{Smax}	G_{Omin}	G_{Omax}	
P_{gen}	−0.100	0.100	0.000	P_{max}	

where T_p, T_r, T_g and T_w are in seconds.

(b) Electrical–Hydraulic (E–H) Governor and Steam Turbine System

Table 4.6: Data of E–H Governor and Steam Turbine

K_g	T_{sm}	T_{CH}	C_g
20.000	0.100	0.400	P_{gen}
G_{Smin}	G_{Smax}	G_{Omin}	G_{Omax}
−0.100	0.100	0.000	P_{max}

where T_{sm} and T_{CH} are in seconds.

In the governor and turbine system data, the interfacing factor C_g has a value of the rated power output P_{gen} of the generator. The maximum gate or valve opening G_{Omax} corresponds to the maximum power output which may be certain percent over the rated power output, for example, P_{max} may be 1.2 times of P_{gen}.

Power System Stabilizers

The power system for the given operating condition is originally unstable in term of system low frequency oscillations. For voltage stability studies, this conventional angle stability problem should be removed from the system. This can be done with the applications of power system stabilizers (PSS's). For the given system operating condition, three power system stabilizers are furnished on the generators at buses 4, 8, and 9 to provide a supplementary excitation control to quench the osillations [44]. The corresponding PSS parameters are given below. For different system loading conditions, these parameters may have to be adjusted so as to give the best damping performance.

Table 4.7: Data of PSS's for Given Operating Condition

Generator Bus	K_C	T_s	T_{1s}	T_{2s}
4	18.057	5.000	0.103	0.035
8	28.271	5.000	0.104	0.035
9	31.352	5.000	0.124	0.035

where T_s, T_{1s} and T_{2s} are in seconds.

4.2 The Critical System Load Buses

4.2.1 Analysis of the System Operating Condition

For the given system operating condition, load flow studies show that the system is highly power stressed. A large amount of power is transferred from some remote generating plants, for instance, at buses 4, 5, 8, 9, and 10, and to some remote loads, such as loads at buses 14, 19, and 21. The long distant power transmission results in a heavy reactive power loss in the transmission lines and transformers. As a matter of fact, all the reactive power supply from generators is consumed in the transmission system, as indicated in Table 4.8. As a result, the large capacity reactive power compensation at bus 21 becomes critical for the system to maintain a nearly normal voltage profile as shown in Table 4.9.

Table 4.8: System Power Generation and Consumption

	Slack Bus	*Generators*	*Compensations*	*Loads*	*Losses*
Power (P)	1.875	22.000	0.000	23.4000	0.475
Reactive Power (Q)	0.969	7.104	1.700	1.500	8.273

Table 4.9: Voltage Profile of the Given System Condition

V_1	V_2	V_3	V_4	V_5	V_6	V_7
1.060	1.040	1.035	1.030	1.035	1.040	1.040
V_8	V_9	V_{10}	V_{11}	V_{12}	V_{13}	V_{14}
1.010	1.015	1.060	1.032	1.008	1.021	0.981
V_{15}	V_{16}	V_{17}	V_{18}	V_{19}	V_{20}	V_{21}
0.994	0.984	0.969	0.956	0.967	0.999	1.004

As a result, the system operation becomes voltage vulnerable due to its critical dependence on the heavy reactive power compensation. This means that system voltage may collapse due to system disturbances that reduce the compensation.

4.2.2 Critical System Load Buses

Critical load buses of the system are identified and used to investigate the effects of load and control dynamics on system voltage stability. The critical system load bus is defined as the bus that is most voltage sensitive among all system load buses. This suggests that the load increase at a critical load bus will have a larger influence on the overall system voltage profile than those at other load buses. More specifically, a load increase at the critical load bus will cause large voltage drops at most system load buses. Therefore, the system voltage profile is more sensitive to the load variations at the critical load bus than those at other system load buses.

For a given system generation and loading condition, the steady state system operation can be characterized by the following nonlinear load flow equations.

$$\mathbf{P}\left(\boldsymbol{\Theta},\mathbf{V}\right) = \mathbf{0} \tag{4.1}$$

$$\mathbf{Q}\left(\boldsymbol{\Theta},\mathbf{V}\right) = \mathbf{0} \tag{4.2}$$

where $\mathbf{P}$ and $\mathbf{Q}$ refer to the power and reactive power mismatch equations, respectively. $\boldsymbol{\Theta}$ and $\mathbf{V}$ represents the angles and magnitudes of system bus voltages, respectively.

The system perturbation equations can be obtained by linearizing the load flow equations (4.1) and (4.2) around the system operating point, which gives

$$\boldsymbol{\Delta}\mathbf{P} = \mathbf{P}_{\Theta}\,\boldsymbol{\Delta\Theta} + \mathbf{P}_{\mathrm{V}}\,\boldsymbol{\Delta}\mathbf{V} \tag{4.3}$$

$$\boldsymbol{\Delta}\mathbf{Q} = \mathbf{Q}_{\Theta}\,\boldsymbol{\Delta\Theta} + \mathbf{Q}_{\mathrm{V}}\,\boldsymbol{\Delta}\mathbf{V} \tag{4.4}$$

which may be written in a single matrix equation with the load flow Jacobian matrix as

$$\mathbf{J_{LF}}\,(\mathbf{\Theta}, \mathbf{V}) = \begin{bmatrix} \mathbf{P_\Theta} & \mathbf{P_V} \\ \mathbf{Q_\Theta} & \mathbf{Q_V} \end{bmatrix}$$

$\mathbf{\Delta\Theta}$ and $\mathbf{\Delta V}$ are respectively the angle and magnitude deviations of system bus voltages due to the bus power and reactive power perturbations of $\mathbf{\Delta P}$ and $\mathbf{\Delta Q}$. The Jacobian matrix $\mathbf{J_{LF}}\,(\mathbf{\Theta}, \mathbf{V})$ is essentially a sensitivity matrix, and the corresponding bus voltage sensitivities can be used to identify the most critical system load bus.

Since there is relatively strong coupling between reactive power and voltage magnitude in power system, the voltage–reactive power sensitivity $[\mathbf{\Delta V}/\mathbf{\Delta Q}]$ is a reasonable index to describe the effects of system loading perturbations on the voltage magnitude. Since the effects of changes in the real power injections on the voltage magnitude is usually very small, the relationship between bus reactive power perturbation $\mathbf{\Delta Q}$ and the bus voltage deviation $\mathbf{\Delta V}$ can be obtained as follows.

Let $\mathbf{\Delta P} = \mathbf{0}$ in Equation (4.3) and solve for $\mathbf{\Delta\Theta}$, which gives

$$\mathbf{\Delta\Theta} = -\mathbf{P_\Theta^{-1}}\,\mathbf{P_V}\,\mathbf{\Delta V} \tag{4.5}$$

Substituting $\mathbf{\Delta\Theta}$ in Equation (4.5) into Equation (4.4) gives

$$\mathbf{\Delta Q} = (\mathbf{Q_V} - \mathbf{Q_\Theta}\,\mathbf{P_\Theta^{-1}}\,\mathbf{P_V})\,\mathbf{\Delta V} \tag{4.6}$$

or

$$\mathbf{\Delta V} = \mathbf{S}\,\mathbf{\Delta Q} \tag{4.7}$$

where

$$\mathbf{S} = [\mathbf{Q_V} - \mathbf{Q_\Theta}\,\mathbf{P_\Theta^{-1}}\,\mathbf{P_V}]^{-1} \tag{4.8}$$

and $\mathbf{S}$ may be referred to as system voltage and reactive power sensitivity matrix.

In Equation (4.7), the element $\mathbf{S}_{ij}$ of matrix $\mathbf{S}$ has a value equal to the voltage deviation ΔV_i at load bus i, due to one per unit change in reactive power $\Delta Q_j = 1$ at load bus j, assuming no load changes at other load buses. From this point, a critical system load bus is defined as the bus which, when having a load increase, will cause large voltage drops at most system buses. On the other hand, a load bus which, when having a load increase, will influence the voltages of only its own or/and a few adjacent buses, is not critical to the overall system voltage profile.

For the given system operating condition of the sample power system, the system voltage and reactive power sensitivity matrix $\mathbf{S}$ calculated from equation (4.8) is shown in Table 4.10. The values in the jth column of the matrix are the voltage deviations at all system load buses due to the per unit change in reactive power at load bus j. The larger the value is, the larger is the influence of the bus j on the corresponding buses. If 1 percent of voltage deviation due to 1 per unit reactive power change is taken as the threshold of large influence, the number of buses whose voltages are largely affected by the change of reactive power at bus j, ($j = 11, 12, \cdots, 21$) are given in Table 4.11.

Table 4.10: System Voltage Sensitivity Matrix

Bus i	$\frac{\Delta V_i}{\Delta Q_{11}}$	$\frac{\Delta V_i}{\Delta Q_{12}}$	$\frac{\Delta V_i}{\Delta Q_{13}}$	$\frac{\Delta V_i}{\Delta Q_{14}}$	$\frac{\Delta V_i}{\Delta Q_{15}}$	$\frac{\Delta V_i}{\Delta Q_{16}}$	$\frac{\Delta V_i}{\Delta Q_{17}}$	$\frac{\Delta V_i}{\Delta Q_{18}}$	$\frac{\Delta V_i}{\Delta Q_{19}}$	$\frac{\Delta V_i}{\Delta Q_{20}}$	$\frac{\Delta V_i}{\Delta Q_{21}}$
11	−0.026	−0.001	−0.001	−0.005	−0.014	−0.001	−0.002	−0.003	−0.002	−0.002	−0.004
12	−0.001	−0.063	−0.008	−0.003	−0.002	−0.001	−0.002	−0.002	−0.005	−0.006	−0.004
13	−0.001	−0.008	−0.010	−0.004	−0.002	−0.001	−0.002	−0.003	−0.006	−0.007	−0.004
14	−0.005	−0.003	−0.004	−0.030	−0.016	−0.007	−0.010	−0.016	−0.011	−0.012	−0.022
15	−0.014	−0.002	−0.002	−0.016	−0.045	−0.004	−0.005	−0.008	−0.006	−0.006	−0.012
16	−0.001	−0.001	−0.001	−0.007	−0.004	−0.026	−0.023	−0.016	−0.011	−0.006	−0.008
17	−0.001	−0.002	−0.002	−0.009	−0.005	−0.022	−0.032	−0.023	−0.011	−0.007	−0.011
18	−0.002	−0.002	−0.002	−0.016	−0.008	−0.016	−0.023	−0.055	−0.011	−0.008	−0.014
19	−0.002	−0.005	−0.006	−0.011	−0.006	−0.012	−0.012	−0.011	−0.110	−0.031	−0.016
20	−0.002	−0.006	−0.007	−0.012	−0.006	−0.006	−0.007	−0.008	−0.031	−0.038	−0.017
21	−0.004	−0.004	−0.005	−0.023	−0.012	−0.008	−0.011	−0.015	−0.016	−0.018	−0.035

Table 4.11: Number of Buses Largely Affected by Bus j

Bus j	11	12	13	14	15	16	17	18	19	20	21
No. of Buses Largely Affected	2	1	1	6	4	4	6	6	7	4	7

According to Table 4.11, the system load buses may be classified into three groups in terms of voltage sensitivity, the strong bus group, buses 11, 12, and 13, which are less system voltage sensitive, the weak bus group, buses 14, 17, 18, 19, and 21 with the most critical buses 19 and 21, which have the largest effects on system voltage profile, and the third group, buses 15, 16, and 20, which have the effects in between.

Since the load and control effects on the system voltage stability can be clearly demonstrated at the system critical buses, and the system voltage profile is largely dependent on the reactive power compensation at bus 21, the load bus 21 is then chosen for subsequent voltage stability studies. Thus, the load at bus 21 will be substituted by a typical load for each case study. The effect of reactive power controls will also be examined at bus 21.

4.3 Effects of System Loads on Voltage Stability

The effects of the system bus loads described in Chapter 2 on the system voltage stability are studied in this section. In the study, a system bus load is represented by a particular type of load, a transformer with on load tap changer, and a distribution link connected to the transmission system bus as in Figure 4.2. The distribution link impedance is included in the transformer model. When the effect of a typical load itself is investigated, the tap changing may not be considered, that is, $\mu = 0$. An induction motor load, an exponential form static load and a persistent PQ load are included in this part of study.

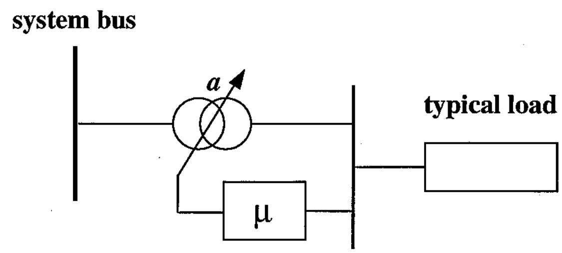

Figure 4.2: A System Bus with Typical Load

4.3.1 Effect of an Induction Motor Load

The basic data of an equivalent induction motor is as follows:

Table 4.12: Data of an Induction Motor Load

H	r_s	x_o	x'	T_o'	T_L
6.700	0.010	4.209	0.142	1.600	2.4

where H and T_o' are in seconds, and the motor load torque T_L may subject to change in different case studies.

With the induction motor load connected at bus 21, the system will have a low voltage profile due to the large reactive power consumed by the motor. To have a system operation with a fairly normal voltage profile, some of the generator voltage references are raised to a higher level and the parameters of the PSS's are adjusted to give the best damping to the system unstable mechanical modes. The system adjustments are as follows.

Table 4.13: Adjusted System Voltage Profile

V_1	V_2	V_3	V_4	V_5	V_6	V_7
1.060	1.040	1.035	1.050	1.035	1.050	1.050
V_8	V_9	V_{10}	V_{11}	V_{12}	V_{13}	V_{14}
1.050	1.050	1.060	1.026	1.004	1.017	0.960
V_{15}	V_{16}	V_{17}	V_{18}	V_{19}	V_{20}	V_{21}
0.984	0.988	0.972	0.960	0.956	0.982	0.966

Table 4.14: Adjusted PSS Parameters

Generator Bus	K_C	T_s	T_{1s}	T_{2s}
4	37.573	5.000	0.080	0.035
8	34.056	5.000	0.128	0.035
9	26.251	5.000	0.121	0.035

Case Study 1: An Induction Motor Near Critical State

In this case study, the induction motor with a constant load torque $T_L = 2.4$ is considered. The motor is connected to bus 21. Other system loads are assumed to be constant impedance loads. Transformer tap changing effect is not considered. The initial system voltage profile is shown in the Table 4.13 and the motor related variables are given in Table 4.15.

Table 4.15: Initial State of the Induction Motor

Terminal Voltage	*Motor Slip*	*Power*	*Reactive Power*
0.965	0.024	2.480	1.404

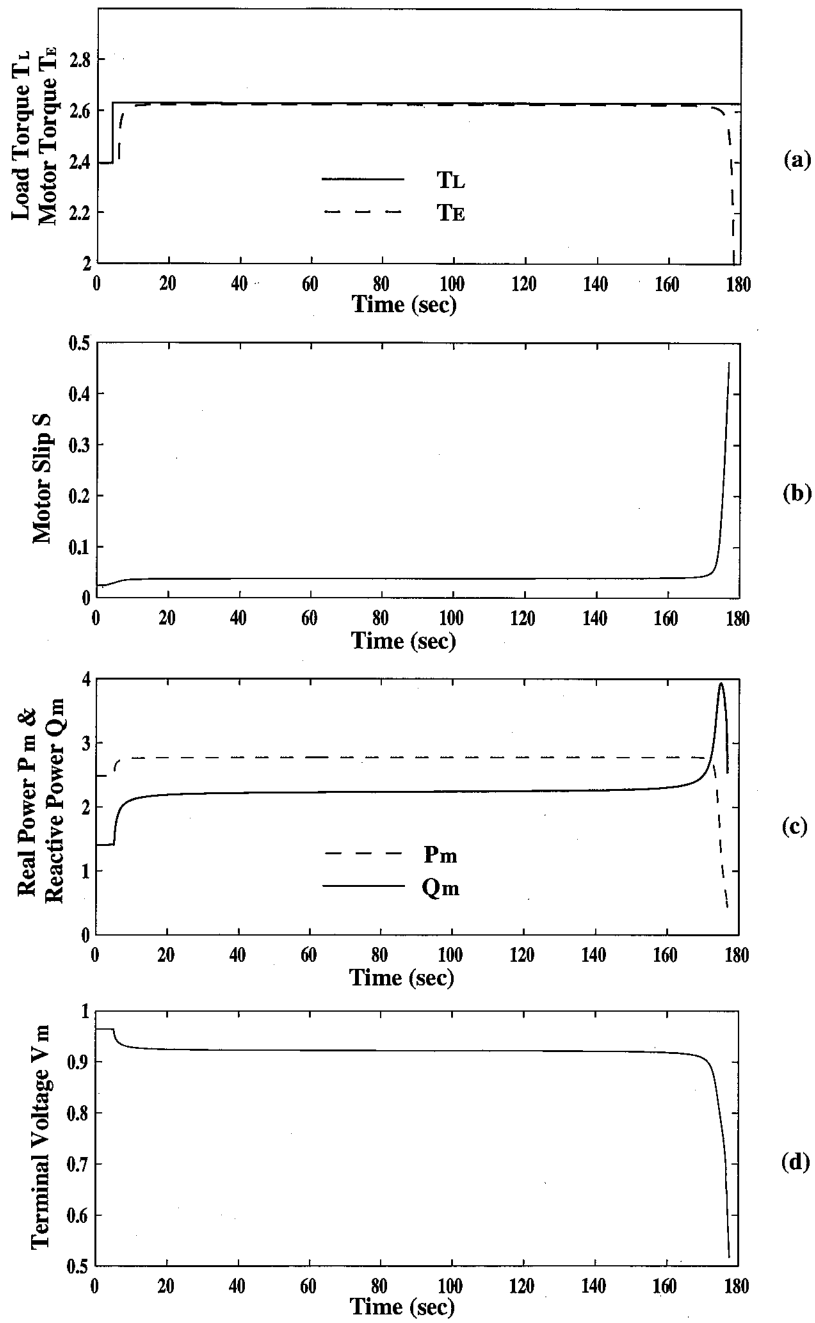

Figure 4.3: Motor Response to Step Change in Load Torque

A step load torque increase of 0.23 is then applied to the motor as a system disturbance. System responses recorded in the figures show a voltage instability phenomenon of slow system dynamics followed by a sudden voltage collapse.

Figure 4.3 shows the dynamic behavior of the induction motor. Following the step increase in load torque at $t = 5$ second as in Figure 4.3a, there is a transient period of about 10 seconds. Following the disturbance, the motor slip begins to increase according to the rotor motion equation (2.1). Both motor power and reactive power drawn from the system increase accordingly to pick up the load. As a result, the larger motor current causes extra voltage drops in the transmission system, leading to a decrease of motor terminal voltage and other system bus voltages as well, as shown in Figure 4.3d and Figure 4.5. During this transient, generator bus voltages are maintained at the same level as those in the pre–disturbance system condition by generator excitation controls as shown in Figure 4.4.

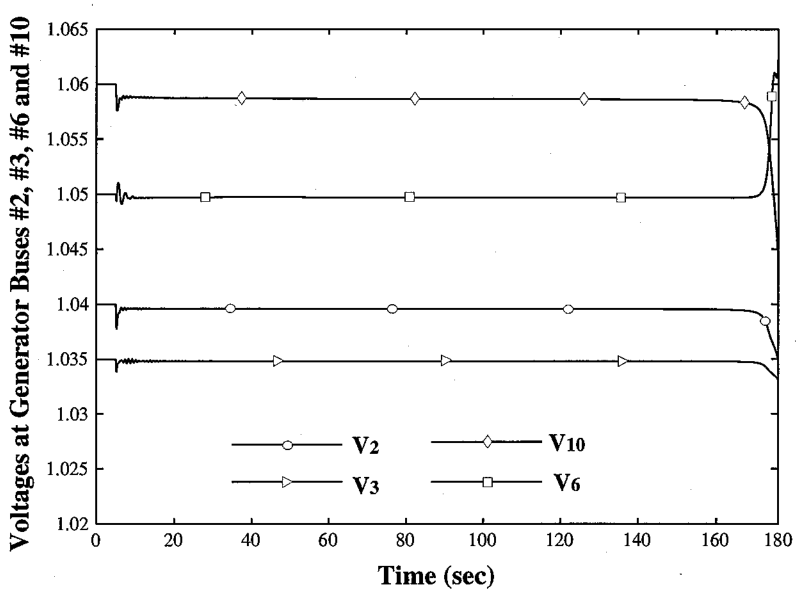

Figure 4.4: Some Generator Bus Voltages

After the transient, the motor slip continues to increase gradually, and the system experiences a rather slow system dynamics, in which the system load bus voltages remain fairly normal, and the system frequency is fixed at 60 Hz, as shown in Figure 4.5 and Figure 4.7. During this slow dynamics, the electromagnetic torque developed by the motor is slightly less than the motor load torque. Motor slip begins to approach its critical value over which the motor will start stalling. At around $t = 105$ second, the motor slip reaches its critical value $S_c \approx 0.038$ with a maximum motor torque $T_E = 2.627$, which is still less than the load torque $T_L = 2.63$. After that, the motor slip continues to increase while the motor developed torque begins to drop. The motor starts stalling. The motor reactive power begins to increase. This causes the motor terminal voltage to dip further, which in turn reduces the motor torque. This interacting dynamics continues until a rapid change occurs at about $t = 170$ second. Due to the fast decreases in motor developed torque shown in Figure 4.3a, the motor slip increase rapidly as shown in Figure 4.3b. Although the motor power drops quickly, its reactive power goes up rapidly as shown in Figure 4.3c. It is this rapid increase of the motor reactive power demand that causes a sharp drop in motor terminal voltage as shown in Figure 4.3d. Other system load buses have similar phenomena, and the results are shown in Figure 4.5, in which only voltages at load buses 13, 16, and 21 are shown for the sake of clarity.

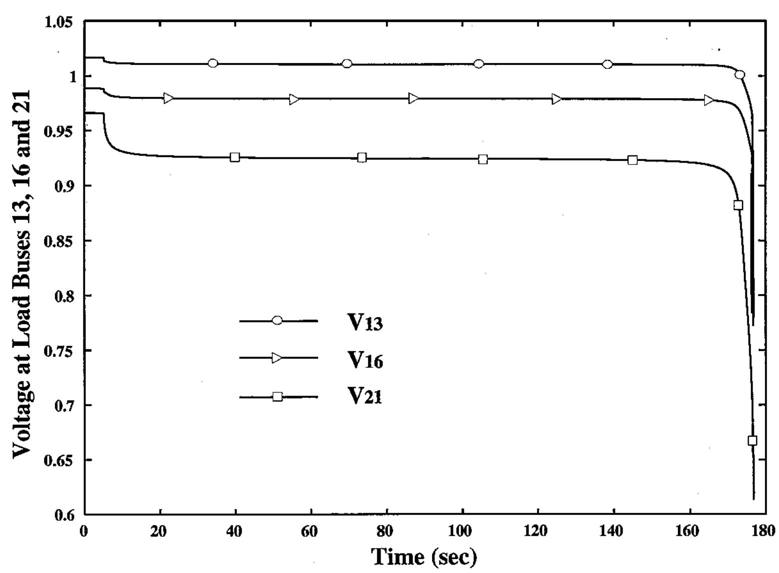

Figure 4.5: System Voltages at Some Load Buses

At about $t = 175$ second, the motor reactive power begins to decrease but the motor terminal voltage continues to drop. This means that the system operation has reached the lower part of Q–V curve of motor terminal bus as shown in Figure 4.6. The system loses voltage control at motor terminal bus after $t = 175$ second. Figure 4.6 also shows that the maximum motor power limit occurs at $t = 165$ second, while that of reactive power occurs at $t = 175$ second. This suggests that although the motor operates on the lower part of the P–V curve after $t = 165$ second, the motor terminal voltage still can be controlled if there is a sufficient reactive power compensation near the motor terminal bus.

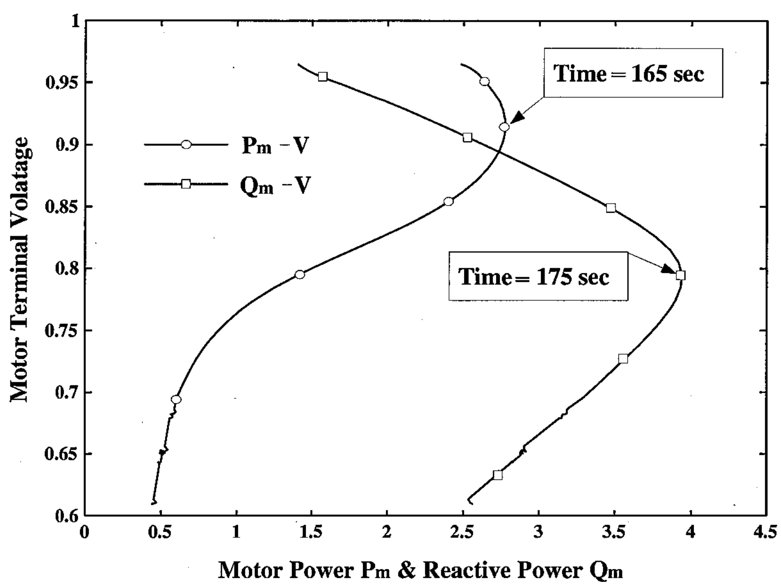

Figure 4.6: Transient P–V and Q–V curves of Motor Terminal Bus

Since all system loads except the induction motor load are constant impedance loads, the large system voltage drops after $t = 175$ second cause a large load reduction to the entire system. This load reduction happens so fast that the governors and turbines are not in time to respond so as to reduce the mechanical inputs to the generators. As a result, all generators are speeded up and ultimately pulled out of synchronous operation successively, which causes a complete system collapse as shown in Figure 4.7 where the rotor angles of generators at buses 2, 6, 8, and 10 are recorded. Other generators have similar angular instabilities.

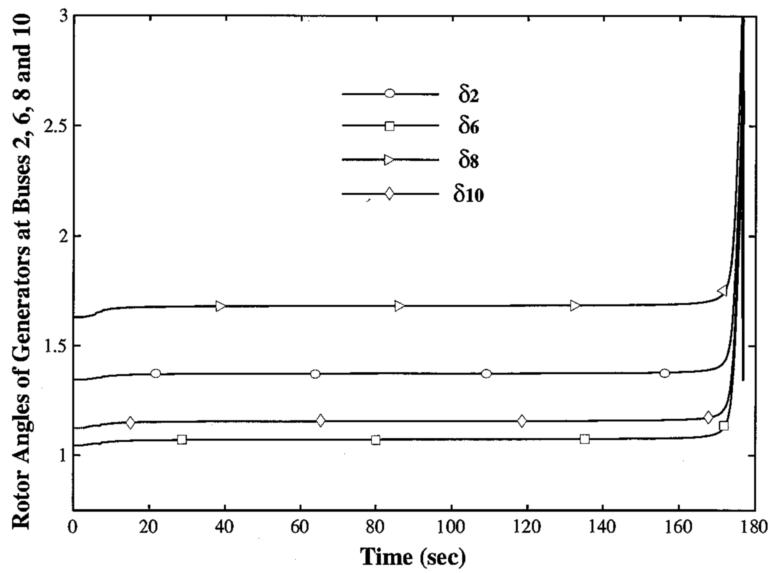

Figure 4.7: Some Generator Rotor Angles

In summary, the results of this case study show that an induction motor load could cause a slow voltage deterioration followed by a sudden voltage collapse when the motor operates near its critical condition. The stable operation of an induction motor depends on its terminal voltage and its critical slip.

When a motor operates over its critical state, both motor developed torque and power will drop, but it will draw more reactive power from the system, which will, in turn, aggravate the motor terminal voltage deterioration. If this interacting process is unchecked, a sharp voltage collapse will occur. In addition, from Figure 4.6, we can see that although system operates at the unstable branch of P–V curve of motor terminal bus, the system has not yet lost its voltage control until the maximum reactive power is reached. If sufficient Var compensations were added at motor terminal bus before this reactive power limit is reached, the system voltage would have been controlled, and the motor would move back to stable operation. Therefore, for the system with induction motor loads, the system voltage stability can not be judged by P–V curve alone.

Case Study 2: Transient Stability with Induction Motor Load

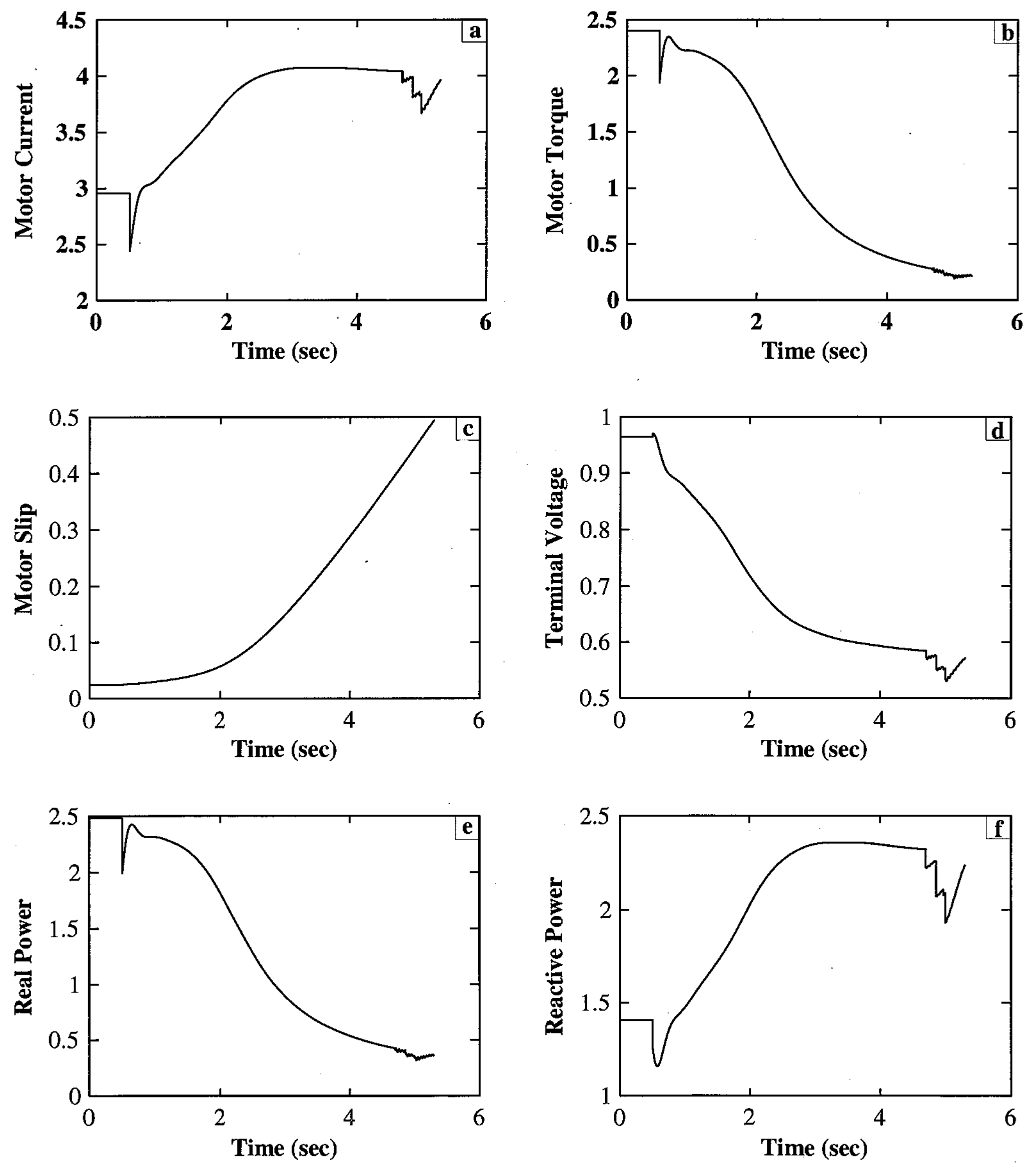

Figure 4.8: Transient Responses of Motor Variables

In this case study, an induction motor load is connected at system bus 21 through a distribution link. All other system loads are assumed to be constant impedance loads. The initial system condition is the same as that in case study 1. But the system loses a line between buses 14 and 21 at $t = 0.5$ second. The system responses shown in the Figure 4.8 demonstrate a transient voltage instability of the system.

Figure 4.8 shows the motor responses to the system disturbance. At the instant of the disturbance, the motor internal voltages (not shown) and motor slip remain unchanged. The motor terminal voltage and current change instantly. The disturbance causes the motor current to change in such a way that the motor developed torque, and hence the motor power and reactive power dip suddenly. The motor terminal voltage goes up a bit. Following that, motor slip begins to increase quickly until the critical slip is reached at $t = 1.2$ second. The motor developed torque has reached the maximum which is, however, still less than the load torque as shown in Figure 4.8b. After that, the motor starts stalling. Both motor torque and power decrease quickly. The motor reactive power demand increases rapidly causing motor terminal voltage collapse within 4 seconds. The results of this case study show that a system with induction motor loads may involve a transient voltage instability when the operation of the induction motor is upset by system disturbances. More reactive power demand of an induction motor against voltage decline adds an strict constraint on system voltage stability.

4.3.2 Effect of Exponential PQ Loads

The effect of a general static PQ load of the exponential form on system voltage stability is examined, which includes three special cases: the constant impedance, the constant current, and the constant power loads.

Case Study 3: Constant Power, Current, or Impedance Load

The initial system condition is the same as that in case study 1. An induction motor with an initial load torque of 2.4 is again connected to system bus 21 through a distribution link. An step load torque increase of 0.23 is applied to the motor as a system disturbance. All other system bus loads are assumed to be exponential PQ loads. The effects of three different types of the loads, the constant impedance, the constant current, and the constant power loads are examined and compared. Tap changing effects are not considered in this study.

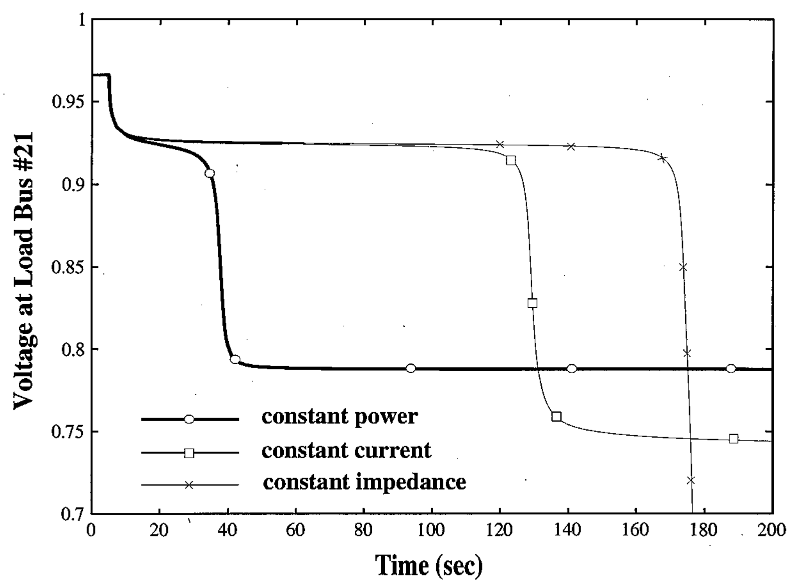

Figure 4.9: Voltage Response at a Load Bus

Comparison of the results for the three special types of PQ loads reveals some interesting points. A constant impedance load ($\alpha = \beta = 2$) is more voltage dependent than a constant current load ($\alpha = \beta = 1$), while a constant power load ($\alpha = \beta = 0$) is not dependent on its terminal voltage at all. Following the disturbance at $t = 5$ second, the induction motor will draw more power and reactive power from the system rapidly, causing voltage drops at all system buses. In responding to the voltage drops, the constant impedance loads will draw less power and reactive from the system, thus having a favorable effect to halt the further decline of system voltage. As a result, the motor can maintain stable operation at a higher terminal voltage for more than 170 seconds. On the other hand, the constant power load will draw the same power and reactive power from the system despite the voltage decreases, which aggravates the system voltage decline. The induction motor starts stalling at about $t = 25$ second, much earlier than that in the case of constant impedance loads. The effect of a constant current load is between the two with motor stalling at about $t = 125$ second, as shown in Figure 4.9.

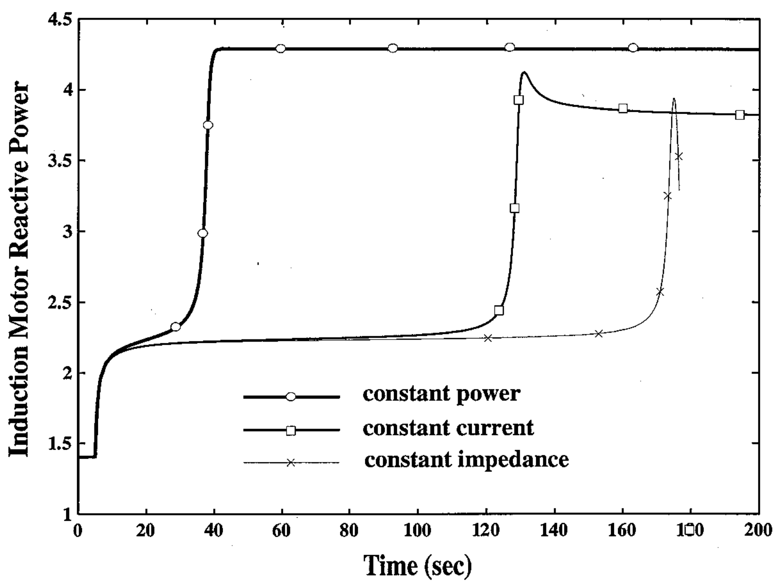

Figure 4.10: Reactive Power Drawn by the Motor

In all three cases, bus voltages collapse sharply when the induction motor starts stalling, which is, however, largely affected by the load characteristics. The more the dependence of a load on its terminal voltage, the better the damping effect it will have on system voltage stability. This damping effect is more crucial to the voltage stability of a power system where critical induction motor loads are supplied, as in this case study.

The motor reactive power response is shown in Figure 4.10, and the voltage response of a representative generator is shown in Figure 4.11.

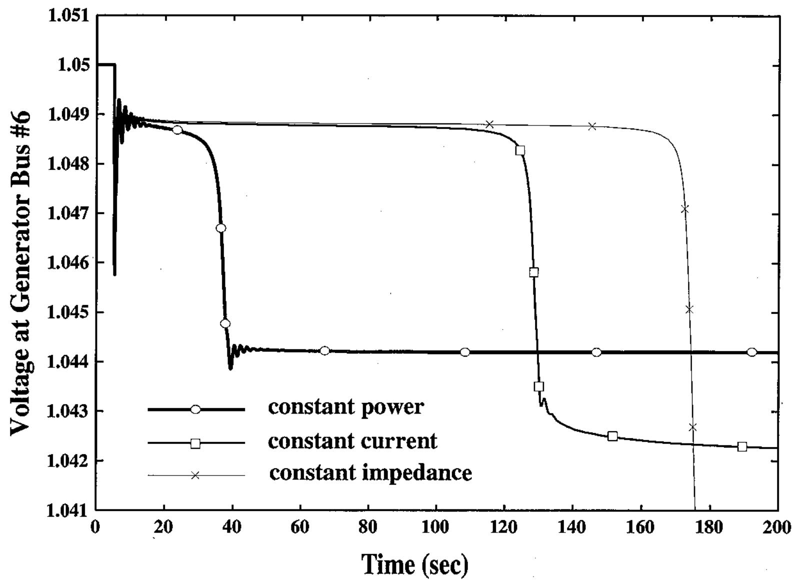

Figure 4.11: Voltage Response at a Generator Bus

It is also observed that with constant impedance loads, the system involves the generator angle instability, while with constant current or constant power loads, the system remains stable in term of system frequency although the stalling of the induction motor causes a voltage collapse at load bus 21, which is clearly demonstrated in Figure 4.12.

In the case of constant impedance loads, large voltage drops due to system disturbance reduce the system load, especially the real power load, causing generators to speed up following the disturbance. System remains stable both in angle and in voltage during the slow system dynamics. At about t = 105 second after the disturbance, the motor begins to stall, resulting in a sharp voltage collapse as shown in Figure 4.9. Both motor power and other system constant impedance loads drop rapidly. The process is so fast that the governors can not respond in time. The imbalance of system real power drives the generators eventually out of step of the synchronism. On the other hand, in the case of constant power loads, system load is not affected by the sharp voltage drop due to the motor's stalling. Only the real power of the induction motor load is lost. The generators speed up in response to this load reduction but remain stable at a higher rotor angles than those before the disturbance, as shown in Figure 4.12.

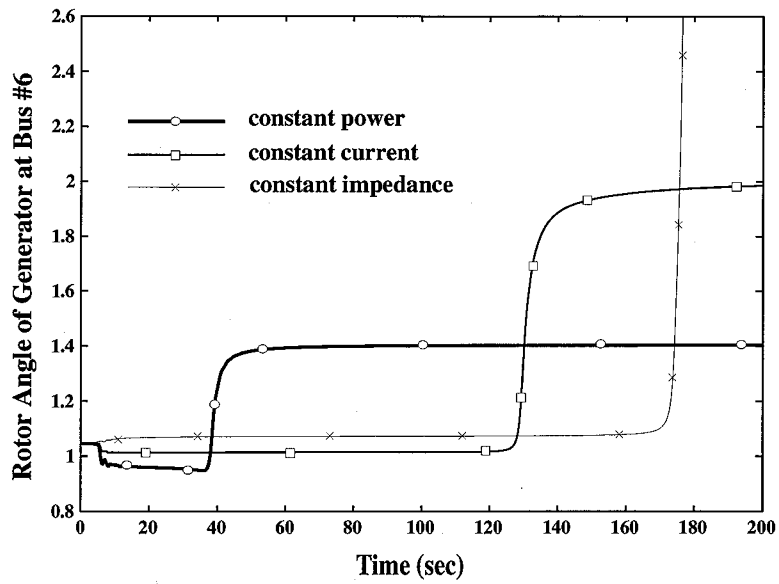

Figure 4.12: Rotor Angle of a Generator

This case study demonstrates the effects of a static voltage dependent load on system stability. Constant impedance loads draw less power and reactive power when voltage decreases, which has a favored damping effect on system voltage stability. On the other hand, the load reduction may tip over the real power balance of the system causing a possible generator angle instability, especially in the cases where rapid voltage collapse may involve. In contrast, constant power loads have an somewhat opposite effect on system stability. Although the constant demand of power and reactive power may aggravate the system voltage decline, which may cause system voltage collapse, it may help to maintain system real power balance when system voltage drops rapidly as in this case study, thus enhancing the system transient stability. This conclusion is drawn from the consideration of load only. The conclusion may be opposite if the loss of system power generations is also involved.

4.3.3 Effect of Persistent PQ Loads

As described in Chapter 2, a persistent PQ load demands constant power and reactive power despite a voltage decline, but involving an inherent time delay constant. This kind of load characteristics is very important to system voltage stability since the insisting demand of constant power and reactive power may cause system collapse, especially when the system loadability is reduced due to system disturbances.

Case Study 4: Effects of Persistent PQ loads on Voltage Stability

To study the effect of this kind of load on system voltage stability, all system loads of the sample system are considered as persistent PQ loads, modeled as changing equivalent admittances and with same recovery time delay of 10 seconds. The same initial system condition as in the previous case studies is obtained by replacing the corresponding induction motor load at bus 21 with a persistent PQ load having an initial loading of $2.48 + j1.40$. The steady state system operation is then disturbed by a loss of a line between buses 14 and 21 at $t = 5$ second. It is anticipated that this system disturbance would greatly reduce the loadability of system bus 21 because the load now must be supplied through the relatively remote buses 17 and 20. The simulation lasts 1000 seconds, and system responses are as follows.

Figure 4.13 records the voltage response at system bus 21, which shows voltage instability. Upon the system disturbance, system voltages dip immediately, causing the instant load power and reactive power load drops as seen in Figure 4.14.

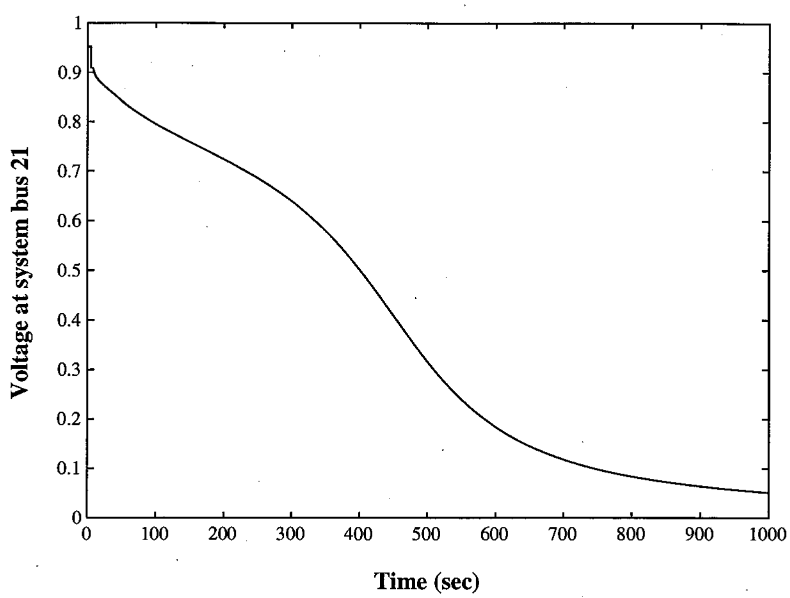

Figure 4.13: Voltage Collapse at Bus 21

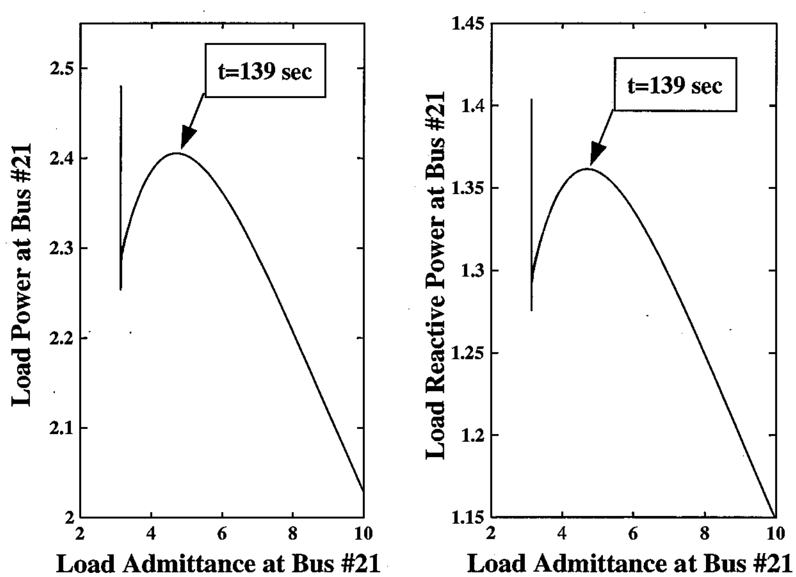

Figure 4.14: Load Power and Reactive Power vs. Load Admittance

After that, the system load admittance begins to increase according to equation (2.8). The load power and reactive power recover gradually while system voltages continue to decline. This process continues until about $t = 139$ second at which load power and reactive power at bus 21 have reached their corresponding maximum values as shown in Figure 4.14. But, the maximum load power and reactive power at bus 21 are still less than the pre–disturbance values. As a result, the load admittance continue increasing. Over that point, the load power and reactive power begin to drop monotonically despite the further increase of the load admittance. The bus voltage goes all the way down as shown in Figure 4.13, which indicates that system has lost voltage control at bus 21.

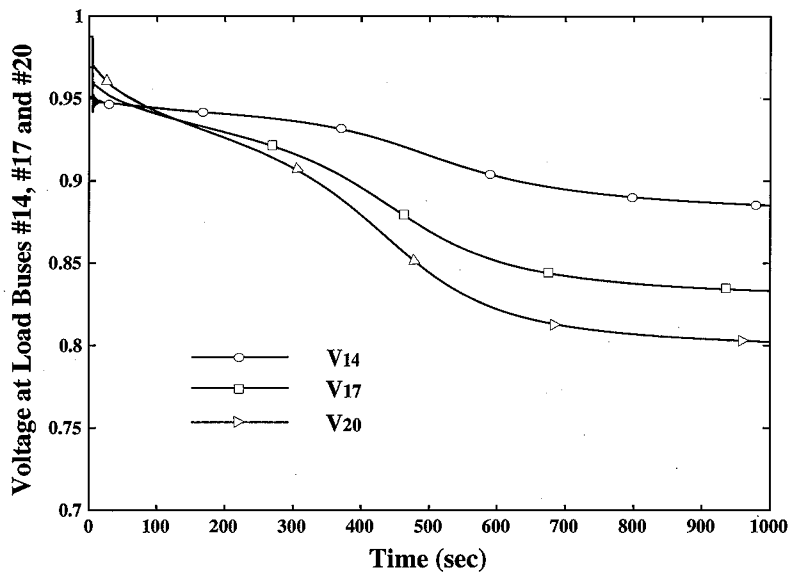

Figure 4.15: Some Other System Load Bus Voltages

Some other load and generator bus voltages of the system are shown in Figure 4.15 and Figure 4.16. The results indicate that the system survives the transient stability and voltages at system load buses other than bus 21 remain a fairly high level. Although the voltage collapses at bus 21, which causes loss of load at that bus, the other system bus loads have recovered to their pre–disturbance levels, some of which are shown in Figure 4.17. The persistent loads demand constant power and reactive power, which exceed the system loadability at bus 21, causing a voltage collapse at that bus, but maintains the system real power balance, avoiding a system angle instability.

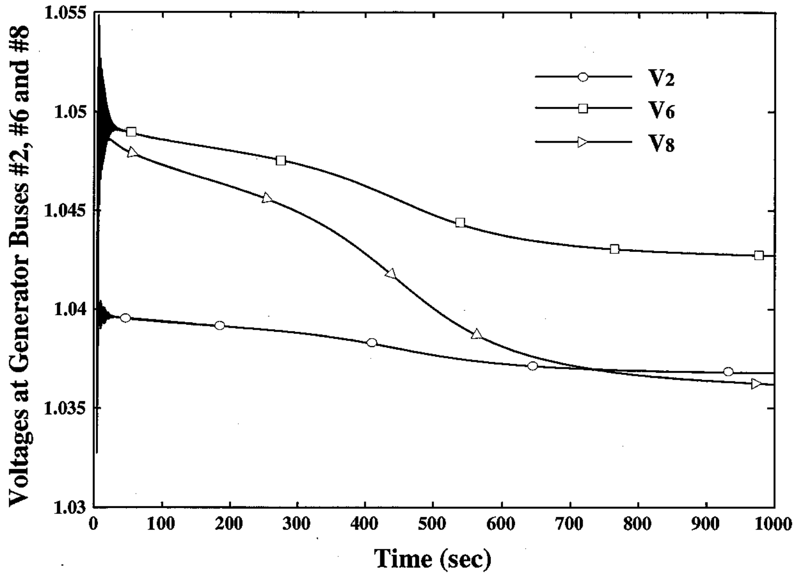

Figure 4.16: Some Generator Bus Voltages

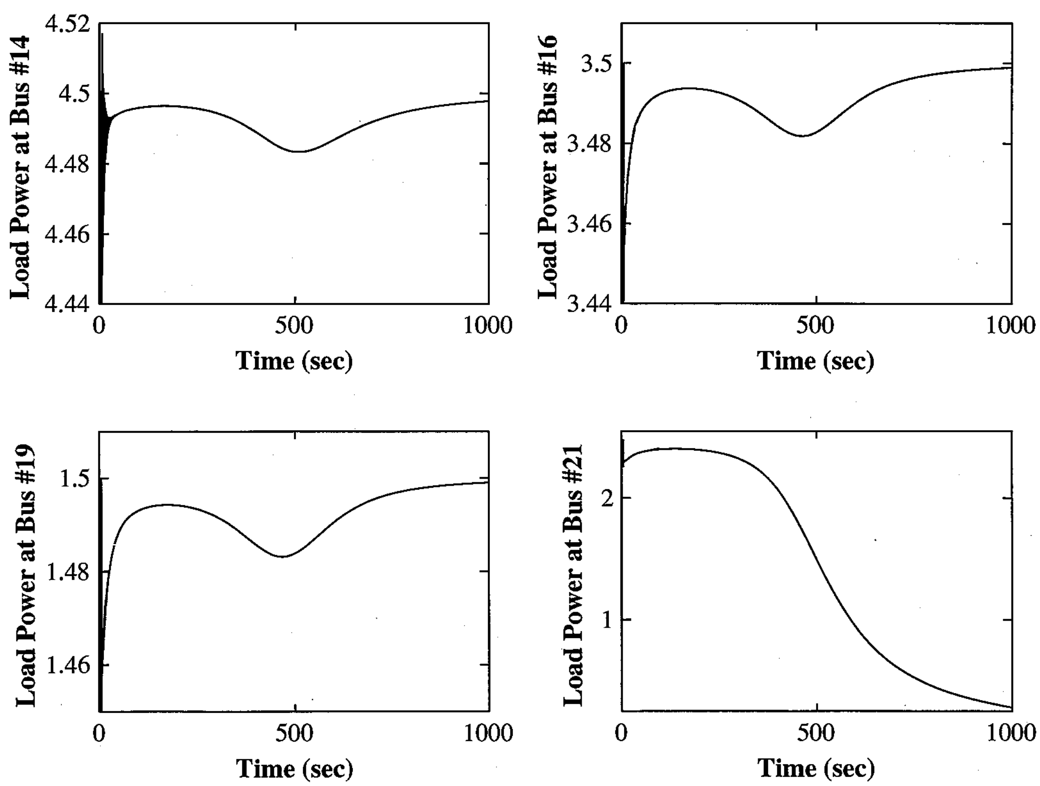

Figure 4.17: Loads at Some System Buses

4.4 Control Effects on System Voltage Stability

All reactive power related system components, such as controls, compensations, and constraints, have large impacts on system voltage stability. These system components may improve or deteriorate system voltage by supporting or restricting the system reactive power supply. The effects of system reactive power components on system voltage stability are examined in this section. Among them are the on load tap changing of a distribution transformer, the reactive power compensation with fixed capacitor banks or with SVC's, and the rotor overheat protection of a generator.

4.4.1 Effect of transformer tap changing

System distribution transformers are equipped with on load tap changers (OLTC's) to maintain normal load side voltages by changing the taps. The dynamics of the OLTC is usually slow comparing with those of other system components, such as generators and motors. Therefore, the effect of an OLTC on system voltage stability may not be considered for fast transient system conditions. But, it must be considered when a slow system dynamics is involved, especially when a system is operating near its critical state.

To study the tap changing effect on system voltage stability, an induction motor load is assumed at load bus 21, and all other system bus loads are assumed to be constant impedance loads. All loads are connected to the system buses through transformer links, and the transformers are equipped with on load tap changers. It is further assumed that each tap of a transformer is 0.025, the time delay of each tap changing is 10 seconds, and the voltage deviation tolerance is $\pm$ 2 percent from the normal voltage. The system disturbance is simulated by a step load torque increase to the motor with an initial load torque of 2.4.

Case Study 5: Tap Changing at Critical Motor Load Bus

In this particular study, the tap changing is only assumed at the transformer link of the motor load bus. The effects of other transformer tap changings are not considered. A step load torque increase of 0.23 is applied to the motor at $t = 5$ second.

To demonstrate the transformer tap changing effect, the result of case study 1 is used for comparison. As shown in Figure 4.18, if the transformer tap changing effect is not considered (as in case study 1), the system voltage will collapse at about $t = 170$ second due to the motor's stalling. Otherwise, the system voltage remains stable if the tap changing effect is considered.

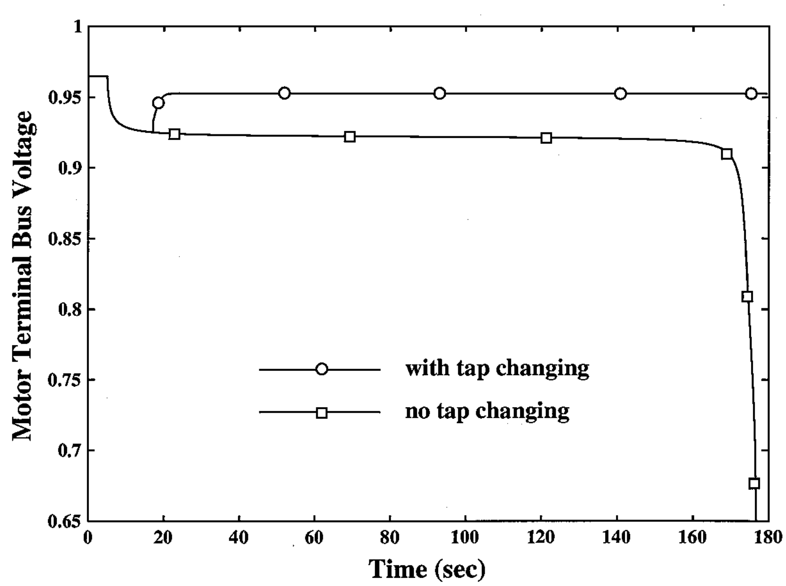

Figure 4.18: Tap Changing Effect on Motor Terminal Voltage

Following the step change in motor load torque at $t = 5$ second, both motor power and reactive power increase along with the increase of the motor slip, which causes the motor terminal voltage to decline due to the extra voltage drops in the transmission system. At $t = 7.13$ second, the motor terminal voltage drops below the specified lower limit and the tap changing is initiated. The tap changing of moving up one tap is completed at

$t = 17.13$ second. This tap changing raises the motor terminal voltage as shown in Figure 4.18. This voltage rise increases the motor developed torque, which becomes larger than the load torque as shown in Figure 4.19.

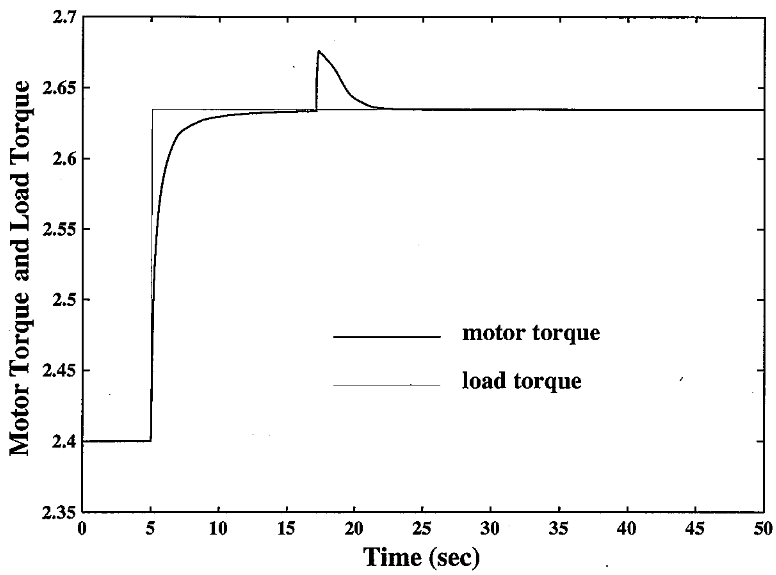

Figure 4.19: Tap Changing Effect on Motor Torque

At the instant of tap changing, the motor slip remains unchanged. Both motor power and reactive power jump suddenly. After that, motor slip begins to decrease, which results in a large motor reactive power decrease as shown in Figure 4.20. This reduction of motor reactive power helps to halt the system voltage from declining, which stabilizes the motor operation with a higher motor load torque of $T_L = 2.63$.

The effect of the tap changing on the P–V curve of the motor terminal bus is shown in Figure 4.21, where the loading limit (the nose of the P–V curve) of the motor terminal bus is appreciably extended by the transformer tap changing.

This study shows that the transformer tap changing is helpful to voltage stability for a load with negative reactive power–voltage characteristics, such as induction motor load.

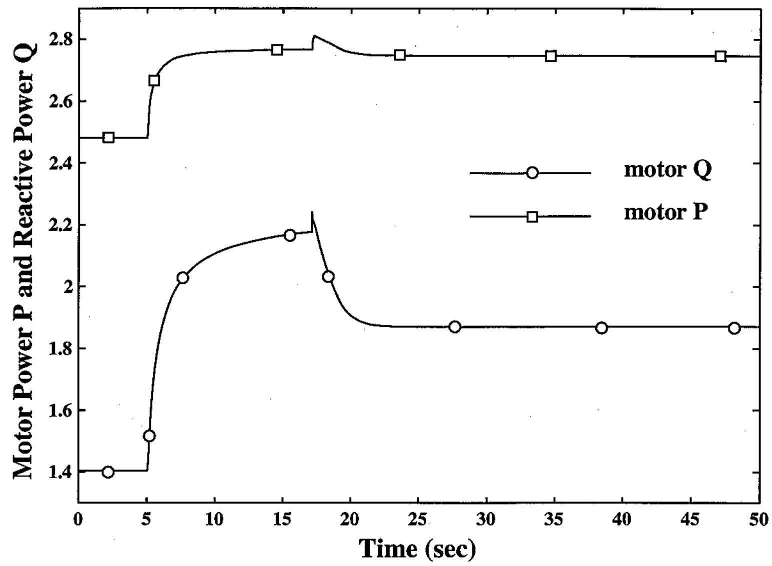

Figure 4.20: Tap Changing Effect on Motor P and Q

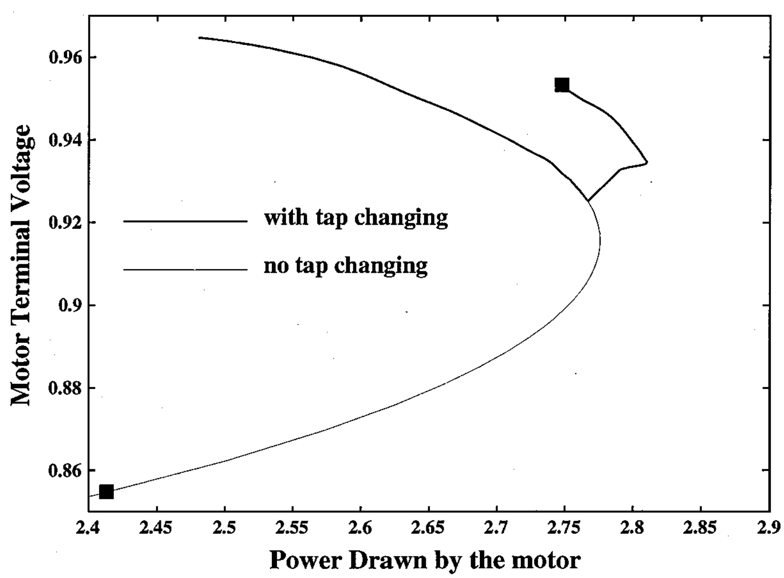

Figure 4.21: Motor P–V Curve with and without Tap Changing

The load side voltage increase due to the tap changing will reduce the load reactive power, which, in turn, enhences the system voltages. This effect of a transformer tap changing is especially crucial when the system operates near its critical state.

Case Study 6: Tap Changing at Other System Load Buses

In this case study, it is assumed that there are transformer tap changings for all system load transformers except for that of the induction motor load. The initial system condition is the same as that in case study 5. But a smaller motor load torque increase of 0.22 is assumed at $t = 5$ second.

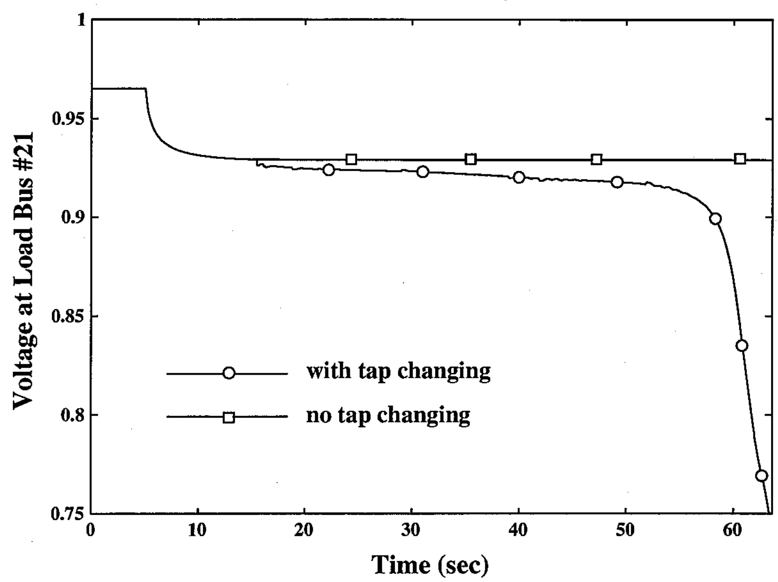

Figure 4.22: Effect of Tap Changing at Other System Load Buses

Figure 4.22 shows that the system voltage will remain stable if no tap changing effects are considered while the system loses voltage stability in the case where the tap changing effects are considered for all load buses but the motor load bus.

Following the system disturbance, system voltage decreases as the motor picks up its load. Since all system loads except the motor load are constant impedance loads, this voltage drop will cause a system load reduction, which has a damping effect to voltage deterioration. If no transformer tap changings are involved, the system will sustain a transient condition, and remain stable at a fairly normal voltage as shown in Figure 4.22.

In the case where the tap changings are considered only at load buses with constant impedance loads, the voltage drops at buses 14, 19, 18, and 17 successively initiate and, after 10 second time delay, activate the tap changers at the corresponding load buses. These tap changings raise the load side bus voltages of transformers, which restores some of the load power and reactive power. More current are then drawn from the transmission system, causing a further voltage decline at system side buses of transformers. As a result, the voltage drop at system bus 21 causes the induction motor to stall at about $t = 55$ second. Following that, a rapid increase in motor reactive power demand leads to a sharp voltage collapse. Figure 4.23 shows the P–V curve of the motor load bus. The dash–line curve shows the case where no tap changings are considered, and the motor remains stable operation at a fairly normal voltage, while the solid–line curve shows the tap changing effects which cause system bus voltage drops, upsetting the motor stable operation. The effects of tap changings on motor power and reactive power is further shown in Figure 4.24.

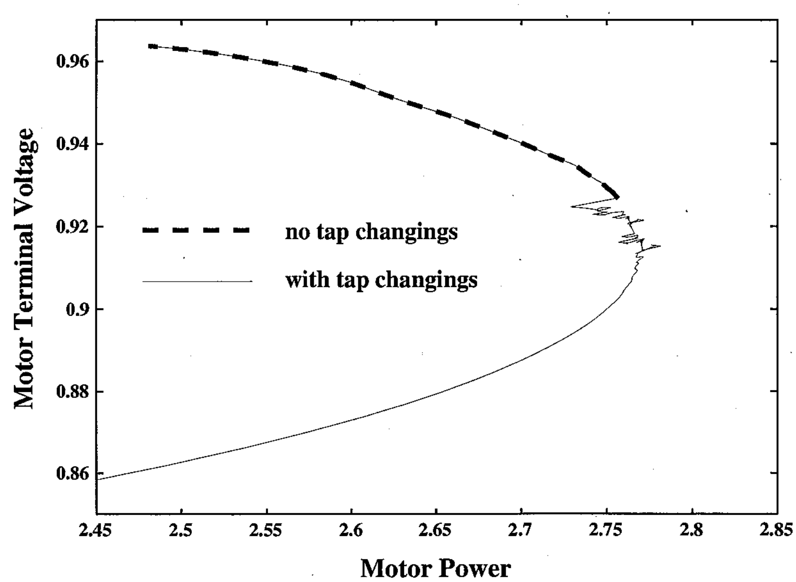

Figure 4.23: Motor Bus P–V Curves

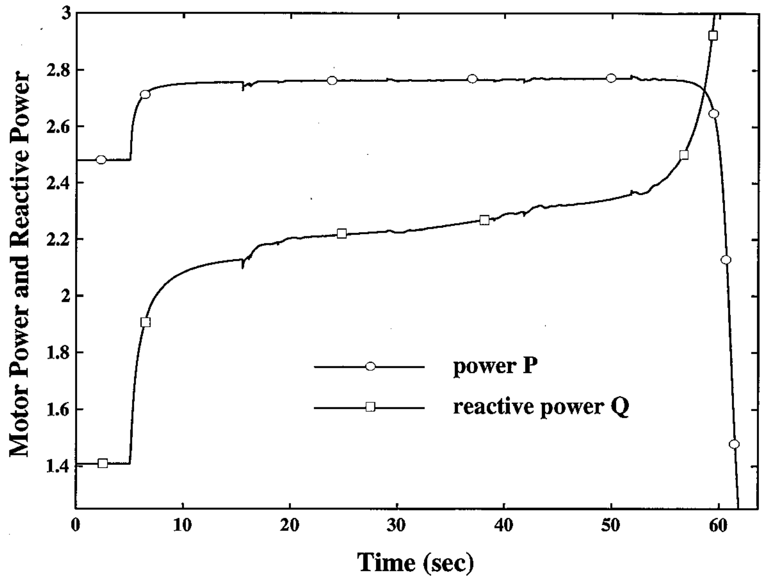

Figure 4.24: Tap Changing Effect on Motor Power and Reactive Power

This case study shows that a transformer tap changing has a detrimental effect on system voltage stability for the system loads with positive reactive power–voltage characteristics, such as an exponential form PQ load with positive exponents. The voltage rise due to a transformer tap changing will increase the load power and reactive power. This, in turn, aggravates the system bus voltage deterioration, which may cause a possible voltage instability as shown in this case study. This effect of a transformer tap changing will become salient when the system is operating near its critical state.

4.4.2 Effect of System VAR Compensation

For a heavily loaded power system, effective reactive power support is crucial to maintain system voltage stability. To study the effects of reactive power control devices on system voltage stability, a fixed capacitor compensation and an SVC are considered and compared for different system operating conditions, which may involve fast system transients and slow system dynamics. The fixed capacitor is modeled as a constant susceptance B_c.

The parameters of the SVC's control circuit are given in Table 4.16.

Table 4.16: Data of SVC Parameters

K_B	T_B	T_{1B}	T_{2B}
100	0.15	1.0	10.0

Case Study 7: VAR Compensation and Fast System Transients

In this case study, the additinal VAR compensations are provided to bus 21. Both fixed capacitor compensation and SVC's with two different capacities are considered. The fixed capacitor susceptance B_c is 0.5. SVC capacity may be represented by the limit of B_2 as shown in Figure 2.10. The SVC of larger capacity has a value of $B_{2max} = 0.35$, while that of smaller capacity $B_{2max} = 0.25$. An induction motor with initial load torque of 2.4 is connected to system bus 21 through a distribution link. Other system loads are assumed to be constant impedance loads. The system disturbance is simulated by a line opening between buses 14 and 21 at $t = 0.5$ second. No tap changings are considered.

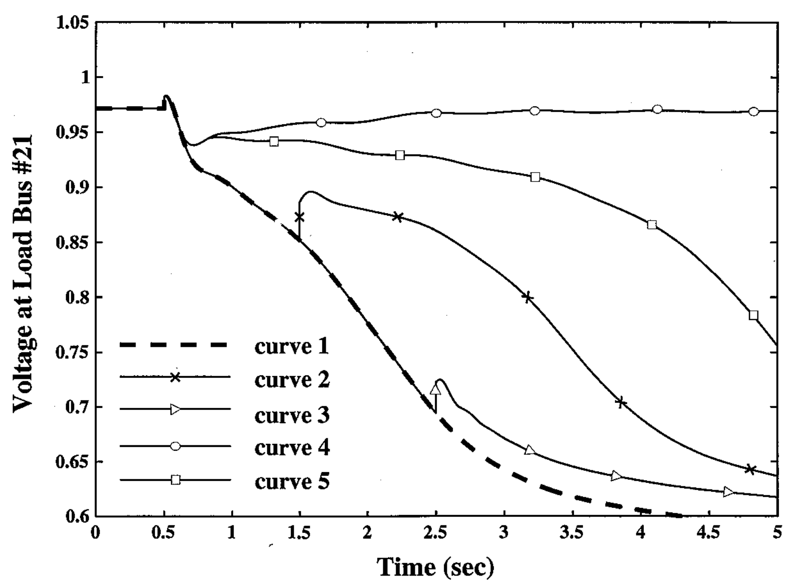

Figure 4.25: Effects of Different VAR Compensations

Figure 4.25 shows voltage responses at load bus 21 with different VAR compensations. After the system disturbance, the voltage at bus 21 drops quickly due to the large current of motor in order to pick up the load, which now has to be supplied from relatively remote system buses 17 and 20. If there is no additional reactive power support at bus 21, the low voltage will cause the motor to stall, and the large reactive power drawn by the stalling motor will result in a voltage collapse within 4 seconds, as shown by Curve 1.

The situations will be different if a fixed capacitor is available at bus 21, in which Curve 2 shows the case where the capacitor is switched in the system at $t = 1.5$ second, while Curve 3 that at $t = 2.5$ second. Although the capacitor is switched in very quickly, it still can not halt the voltage deterioration and collapse in both cases. Curve 2 and Curve 3 also show that the sooner the capacitor is switched in, the better the compensation will present. This is because the reactive power supplied by a capacitor depends on the voltage level, as shown in Figure 4.26. Since the voltage drops quickly in transient conditions, the fixed capacitor compensation is not effective due to the switch time delay.

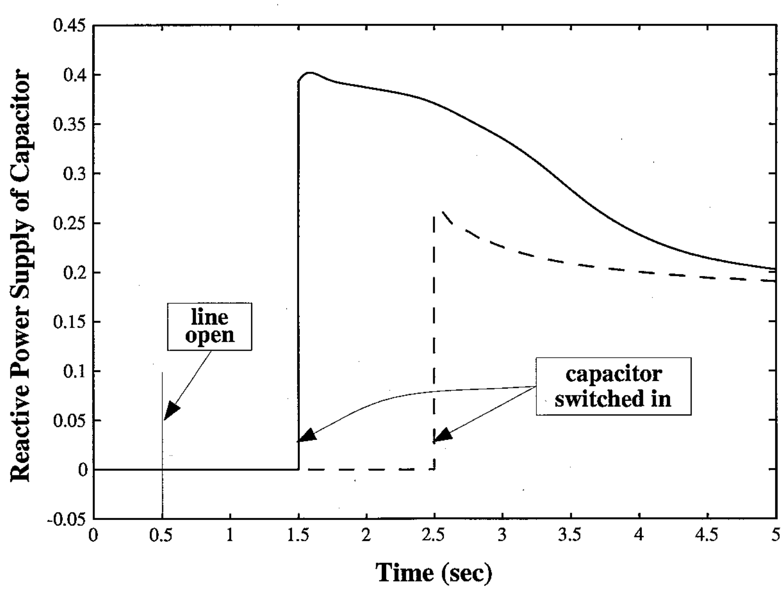

Figure 4.26: VAR Compensation of Fixed C Switched in Different Time

Curve 4 and Curve 5 in Figure 4.25 show the cases where the fixed capacitor at bus 21 is replaced by SVC's. The results demonstrate that system voltage can be effectively stabilized by an SVC of sufficient capacity (Curve 4), but not so for the system with an SVC of limited capacity (Curve 5). In the latter case, the SVC cannot supply enough reactive power compensation because it has reached its limit, and behaves like a fixed capacitor thereafter. As shown by Curve 5, the bus voltage has been controlled at a fairly high level for about 4 seconds, but ultimately collapses.

Figure 4.27 further shows the reactive power compensations of both SVC's. It clearly shows that an SVC can provide reactive power very quickly upon voltage drops, but an SVC must have sufficient capacity in order to stabilize a system voltage.

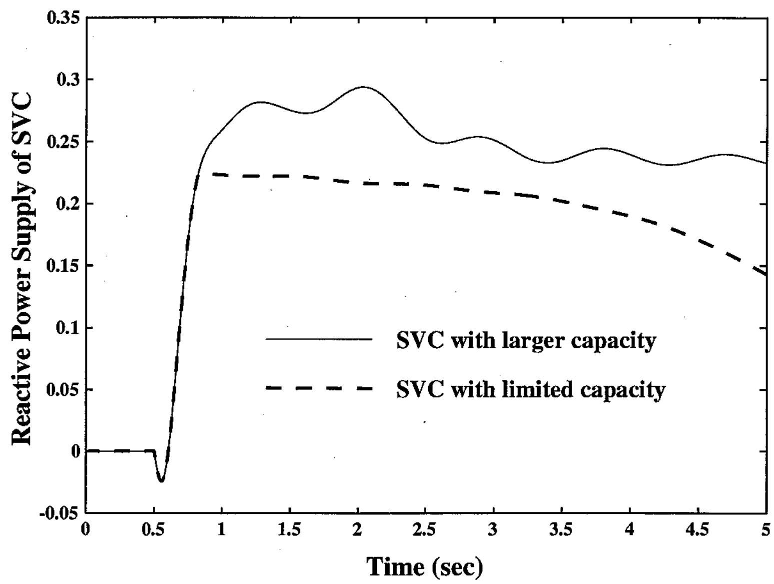

Figure 4.27: VAR Compensation of SVC's with Different Capacities

Case Study 8: VAR Compensation and Slow System Dynamics

In case study 7, system VAR compensation in fast transient system condition is investigated. This case study will show the effects of VAR compensations for a system condition in slow system dynamics. For this, all system loads are modeled as persistent PQ loads with a time constant of 10 seconds. The induction motor load in case study 7 is replaced by a persistent PQ load with the same initial loading. VAR compensations are considered again at bus 21. The system disturbance is simulated by a loss of line between buses 14 and 21 at $t = 5$ second.

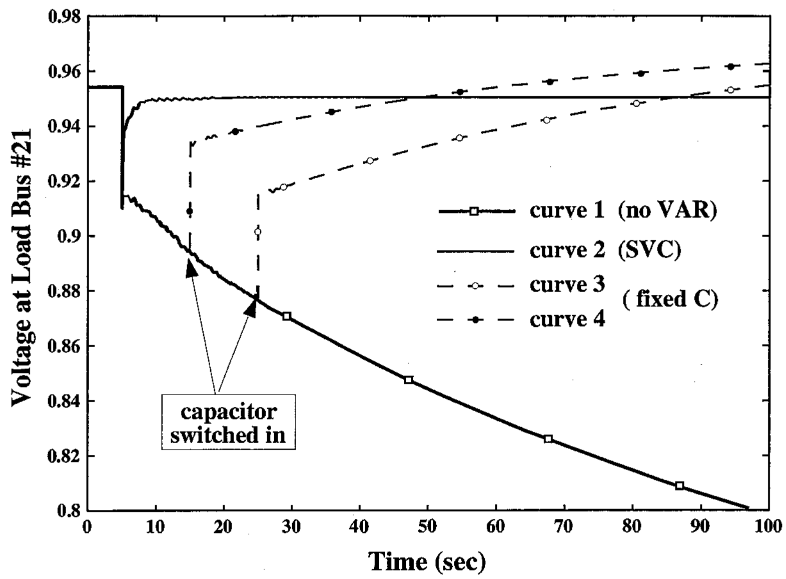

Figure 4.28: Effects of VAR Compensation of Fixed Capacitor and SVC

Figure 4.28 shows the voltage responses at bus 21. Upon the system disturbance, the voltage drops suddenly, and then declines monotonically as the load recovers. If there is no additional VAR compensation available at bus 21, the voltage will ultimately collapse as shown by Curve 1. Comparatively, Curve 2 shows the case where an effective SVC is available at bus 21. The voltage recovers very quickly in about 10 seconds and remains stable at its normal value. The other two dash–line curves, Curve 3 and Curve 4, show the situations where a fixed capacitor at bus 21 is switched in at 10 seconds and 20 seconds respectively after the disturbance. The voltage is stably controlled for both cases. However, there will be more than required reactive power compensation to the system along with the voltage recovery. As a result, the voltage will have a value higher than its pre–disturbance value, and some of capacitor compensations may have to be switched out of the system. This can be very critical when a system has major load with negative reactive power–voltage characteristics, that is, the load demands more reactive power when its terminal voltage goes down. There is no such problem with SVC compensation, since the reactive power supply is controlled according to the voltage deviations. When voltage is higher than its specified value, VAR compensation of SVC will decrease accordingly. The different VAR compensations are shown in Figure 4.29.

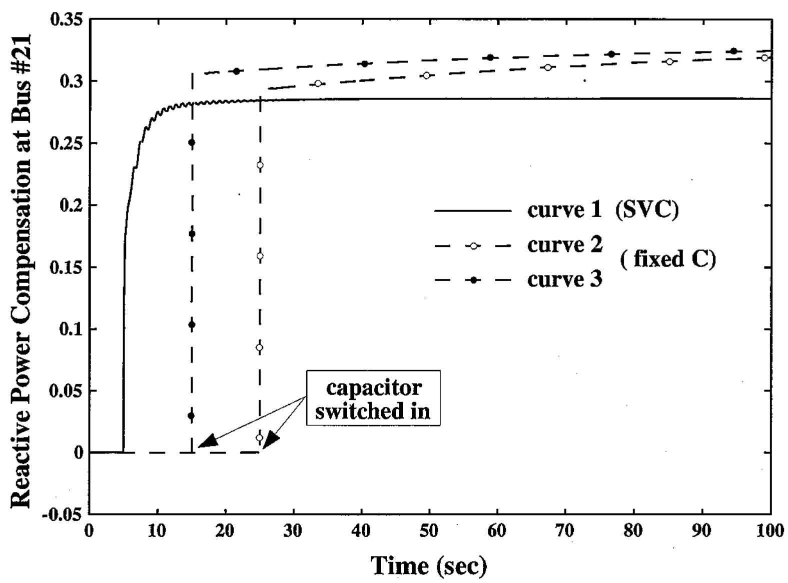

Figure 4.29: VAR Compensation of Fixed Capacitor and SVC

For a heavily loaded power system, an effective reactive power compensation is crucial to system voltage stability since system disturbances changes the power flow in the transmission network, which may cause an extra reactive power loss and a lower system voltage. Depending on the system controls and load characteristics, the system may involve fast transients and/or slow dynamics. For system involving fast transients, the system voltage may drop quickly. In such a case, fixed capacitor compensations are not effective and SVC's with sufficient capacities should be used. For the system involving slow dynamics, the fixed capacitor compensation can be used to support system voltage, but it may cause the voltage to overshoot its normal value because of its positive feedback control characteristics. Therefore, only SVC's with ample capacities can effectively stabilize the voltage of a power system.

4.4.3 Effect of Generator Rotor Overheat Protection

Generators are equipped with rotor overheat protection to prevent the field winding from overheating. The current in the field winding is determined by the winding resistance and the excitation voltage which is controlled by the generator excitation system. When system disturbances cause an extra system reactive power loss, the generator terminal voltages will decrease. To maintain normal terminal voltages, generator excitation voltages must be automatically increased, which will result in larger currents in rotor windings. When the accumulated heat is over the permissive limit, overheat protections will reduce the excitation voltage to a lower level or even trip the generator off the system. Since this protection limits the generator reactive power output or even trips off the generator, it will have a significant impact on the voltage stability of the entire power system.

Case Study 9: Effect of Rotor Overheat Protection

In this case study, the effect of generator rotor overheat protection (ROP) on system voltage stability is investigated. The ROP is usually realized by the generator excitation reduction to its continuous operating limit or the second limit (see in Figure 2.4) when the generator has been operated at a higher excitation level over a prescribed period of time.

In case study 4, the effects of persistent loads on system voltage stability are discussed without considering the generator ROP. The attempt of persistent PQ loads to recover loads to the pre–disturbance level by increasing their equivalent admittances pushes the system over the post–disturbance loading limit of bus 21, which results in a voltage collapse at that bus as shown in Figure 4.13.

In this case study, all system loads are again modeled as persistent PQ loads with recovery time delay of 10 seconds, the same as in case study 4, but the effect of generator ROP on system voltage stability is considered. The pre–disturbance loading at bus 21 in case study 4 is adjusted from $2.48 + j1.40$ to $2.40 + j1.36$. The system disturbance remains unchanged, and is again simulated by a loss of line between buses 14 and 21, which occurs at $t = 5$ second.

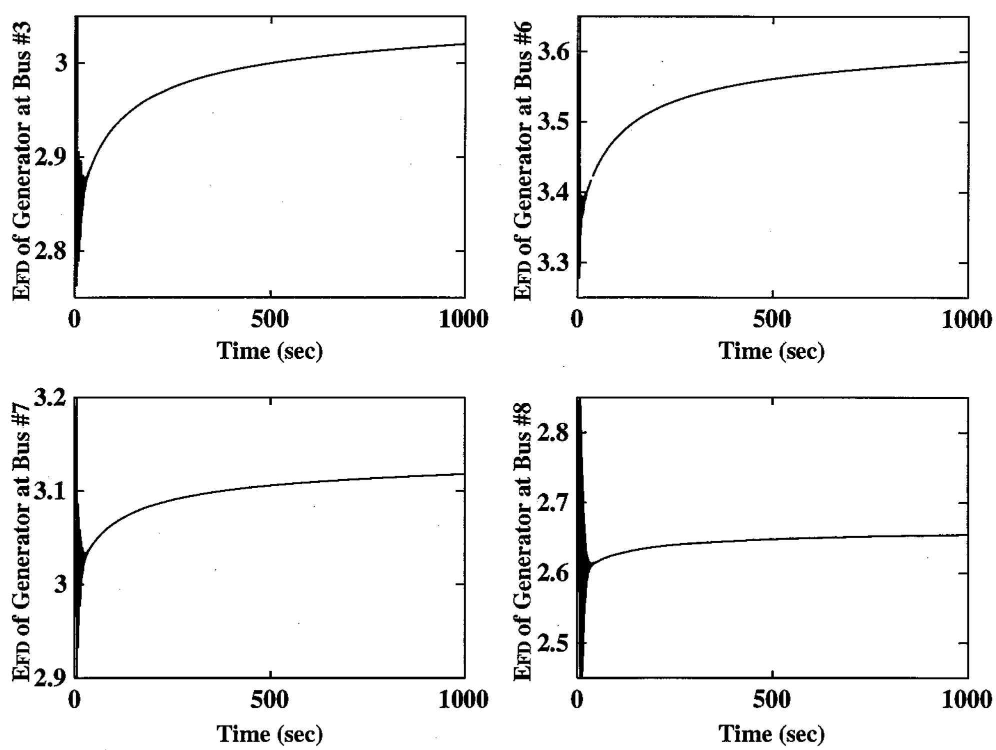

Figure 4.30: Some Generator Excitation Voltages (without Generator ROP's)

Two different cases are examined. In the first case, no generator ROP's are included.

Generators could operate continuously at higher excitations, as shown in Figure 4.30 where excitation voltages of generators at buses 3, 6, 7, and 8 are recorded. This means that the generators could have the ability to maintain their terminal voltages so that large reactive power could be supplied to the system. As a result, the system load bus voltages remain stable at a fairly higher values as shown in Figure 4.31.

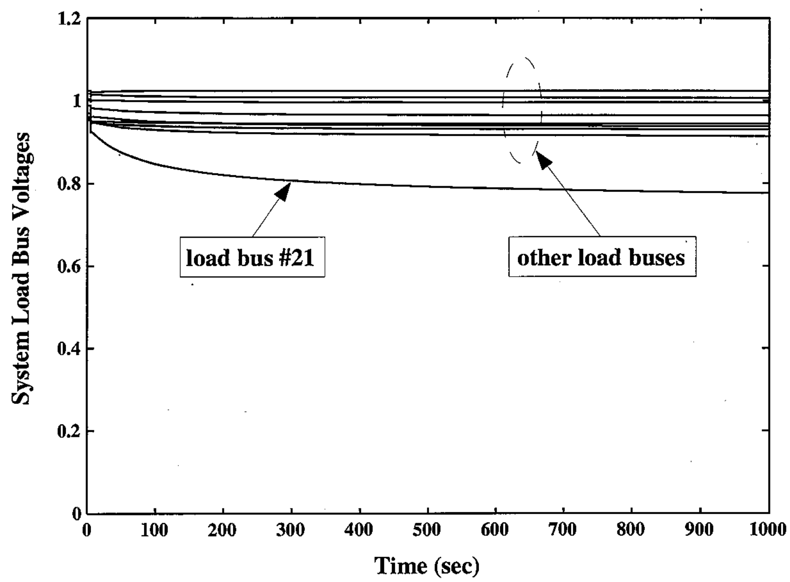

Figure 4.31: System Load Bus Voltages (without Generator ROP's)

In the second case, the continuous operating limit, or the second limit, of excitation voltage for each generator is assumed to be 10 percent over the corresponding pre–disturbance level. If a generator has been operated continuously at a higher excitation than its second limit over 100 seconds, the rotor overheat protection will cramp the generator excitation to this limit.

Simulations show that after system transients, the excitation voltage of the generator at bus 6 exceeds its second limit at t = 142 second and is cramped at t = 242 second since it has operated continuously at the higher excitation over 100 seconds.

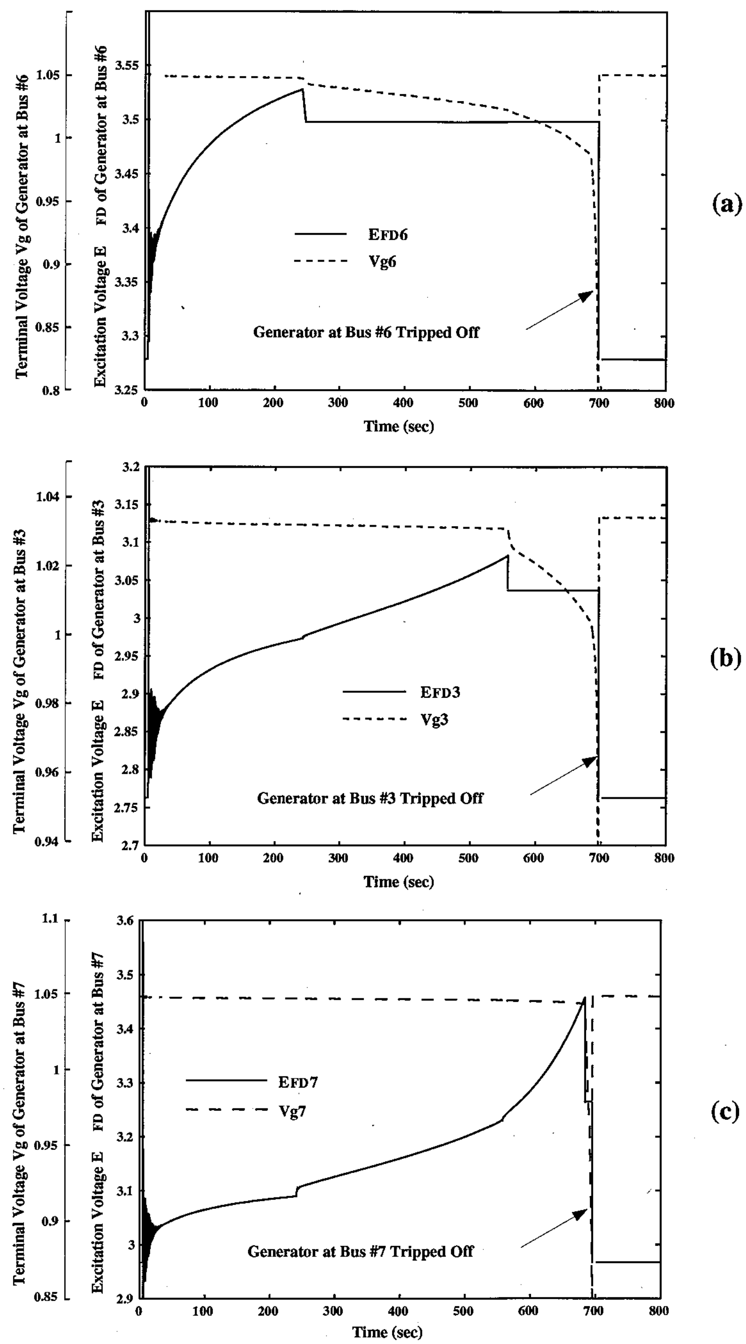

Figure 4.32: Generator Excitation and Terminal Voltages (with ROP's)

As a result, this generator loses its voltage control ability and its terminal voltage begins to decline as shown in Figure 4.32a. Immediately after the excitation reduction of the generator at bus 6, the reactive power burden is transferred to other generators. As shown in Figure 4.32b and Figure 4.32c, generators at buses 3 and 7 increase their excitation rapidly to pick up the system reactive power load.

Consequently, the excitation voltage of generator at bus 3 remains over its second limit from t = 457 second and then is reduced to the second limit after 100 seconds. The loss of reactive power control of generator at bus 3 aggravates the system voltage deterioration. This causes the generator at bus 7 to increase its excitation more quickly. At t = 576 second, the excitation voltage exceeds its second limit and is cramped at t = 676 second. The loss of voltage controls of generator at bus 7 causes large voltage drops at system load buses as shown in Figure 4.33. Although other generators attempt to increase excitations to supply more reactive power, the rapid voltage collapse initiates a system transient instability with generators tripped off consecutively due to their losses of synchronism.

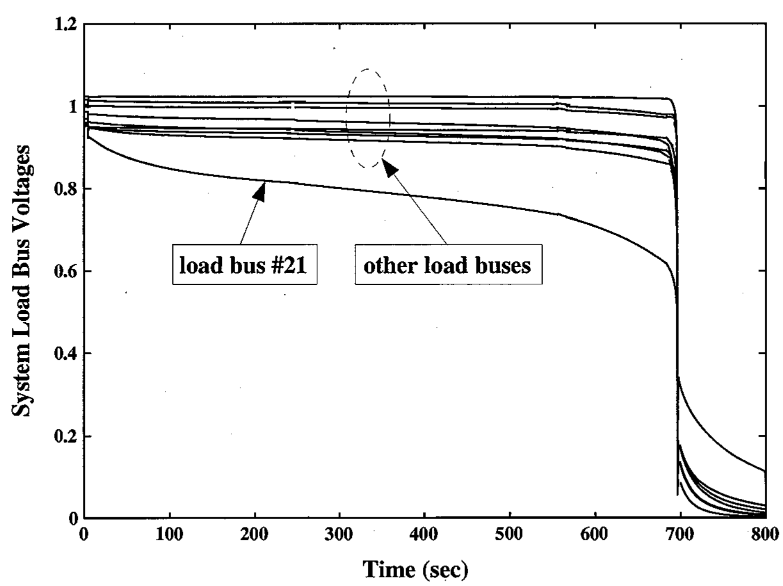

Figure 4.33: Effect of Generator Overheat Protections

This case study shows the important effect of generator rotor overheat protection on system voltage stability. Under heavy system loading conditions, generators are usually operated at high excitation levels in order to maintain a normal system voltage profile. When a system disturbance causes a further system reactive power loss due to the increased the electrical distance between generators and loads, some generators may be operated with overexcitation, such as generator at bus 6 in this case study. Once the excitation of the overexcited generator is reduced by its rotor overheat protection, some of its reactive power supply must be transferred to other machines which may be again successively protected, such as generators at buses 3 and 7. The successive losses of voltage control at generator buses will then aggravate the system reactive power shortage. System voltage may therefore collapse if there are no other reactive power controls available to the system. This study also suggests that for a heavily loaded system, local load reactive power compensation should be effectively used for system voltage control rather than heavily counting on the reactive power supply from remote generators.

4.5 Maximum Loading Limit by Load Flow and Simulation

In previous sections, various effects of loads and controls on voltage stability are examined. Due to the system disturbances, the system operation may approach its critical state dynamically, which is affected by load and control characteristics. Since the system critical state is usually characterized by the system MLL which is crucial to voltage stability analysis and control, methods based on the traditional load flow analysis and the dynamic simulation as proposed in this thesis are compared in this section.

Case Study 10: System Loading Limit with Persistent PQ loads

In this case study, all system loads are modeled as constant PQ loads for load flow study except that a variable admittance load with initial loading of $P+jQ = 2.48+j1.40$

is assumed for bus 21. Persistent PQ loads with the same time constant of 10 seconds are used for the simulation study. The initial and final system loading conditions, and load power factors are the same for both studies. A loss of the line between buses 14 and 21 is assumed as the system disturbance.

Load flow studies are made for both normal and post–disturbance system conditions by increasing load admittance at bus 21. The system loading limits of bus 21 are observed as $P + jQ = 5.77 + j3.26$ for the normal system condition, and $P + jQ = 2.94 + j1.67$ for the post–disturbance system condition. For the simulation study, the disturbance is applied to the system at $t = 5$ second, and the simulation lasts 1000 seconds. P–V curves of bus 21 of both load flow and simulation studies are shown in Figure 4.34.

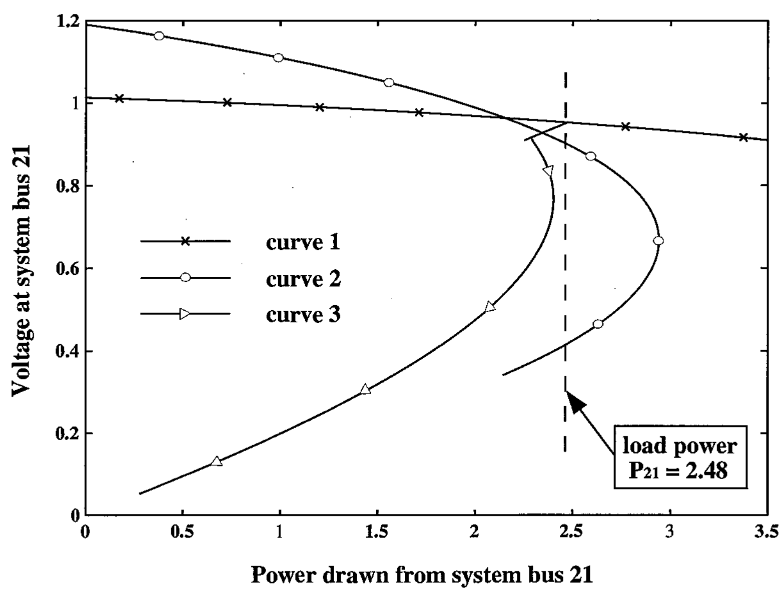

Figure 4.34: P–V Curves of Load Bus 21

Figure 4.34 shows the results of P–V curves of various studies: Curve 1 from load flow for the normal system condition, Curve 2 also from load flow but for the post–disturbance system condition, and Curve 3 from simulation for the system being disturbed. From load flow studies, although the disturbance greatly reduces the loadability of load bus 21, the system loading still lies within its limit, which leads to a conclusion that the post–disturbance system voltage remains stable. However, for the system being disturbed, Curve 3 of Figure 4.34 shows that the system loading limit is less than the load demand, and the system voltage at bus 21 collapses. This concludes that load flow study usually gives the upper bound of a system maximum loading limit.

Case Study 11: System Loading Limit with An Induction Motor Load

The system loading conditions of this case study are the same as those of case study 10 except that the load at bus 21 is replaced by an induction motor load. The initial load torque T_L for both load flow and simulation studies is 2.0. Load flow study is carried out to find the system loading limit by increasing the motor load torque until the load flow solution disappears, and the result is shown as Curve 1 of Figures 4.36 and 4.37. The results show that the system reaches its loading limit at a motor load torque $T_L = 2.47$ ($P_m = 2.56$) at which the load flow diverges.

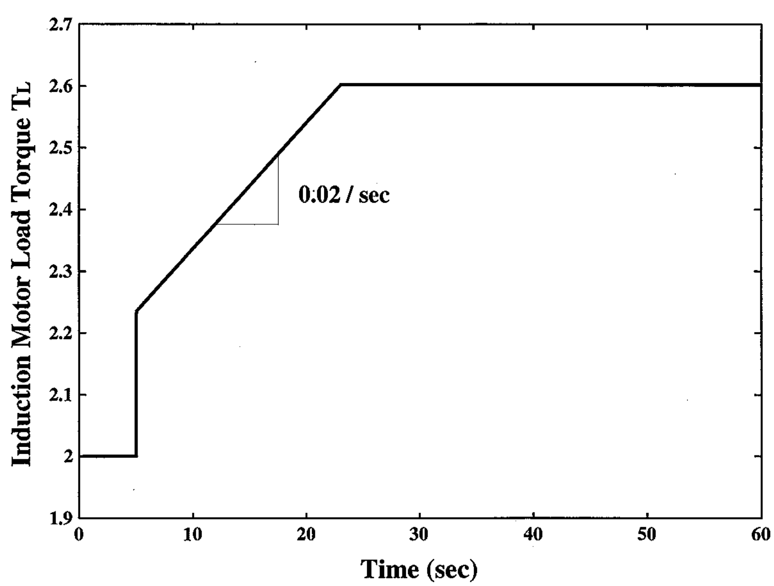

Figure 4.35: Motor Load Torque Changes in Simulation Study

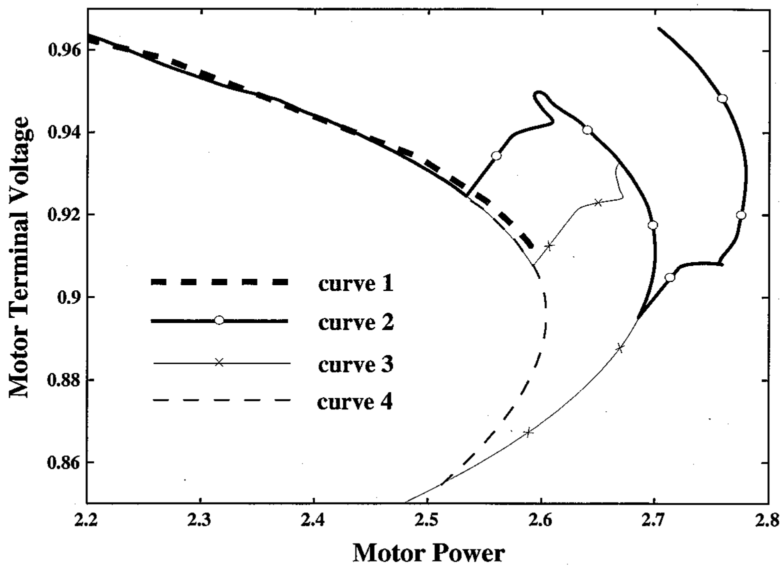

Figure 4.36: P–V Curves of Motor Terminal Bus

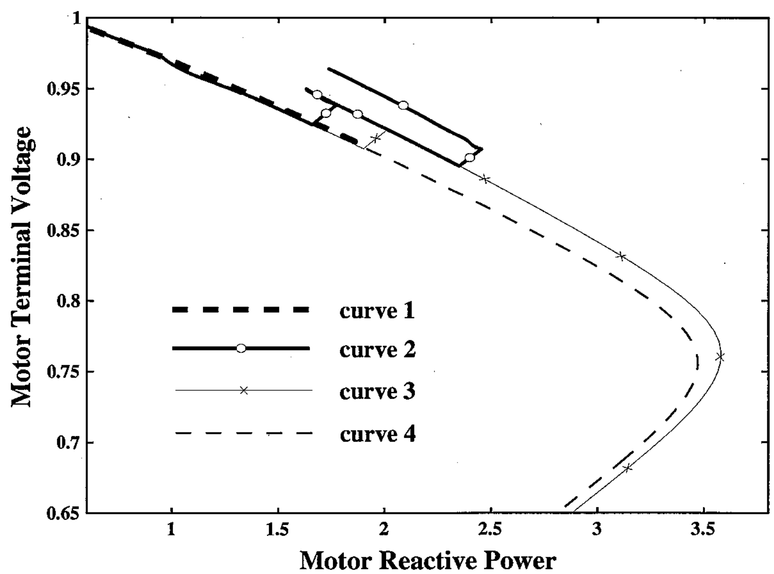

Figure 4.37: Q–V Curves of Motor Terminal Bus

For simulation study, it is further assumed that the motor load torque has a step change of 0.23 at $t = 5$ second, and then a gradual increase of 0.02/sec until it reaches $T_L = 2.6$ at $t = 23$ second as shown in Figure 4.35. The P–V and Q–V curves are shown in the Figure 4.36 and Figure 4.37, respectively, as Curves 2, 3, and 4.

The results show that the voltage control due to the transformer tap changing at motor load bus can increase the system loading limit, but is also affected by the time delay of the tap changing. The simulations show that the motor load torque of $T_L = 2.6$ is still within system loading limit if the time delay of tap changing is less than 10 seconds. Due to the slow recovery of system persistent PQ load and the slow increase in motor load torque after the step change, there is enough time for the transformer tap changer to respond before the voltage collapses.

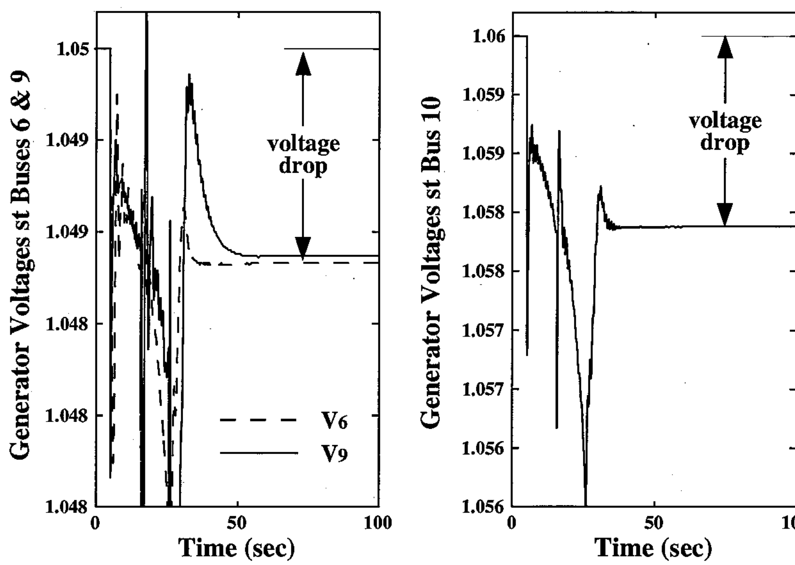

Figure 4.38: Some Generator Bus Voltages

Curve 2 of Figure 4.36 and Figure 4.37 shows the case that the tap changing time delay is 10 seconds. The tap changes at $t = 15.77$ second and $t = 25.77$ second raise the motor terminal voltage, and extend the motor bus loading limit. After the second tap change, the motor developed torque becomes larger than the load torque of $T_L = 2.6$. The motor slip begins to decrease, and hence the reactive power drops accordingly. Although the final generator voltages shown in Figure 4.38 are below their normal levels, the motor remains stable at the normal voltage with the load torque of 2.6 and other bus loads totally recovered as shown in Figure 4.39.

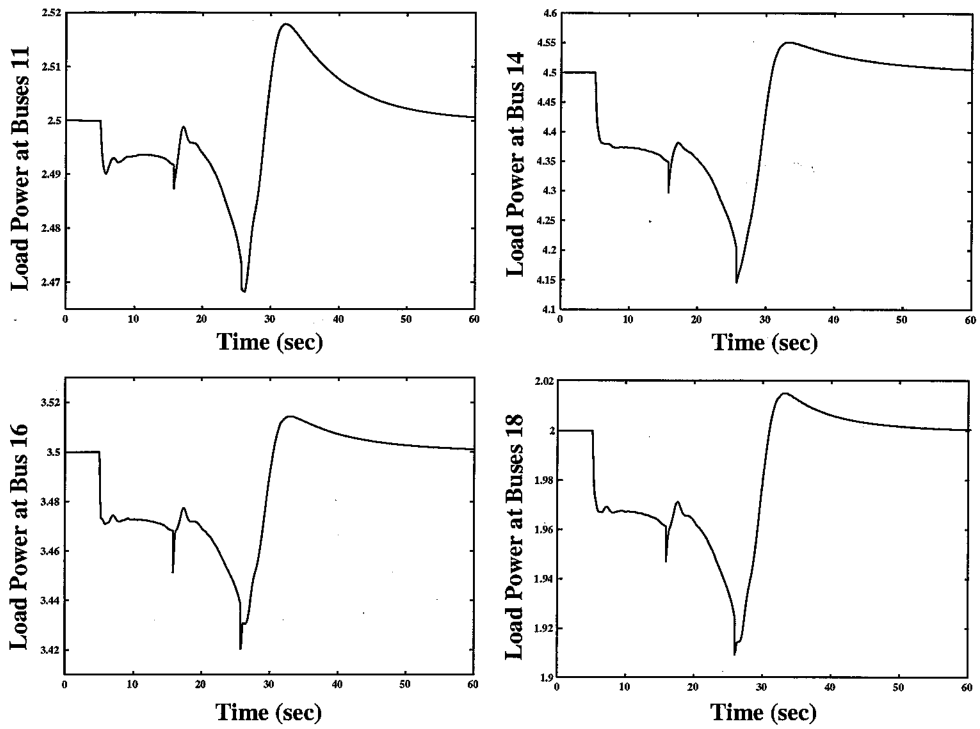

Figure 4.39: Some System Bus Loads

Curve 3 of Figure 4.36 and Figure 4.37 shows the case that the time delay of tap changing is set to 15 seconds. The tap changer responses at $t = 20.77$, which increases the system loading limit. But this limit is again exceeded at $t = 21$ second due to system load recovery. As a result, the motor power begins to decrease, while its reactive power increases despite voltage drop. Finally, before the second tap change could occur at $t = 35.77$ second, the system has lost voltage stability at motor terminal bus at $t = 30.7$ second. After that, both motor power and reactive power drops along with the voltage collapse. For comparison, the case where no tap changer is considered is also presented by Curve 4 of Figure 4.36 and Figure 4.37.

This case study demonstrates that although the system loading limit in steady state can be determined from load flow related static methods, the loading limit for system being disturbed must be evaluated by detailed system simulations. Moreover, the voltage control effect of transformer tap changing, if fast enough, can effectively increase the MLL of a system being disturbed to the extent even larger than the MLL of steady state from load flow.

Chapter 5

CONCLUSIONS AND REMARKS

5.1 Conclusions of the Thesis

This thesis project is mainly concentrated on the analysis of voltage stability of a power system through time domain simulation techniques. Better understandings of system voltage instability phenomenon are gained through close examinations of the effects of load and control components on system voltage stability.

A 21 bus sample power system is chosen for the simulation studies. Steam and hydro–electric generating units, various types of loads, and many reactive power control devices are modeled with emphasis on the dynamic behaviors of system loads and reactive power related components. System critical buses are defined and identified from voltage–reactive power sensitivity analysis for the voltage stability study.

A comprehensive time domain simulation program is developed based on the implicit Trapezoidal integration rule and the step doubling integration step size control algorithm. A new variable elimination method is devised for some dynamic load to include the related nonlinearities in load flow iterations so that the variable extension and convergence problems can be avoided. A new two–step procedure is also developed for efficient and systematic solution of high order system Jacobian matrix equations.

The effects of various types of loads and reactive power controls on the voltage stability are thoroughly examined through designed case studies so that the dynamic voltage behavior of a power system in various operating conditions can be clearly demonstrated and clarified.

From case studies in this thesis, the conclusions are drawn as follows.

1. Voltage instability of a dynamic power system is a very complicated phenomenon. It may involve a fast transient voltage instability and/or a slow voltage decline followed by a sudden collapse, depending on the system operating conditions, system load and control dynamics, and types, locations, and severities of system disturbances.

2. Induction motor loads, which constitute the major part of industrial loads, may have great influences on system voltage stability due to its more or less constant power and negative Q–V characteristics which means that the motor will draw more reactive power when its terminal voltage decreases.

   When a system voltage drops, which causes a reduction of motor developed torque, the motor will pick up the load very quickly by increasing its slip. More current will be drawn from the system, which causes further voltage decrease. Depending on the magnitude of a disturbance, this interaction between the motor and the supply system may experience either a slow system dynamics which drives the motor towards its critical state for a long time before it starts stalling, or a fast system transients which upsets the motor's stable operation so quickly and causes the motor stalling in a few seconds. During the motor stalling, the reactive power demand increases very quickly, which causes the system voltage collapse.

   Unlike system angle instability which is caused by the generator power imbalance, the voltage instability caused by the loss of motor stable operation can not be judged by the power imbalance alone. It also involves the reactive power equilibrium of the system. This means that the loss of motor power due to the motor stalling does not necessarily result in a voltage instability since the motor terminal voltage can be controlled before the motor Q–V characteristics becomes positive.

3. When a disturbance causes system voltage drop, a constant impedance load will draw less power and reactive power from the supply system than that of a constant power load, which has a favored damping effect to halt the further voltage decline. This damping effect is crucial to system voltage stability when there are induction motors operating near their critical state. Constant power load, which is not voltage sensitive, is therefore a stiff system load. This load characteristics is harmful to system voltage stability because it will draw the same power and reactive power from the supply system despite voltage decline.

   Although a voltage dependent load has a favored effect on system voltage stability, it has different impacts on system angle stability. On the one hand, when a disturbance causes a system power supply shortage, such as loss of a generator, voltage sensitive loads will draw less power due to voltage decrease. This load reduction is helpful to balance system power so as to stabilize the generator operation. On the other hand, when a disturbance causes system voltage collapse due to, for example, the loss of a motor stable operation, the rapid decrease of loads due to voltage collapse may upset the system power balance causing a transient system angle instability.

4. A persistent PQ load may demand constant power and reactive power but involving a time delayed recovery. The attempt to maintain pre–disturbance load level by increasing load equivalent admittance despite voltage decline may cause some particular system load bus exceeding its post–disturbance loading limit, causing voltage instability at that bus.

   If the post–disturbance system operating condition is such that the voltage collapsed bus has a relatively short electrical distance with other system buses, the loss of voltage control at that particular bus may spread out to the other parts of the system causing a complete system voltage collapse. On the other hand, if the voltage collapsed bus is far away electrically from the rest of the system, it may has little impact on the other bus voltages, and then the rest part of the system may have a chance to maintain both voltage and angle stability.

5. A transformer tap changing may have either beneficial or detrimental effect on system voltage stability depending on its location and load characteristics. Its effect is crucial when a system operates near its critical state.

   The effect of tap changing at step–up transformer of a generator is always beneficial to system voltage stability since it raises the transmission voltage, and hence reduces the network current and the corresponding reactive power loss.

   The tap changing of distribution transformer at a system load bus has different effects on system voltage stability depending on load characteristics. For a load with positive Q–V characteristics, such as an exponential form PQ load with positive exponents, tap changing which raises the load side voltage, will result in more reactive power drawn from the system causing system side voltage to decline further. This may push the system over its loading limit causing a possible voltage collapse if the system has operated near its critical state. On the other hand, for a load with negative Q–V characteristics, such as an induction motor load, the voltage increase by changing the transformer tap will reduce the reactive power drawn from the system so as to stabilize the system side voltage.

6. Effective system VAR control and adequate compensation is very important to maintain system voltage stability. The effectiveness of a VAR compensation depends on the types and locations of VAR devices, the system operating conditions,

the VAR control speed, and the VAR capacities.

Since the VAR compensation with a fixed capacitor are directly proportional to the square of the bus voltage regardless of load demands, it may not be effective in most system situations involving fast voltage drop. This also suggests that a heavy fixed capacitor compensated system may be vulnerable to voltage instability. For a system operating condition involving slow voltage decline, fixed capacitors compensation can be used to support system voltage, but some of the capacitors should be switched out of the system to avoid over–compensation when system voltage is back to normal. This is especially crucial when the bus load has a negative Q–V characteristic.

The VAR compensation with an SVC of sufficient capacity is very effective to stabilize the voltage of a power system. It is effective in both fast transient and slow dynamic operating conditions due to the fast response of the negative feedback control. However, there is a dynamic interaction between an SVC voltage control and a generator excitation control, which may cause a system oscillation. This observation suggests that the SVC voltage control must be coordinated with the power system stabilizer(PSS) design.

7. In a heavily loaded system, a generator rotor overheat protection may limit its rotor winding current by cramping the excitation voltage. As a result, it will reduce the reactive power supply to the system, and that reactive power burden must be transferred to other generators which could be also protected. The successive losses of voltage controls at generator buses will aggravate system reactive power shortage, which may cause a possible system voltage collapse. This also suggests that an effective system wide VAR compensation should be effectively designed, and a heavy dependence of reactive power supply from remote generators could

result in voltage instability due to the possible generator rotor overheat protection.

8. Case studies in this thesis demonstrate the importance of dynamic effects of system loads and control devices on system voltage stability. Although the MLL determined by load flow for power system in steady state is generally larger than the MLL determined by simulation for a system being disturbed, the voltage control effect of transformer tap changing, if fast enough, can increase the MLL of an induction motor load even larger than that determined from load flow.

5.2 Future Research Work

The following aspects are suggested for future research work.

1. Although the effects of individual system typical loads on system voltage stability are closely examined with a sample power system, the real system bus load is far more complicated. It may be a combination of these typical loads or more, which requires further investigation. The study may involve more detailed modeling of bus load, estimation of some other unknown loads, and identification of load parameters.

2. Since all reactive power components of a power system, generation, consumption, control, and constraints, are important to voltage stability, the coordinations of the functions of these components, both locally and system wide, are necessary for a power system to maintain voltage stability. More research work shall be done in this regard.

3. It is realized that the voltage stability of a power system can not be improved by voltage oriented control alone without coordination of the angle stability control. Therefore, both voltage stabilizer and angle stabilizer must be designed together. This suggests another important research project in the future.

Bibliography

[1] IEEE Publication 90TH0358–2–PWR, "Voltage stability of power systems: concepts, analytical tools, and industry experience," IEEE Service Center, New Jersey, 1990.

[2] B.M. Weedy and B.R. Cox, "Voltage stability of radial power links," IEE Proceedings, Vol. 115, No. 4, pp.528–536, April, 1968.

[3] R.K. Gupta, Z.A. Alaywan, R.B. Stuart and T.A. Reece, "Steady state voltage instability operations perspective," IEEE/PES Winter Meeting, 90 WM 037–2 PWRS, Atlanta, February 4–8, 1990.

[4] A. Cheimanoff and C. Curroyer, "The power failure of December 19, 1978," Revue Generale de l' electricite, Vol.89, pp.280–320, April, 1980.

[5] F. Bourgin, G. Testud, B. Heilbronn and J. Verseille, "Present practices and trends on the French power system to prevent voltage collapse," IEEE/PES Summer Meeting, 92 SM 394–7 PWRS, Seatte, July 12–16, 1992.

[6] K. Takahashi and Y. Nomura, "The power failure on July 23, 1987 in Tokyo," Report to CIGRE Study Committee 37, Montreal, September 22–25, 1987.

[7] A.J. Calvaer and Van Geert, "Quasi steady state synchronous machine linearization around an operating point and application," IEEE Transactions on Power Apparatus and System, Vol. PAS–103, No. 6, pp. 1466–1479, June, 1984.

[8] V.A. Venikov, V.A. Stroev, V.I. Idelchick and V.I. Tarasov, "Estimation of electric power steady–state stability in load flow calculations," IEEE Transactions on Power System Apparatus and System, Vol. PAS–94, No. 3, May/June, 1975.

[9] Y. Tamura, H. Mori and S. Iwamoto, "Relationship between voltage instability and multiple load flow solutions in electric power systems," IEEE Transactions on Power Apparatus and Systems, Vol. PAS–102, No. 5, May, 1983.

[10] H.G. Kwatny, A.K. Pasrija and L.Y. Bahar, "Static bifurcations in electric power networks: loss of steady–state stability and voltage collapse," IEEE Transactions on Circuits and Systems, Vol. CAS–33, No. 10, October, 1986.

[11] N. Flatabo, O.B. Fosso, R. Ognedal, T. Carlsen and K.R. Heggland, "A method for calculation of margins to voltage instability applied on the Norwegian system for maintaining required security level," IEEE/PES Summer Meeting, 92 SM 395–5 PWRS, Seatte, July 12–16, 1992.

[12] T. Van Cutsem, "A method to compute reactive power margins with respect to voltage collapse," IEEE/PES Winter Meeting, 90 WM 097–6 PWRS, Atlanta, February 4–8, 1990.

[13] C.W. Taylor, "Voltage stability analysis with emphasis on load characteristics and undervoltage load shedding," Panel Session on Load Modeling Impact on System Dynamic Performance, IEEE/PES Summer Meeting, Long Beach, July 10, 1988.

[14] M.M. Begovic and A.G. Phadke, "Control of voltage stability using sensitivity analysis," IEEE/PES Winder Meeting, 91 WM 231–1 PWRS, New York, February 3–7, 1991.

[15] R.A. Schlueter, I. Hu, M.W. Chang, J.C. Lo and A. Costi, "Methods for determining proximity to voltage collapse," IEEE/PES Winter Meeting, 90 WM 096–8 PWRS, Atlanta, February 4–8, 1990.

[16] P.W. Sauer and M.A. Pai, "Power system steady–state stability and the load–flow Jacobian," IEEE Transections on Power Systems, Vol. 5, No. 4, November, 1990.

[17] S. Abe, Y. Fukunaga, A. Isono, and B. Knodo, "Power system voltage stability," IEEE Transactions on Power Apparatus and Systems, Vol. PAS–101, No. 10, pp. 3830–3840, October, 1982.

[18] C. Concordia and S. Ihara, "Load representation in power system stability studies," IEEE Transactions on Power Apparatus and Systems, Vol. PAS–101, No. 4, pp. 969–977, April, 1982.

[19] IEEE Task Force on Load Representation for Dynamic Performance, "Load representation for dynamic performance analysis," IEEE/PES Winter Meeting, 92 WM 126–3 PWRD, New York, January 26–30, 1992.

[20] E. Vahedi, M.A. El-Kady, J.A. Libaque-Esaine and V.F. Carvalho, "Load models for large–scale stability studies from end–user consumption," IEEE Transactions on Power Systems, Vol. PWRS–2, No. 4, pp. 864–872, November, 1987.

[21] E. Vaahedi,, H.M.Z. El-Din and W.W. Price, "Dynamic load modeling in large scale stability studies," IEEE Transactions on Power Systems, Vol. 3, No. 3, pp. 1039–1045, August, 1988.

[22] A.E. Hammad and M.Z. El-Sadek, "Prevention of transient voltage instability due to induction motor loads by static VAR compensations," IEEE Transactions on Power Systems, Vol. 4, No. 3, pp. 1182–1190, August, 1989.

[23] M.H. Ment, W.R. Schmus, F.A. McCrackin and L.M. Wheeler, "Dynamic modeling of loads in stability studies," IEEE Transactions on Power Apparatus and Systems, Vol. PAS–88, No. 5, pp. 756–763, May, 1969.

[24] IEEE Computer Analysis of Power Systems Working Group, "System load dynamics simulation effects and determination of load constants,", IEEE Transactions on Power Apparatus and Systems, Vol. PAS–92, No. 2, pp. 600–609, March/April, 1973.

[25] D.J. Hill, "Nonlinear dynamic load models with recovery for voltage stability studies," IEEE/PES Winter Meeting, 92 WM 102-4 PWRS, New York, January 26–30, 1992.

[26] C.P. Arnold, K.S. Turner and J. Arrillaga, "Modeling rectifier loads for a multi–machine transient–stability program," IEEE Transactions on Power Apparatus and Systems, Vol. PAS–99, No. 1, pp. 78–85, January/February, 1980.

[27] T. Smed, G. Andersson, G.B. Sheble and L.L. Grigsby, "A new approach to AC/DC power flow," IEEE/PES Summer Meeting, 90 SM 399-6 PWRS, Minneapolis, July 15-19, 1990.

[28] T.J. Hammons and D.J. Winning, "Comparisons of synchronous machine models in the study of the transient behavior of electric power systems," IEE Proceedings, Vol. 118, No. 10, pp.1442–1458, October, 1971.

[29] IEEE Committee Report, "Computer representation of excitation Systems," IEEE Transactions on Power Apparatus and Systems, Vol. PAS–87, No. 6, pp. 1460–1468, June, 1968.

[30] L.M. Hovey and L. A. Bateman, "Speed regulation tests on hydro station supplying an isolated load," IEEE Transactions on Power Apparatus and Systems, pp.364–371, October, 1962.

[31] IEEE Committee Report, "Dynamic models for steam and hydro turbines in power system studies," IEEE/PES Winter Meeting, T 73 089–0, New York, January 28–February 2, 1973.

[32] Y.N. Yu, "Electric power system dynamics," Academic Press, New York, 1983.

[33] C.C. Liu and F.F. Wu, "Steady state voltage stability region of power systems," Proceedings of the Conference on Decision and Control, pp. 488–493, December, 1984.

[34] J. Medanic, M. Ilic-Spong and J. Christensen, "Discrete Models of slow voltage dynamics for under-load tap-changing transformer coordination," IEEE Transactions on Power Systems, pp. 873–882, November, 1987.

[35] Y.Y. Hsu and C.J. Wu, "Adaptive control of a synchronous machine using the auto–searching method", IEEE Transactions on Power System, Vol. 3, No. 4, pp.1434-1439, November, 1988.

[36] IEEE Publication 87TH0187–5–PWR, "Application of static VAR systems for system dynamic performance," IEEE Publishing Service, New York, 1987.

[37] G.K. Morison, B. Gao and P. Kundur, "Voltage stability analysis using static and dynamic approaches," IEEE/PES Summer Meeting, 92 SM 590–0 PWRS, Seatte, July 12–16, 1992.

[38] J. Arillaga, C.P. Arnold and B.J. Harker, "Computer modeling of electrical power systems," John Wiley & Sons, 1983.

[39] Q.H. Li, "Stabilizer design of dynamic stability control of multimachine power systems," Ph.D Dissertation, Department of Electrical Engineering, The University of British Columbia, December, 1991.

[40] Energy Technology Applications Division, "Power system dynamic analysis – phase 1," EPRI EL–484, Research Project 670–1, July, 1977.

[41] L. Shampine and M. Gordon, "Computer solution of ordinary differential equations," W. H. Freeman and Co., San Francisco, 1975.

[42] K.E. Atkinson, "An introduction to numerical analysis," John Wiley & Sons, New York, 1978.

[43] C.W. Gear, "Numerical initial value problems in ordinary differential equations," Englewood Cliffs, N.J., Prentice–Hall, 1971.

[44] Y.N. YU and Q.H. Li, "Pole–placement power system stabilizer design of an unstable nine–machine system," IEEE Transactions on Power System, Vol. 5, No. 2, pp.353-357, 1990.

[45] P.C. Krause, "Method of multiple reference frames applied to the analysis of symmetrical induction machinery," IEEE Transactions on Power Apparatus and Systems, Vol. PAS–87, No. 1, pp.218-227, 1968.

[46] J. Goossens, "Reactive power and system operation — incipient risk of generator constraints and voltage collapse," 1989 IFAC Symposium on Power System and Power Plant Control, pp.3-12, 1989.

[47] W.R. Lachs, "Dynamic study of an extreme system reactive power deficit," IEEE Transactions on Power Apparatus and System, Vol. PAS–104, No. 9, pp.2420-2426, September, 1985.

[48] G.A. Jones, "The effects of system voltage reductions on various static load models," IEEE/PES Summer Meeting and Energy Resource Conference, C 74 349–7, Anaheim, July 14–19, 1974.

[49] H.K. Clark, "Experience with load models in the simulation of dynamic phenomena," Panel discussion: Load Modeling Impact on System Dynamic Performance, IEEE/PES Summer Meeting, Long Beach, July 10, 1989.

[50] C. Rajagopalan, B. Lesieutre, P.W. Sauer and M.A. Pai, "Dynamic aspects of voltage/power characteristics," IEEE/PES Summer Meeting, 91 SM 419-2 PWRS, San Diego, July 28 – August 1, 1991.

[51] Y. Sekine and H. Ohtsuki, "Cascaded voltage collapse," IEEE/PES Summer Meeting, 89 SM 710-5 PWRS, Long Beach, July 9–14, 1989.

[52] Y.N. Yu and W.J. Zhang, "Nature of induction motor load and voltage stability," International Conference on Power System Technology, Vol. 1, pp.353-357, 1990.

[53] Y.N. Yu and W.J. Zhang, "Computer simulation study of voltage stability of a power system," 1993 Canadian Conference on Electrical and Computer Engineering, Vol. 2, pp.927-932, 1993.

[54] M.K. Pal, "Voltage stability conditions considering load characteristics," IEEE/PES Summer Meeting, 91 SM 490-3 PWRS, San Diego, July 28 – August 1, 1991.

[55] C.W. Taylor, "Concepts of undervoltage load shedding for voltage stability," IEEE/PES Winter Meeting, 91 WM 162-8 PWRD, New York, February 3–7, 1991.

[56] A.R. Mahran, B.W. Hogg and M.L. El-Sayed, "Co-ordinated control of synchronous generator excitation and static VAR compensator," IEEE/PES Winter Meeting, 92 WM 019-0 EC, New York, January 26–30, 1992.

[57] I.A. Hiskens and C.B. Mclean, "SVC behavior under voltage collapse conditions," IEEE/PES Summer Meeting, 91 SM 489-5 PWRS, San diego, July 28 – August 1, 1991.

[58] B. Gao, G.K. Morison and P. Kundur, "Voltage stability evaluation using model analysis," IEEE/PES Summer Meeting, 91 SM 420-0 PWRS, San diego, July 28 – August 1, 1991.

[59] J. Deuse and M. Stubbe, "Dynamic simulation of voltage stability," IEEE/PES Summer Meeting, 92 SM 396-2 PWRS, Seattle, July 12–16, 1992.

[60] C. Concordia, "Dynamic performance and security of interconnected systems," IEEE Power Engineering Review, pp.11-14, March, 1992.

[61] W.R. Lachs and D. Sutanto, "Voltage instability in interconnected power systems: a simulation approach," IEEE Transections on Power System, Vol. 7, No. 2, pp.753-761, May, 1992.

[62] N. Yorino, H. Sasaki, Y. Masuda, Y. Tamura, M. Kitagawa and A. Oshimo, "An investigation of voltage instability problems," IEEE/PES Winter Meeting, 91 WM 202-2 PWRS, New York, February 3–7, 1991.

[63] H.D. Chiang, I. Dobson, R.J. Thomas, J.S. Thorp and L. Fekih-ahmed, "On voltage collapse in electric power systems," IEEE 1989 PICA Conference, 89CH2747-4, pp.342-349, Seattle, May 1–5, 1989.

[64] M.M. Begovic and A.G. Phadke, "Dynamic simulation of voltage collapse," IEEE 1989 PICA Conference, 89CH2747-4, pp.336-341, Seattle, May 1–5, 1989.

[65] W.R. Lachs and D. Sutanto, "Different types of voltage instability," IEEE/PES Summer Meeting, 93 SM 518-1 PWRS, Vancouver, July 18–22, 1993.

Appendix A

DERIVATION OF STEADY–STATE MOTOR EQUATIONS

In this appendix, the steady-state induction motor power equation (2.5) is derived from motor equivalent circuit which can be obtained from a ψ model for the motor.

Similar to the Park's equations for synchronous machines, the voltage equations of a three phase symmetrical induction motor can be described in a d–q frame of reference rotating at synchronous speed ω_b as

(a) Stator winding voltage equations:

$$V_{ds} = r_s I_{ds} - \psi_{qs} + \frac{1}{\omega_b} \dot{\psi}_{qs} \tag{A.1}$$

$$V_{qs} = r_s I_{qs} + \psi_{ds} + \frac{1}{\omega_b} \dot{\psi}_{ds} \tag{A.2}$$

(b) Rotor winding voltage equations:

$$V_{dr} = r_r I_{dr} - (1 - \omega_r)\psi_{qr} + \frac{1}{\omega_b} \dot{\psi}_{qr} \tag{A.3}$$

$$V_{qr} = r_r I_{qr} + (1 - \omega_r)\psi_{dr} + \frac{1}{\omega_b} \dot{\psi}_{dr} \tag{A.4}$$

In the foregoing equations, r's are winding resistances, ω_r is motor speed, V_d's and V_q's are winding voltage d–q components with $V_{dr} = V_{qr} = 0$ for the rotor, I_d's and I_q's are winding current d–q components, and ψ's are corresponding winding flux linkages, in Webers per second, which have the following relations.

$$\psi_{ds} = (X_{ls} + X_m) I_{ds} + X_m I_{dr} \tag{A.5}$$

$$\psi_{qs} = (X_{ls} + X_m) I_{qs} + X_m I_{qr} \tag{A.6}$$

$$\psi_{dr} = (X_{lr} + X_m)\, I_{dr} + X_m\, I_{ds} \tag{A.7}$$

$$\psi_{qr} = (X_{lr} + X_m)\, I_{qr} + X_m\, I_{qs} \tag{A.8}$$

where X_{ls} and X_{lr} are respectively the stator and rotor winding leakage reactances, and X_m is the magnetizing reactance.

For steady state conditions, the winding transients are not included. The corresponding steady state voltage equations can then be obtained by dropping the derivative terms from equations (A.1) – (A.4), which gives

(a) Stator winding voltage equations:

$$V_{ds} = r_s\, I_{ds} - \psi_{qs} \tag{A.9}$$

$$V_{qs} = r_s\, I_{qs} + \psi_{ds} \tag{A.10}$$

(b) Rotor winding voltage equations:

$$0 = r_r\, I_{dr} - (1 - \omega_r)\, \psi_{qr} \tag{A.11}$$

$$0 = r_r\, I_{qr} + (1 - \omega_r)\, \psi_{dr} \tag{A.12}$$

The steady state equations of an induction motor can also be expressed in phasors. For this, substitute equations (A.5) – (A.8) into equations (A.9) – (A.12), and define motor slip $s = 1 - \omega_r$, terminal voltage $\mathbf{V} = V_{ds} + j\, V_{qs}$, stator current $\mathbf{I_s} = I_{ds} + j\, I_{qs}$, and rotor current $\mathbf{I_r} = I_{dr} + j\, I_{qr}$, which, through some manipulations, gives

$$\mathbf{V} = (r_s + X_{ls})\, \mathbf{I_s} + j\, X_m\, (\mathbf{I_s} + \mathbf{I_r}) \tag{A.13}$$

$$\mathbf{0} = (\frac{r_r}{s} + X_{lr})\, \mathbf{I_r} + j\, X_m\, (\mathbf{I_s} + \mathbf{I_r}) \tag{A.14}$$

Equations (A.13) and (A.14) lead to the well–known equivalent circuit of an induction motor as shown in Figure A.1.

Defining $\mathbf{Z_s} = r_s + j\, X_{ls}$, $\mathbf{Z_r} = r_r + j\, X_{lr}$, $\mathbf{Z_m} = j\, X_m$, $R_a = \frac{1-s}{s} r_r$, and $\mathbf{Z_a} = \mathbf{Z_r} + R_a = \frac{r_r}{s} + j\, X_{lr}$, the impedance $\mathbf{Z}$ as seen from the motor terminal becomes

$$\mathbf{Z} = \mathbf{Z_s} + \mathbf{Z_m} \,||\, \mathbf{Z_a} \tag{A.15}$$

where the symbol " || " means "parallel with."

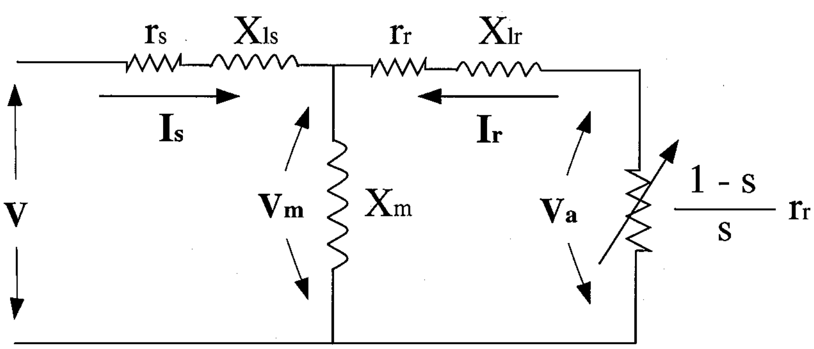

Figure A.1: Equivalent Circuit of An Induction Motor

The voltages $\mathbf{V_m}$ across X_M, and $\mathbf{V_a}$ across $\frac{1-s}{s} r_r$ as shown in Figure A.1 can be expressed as

$$\mathbf{V_m} = \frac{\mathbf{V}}{\mathbf{Z}} (\mathbf{Z_m} \,||\, \mathbf{Z_a}) \tag{A.16}$$

$$\mathbf{V_a} = \frac{\mathbf{V_m}}{\mathbf{Z_a}} R_a \tag{A.17}$$

Substituting equation (A.16) into (A.17) gives

$$\mathbf{V_a} = \frac{(\mathbf{Z_m} \,||\, \mathbf{Z_a}) R_a}{\mathbf{Z} \mathbf{Z_a}} \mathbf{V} \tag{A.18}$$

The torque and power equation (2.5) can be derived as follows.

(a) Air gap power P_E

$$\begin{aligned} P_E &= Re[\mathbf{V_a} \mathbf{I_r^*}] \\ &= Re[\mathbf{V_a} (\mathbf{V_a}/R_a)^*] \\ &= Re[|\mathbf{V_a}|^2/R_a] \\ &= |\mathbf{V_a}|^2/R_a \end{aligned} \tag{A.19}$$

(b) Motor developed torque T_E

$$T_E = \frac{P_E}{1-s} \tag{A.20}$$

(c) Power drawn by the motor P_m

$$\begin{aligned} P_m &= Re[\mathbf{V}\mathbf{I}_s^*] \\ &= Re[\mathbf{V}\,(\mathbf{V}/\mathbf{Z})^*] \\ &= |\mathbf{V}|^2/Re[\mathbf{Z}^*] \end{aligned} \tag{A.21}$$

(d) Reactive power drawn by the motor Q_m

$$\begin{aligned} Q_m &= Im[\mathbf{V}\mathbf{I}_s^*] \\ &= Im[\mathbf{V}\,(\mathbf{V}/\mathbf{Z})^*] \\ &= |\mathbf{V}|^2/Im[\mathbf{Z}^*] \end{aligned} \tag{A.22}$$

The above equations can be expanded and re–organized in such a way that the motor torque and powers can be expressed explicitly in terms of motor slip s, the terminal voltage $\mathbf{V}$, and the motor parameters $\mathbf{p}$ with $\mathbf{p} = \{r_s, r_r, X_{ls}, X_{lr}, X_m\}$.

Let

$$\begin{aligned} a_1 &= r_s r_r \\ a_2 &= X_{ls} X_{lr} + X_{ls} X_m + X_{lr} X_m \\ a_3 &= r_r (X_{ls} + X_m) \\ a_4 &= r_s (X_{lr} + X_m) \\ a_5 &= r_r X_m^2 \end{aligned}$$

$$\begin{aligned} b_1 &= r_s (X_{lr} + X_m)^2 \\ b_2 &= r_r X^2 M \\ b_3 &= r_s r_r^2 \end{aligned}$$

$$
\begin{aligned}
c_1 &= (X_{lr} + X_m)\, a_1 \\
c_2 &= r_r\, a_3
\end{aligned}
$$

$$
\begin{aligned}
d_1 &= a_2^2 + a_4^2 \\
d_2 &= 2\, r_s\, r_r\, X_m^2 \\
d_3 &= a_1^2 + a_3^2
\end{aligned}
$$

the motor torque and power can then be expressed as follows.

$$
T_E = \frac{a_5\, s}{d_1\, s^2 + d_2\, s + d_3} \mathbf{V}^2 = f_E\,(s, \mathbf{p})\, \mathbf{V}^2 \tag{A.23}
$$

$$
P_m = \frac{b_1\, s^2 + b_2\, s + b_3}{d_1\, s^2 + d_2\, s + d_3} \mathbf{V}^2 = f_P\,(s, \mathbf{p})\, \mathbf{V}^2 \tag{A.24}
$$

$$
Q_m = \frac{c_1\, s^2 + c_2}{d_1\, s^2 + d_2\, s + d_3} \mathbf{V}^2 = f_Q\,(s, \mathbf{p})\, \mathbf{V}^2 \tag{A.25}
$$

Equations (A.24) and (A.25) show variable impedance characteristics of an induction motor in steady state operating conditions. The power and reactive power of an induction motor depend on both terminal voltage $\mathbf{V}$ and motor slip s.